Addis Ababa University

Addis Ababa Institute of Technology

School of Mechanical and Industrial Engineering

Design, Simulation and Experimental Test of Solar Assisted Hydraulic Ram Pump

By:

Ashenafi Abebe,

ID: GSR/9896/11

Graduate Program

Advisors: Asfaw Beyene, Ph.D.

Yilma Tadesse, Ph.D.

JUNE 2020

ADDIS ABABA, ETHIOPIA

Certification

We, the undersigned, certify that I read and hear by recommend for acceptance by School of Mechanical and Industrial Engineering, a thesis entitled “Design, Simulation and Experimental Test of Solar Assisted Hydraulic Ram Pump taking Addis Ababa as a case study” in partial fulfillment of the requirements for the degree of Masters of Science in Thermal Engineering.

_____

Asfaw Beyene, Professor (Advisor)

_____

Yilma Tadesse (PhD) (Co-advisor)

Declaration

I, Ashenafi Abebe, declare that this thesis is the result of my work and that all sources or materials used for this thesis have been dually acknowledged. The experimental test was done by a team of mechanical engineering senior design students Dan Inocencio, David Orozco Gamez, Cameron Sacks, and Christian Solorzano at San Diego State University under the close supervision of Professor Asfaw Beyen. This work is submitted in partial fulfillment of the requirements for a Master's Degree in Thermal Engineering at Addis Ababa University, School of Mechanical and Industrial Engineering. I certainly declare that this thesis has not been submitted to any other institution anywhere for the award of any academic degree, diploma, and/or certificate.

Ashenafi Abebe

_____

Addis Ababa University

Institute of Technology

School of Graduate Studies

School of Mechanical Engineering

This is to certify that the thesis prepared by Ashenafi Abebe entitled "Design, Simulation and Experimental Test of Solar Assisted Hydraulic Ram Pump taking Addis Ababa as a case study" in partial fulfillment of the requirements for the degree of Masters of Science in Thermal Engineering compiles with the regulation of Addis Ababa University and meets the accepted standards concerning originality and quality.

Board of Examining Committee:

Advisors:

1. Asfaw Beyene (Professor) Signature: _____ Date: 08/07/2020
2. Yilma Tadesse (PhD) Signature: _____ Date: 08/07/2020

External examiner:

Dr. Gouadwossen Bopal Signature: _____ Date: 08/07/2020

Internal examiner:

Abdulkadir Aman (PhD) Signature: _____ Date: 06/07/2020

Addis Ababa Institute of Technology Graduate Program Director

_____

Chair of Department or Graduate program coordinator

Acknowledgments

I would like to give heart full gratitude for the Almighty GOD with his HOLY FAMILIES.

My gratitude goes to several individuals who supported me to acquire deep and invaluable knowledge and experience. First I would like to take this opportunity to give my special thanks to my advisors Professor Asfaw Beyene and Dr. Yilma Tadesse. Their guidance and generosity with their time for this thesis at every stage their devotion, clarity, and sharing their invaluable ideas as well as experience is greatly appreciated.

Second, my acknowledgment goes to Dr. Shaffar and the team of mechanical engineering senior design students Dan Inocencio, David Orozco Gamez, Cameron Sacks, and Christian Solorzano for the experimental test at San Diego State University Laboratory.

Last but not least I would like to acknowledge all of my friends who stood beside me and gave critical feedback and many helpful ideas.

Abstract

This research aims at designing, simulating, and experimentally testing a solar-assisted hydraulic ram pump, which is an automatic water-lifting device convenient to pump water, by adding energy to the chamber. Low level performance of HRP triggered working on performance improvements. The approach to achieve the objective involves knowing the basic working principle of regular hydram and water hammer effect, data collection and synthesis with understanding of fundamental thermo-fluid and heat transfer principles, development of a mathematical model, CFD simulation of the thermal effect inside the pressure chamber and finally experimental test.

The efficiency of regular hydram can reach 65% delivering around 5 liters per minute with the net head of 6m. The mathematical model gives maximum water hammer pressure change of 268.4 kPa, whereas experimental test results 183.33kPa. Flow rate at the exit of the pump was 4.72 L/minute with source flow of 12 liters every minute and supply head of 2.18m. Experimental test getting a source flow of 34 liters every minute gave 11.72 liters per minute.

The regular hydraulic ram pump was assisted with solar thermal system to improve its performance. The temperature generated from thermal collector was applied to the chamber. For the experimental test, equivalent controllable electrical heater was selected having a temperature of 200 ^{o}C.

The temperature effect results 33kPa pressure rise when computed analytically with approximate chamber temperature of 150 ^{o}C. While CFD provides 50kPa with chamber temperature of 145 ^{o}C. The exit flow rate was 1.35 and 1.667 liters per minute for the analytical and CFD modeling respectively at source flow of 12 liters each minute.

Superposition of thermal and water hammer effect gave 301.4 and 318.4 kPa analytical and CFD simulation respectively. Thermal infusion test, conducted at San Diego State University, measured maximum chamber pressure of 342.32 kPa with chamber temperature of 106.75 ^{o}C. Exit flow rate was 6.07 liters per minute for analytical, 6.387 liters per minute for CFD with supply flow of 12 liters per minute for a pump having 27 mm diameter at supply height of 2.18 m. During the thermal experiment 16.41 liters per minute was recorded with supply of 34 liters per minute. Therefore, after

the application of thermal energy to the pump delivery head was improved by a minimum of three meter.

The heat energy will be generated by using UHVFP collector. The energy is delivered to the chamber through thermal oil, since thermal oils does not need any pumping system. The hot fluid coming out of the solar thermal collector applied around the wall of the chamber.

The power of solar radiation for Addis Ababa was investigated to model the solar thermal potential as case study. The lowest solar radiation occurs in July and its value is 350 W/m^2. Ultra-high vacuum (UHV) collector was selected since it can generate mid-range temperature. A minimum mean temperature difference of 110 ^oC obtained with a collector efficiency of 50%. With the UHV collector fluid outlet temperature, 225 ^oC can be produced during July. Therefore, this newly designed novel hydraulic ram pump can lift water by improving delivery head at least by three meter than regular hydraulic ram pump with higher delivery flow if it is assisted by solar energy.

Keywords: HRP, performance, water hammer, solar assisted, temperature effect, delivery head

Contents

Page

Acronym

CDM - Clean Development Mechanism

CFD – Computational fluid dynamics

EFPC - Evacuated flat plate collector

ETC - Evacuated plate collector

FPC - Flat plate collector

IDRC - International Development Research Centre

NEG - None evaporable getter pump

PVC – Polyvinyl chloride

PTC - Parabolic trough collector

UHV - Ultra-high vacuum collector

UHVFPC - CERN's ultra-high vacuum flat plate collector

Symbols

A_c - Collector area

A_s - Surface area

A_V - Cross-sectional area

a_1 - First-order heat loss coefficient [w/m^2.K]

a_2 - Temperature-dependent heat loss coefficient [w/m^2.K^2]

C - Constant

c_p - Specific heat

c - Wave celerity

D - Drive pipe diameter

$d\dot{m}$ - Differential mass

dQ - Differential heat transfer

dt - Differential time

dU - Differential internal energy

dV - Differential volume

dW - Differential moving boundary work

E - Young's modulus of pipe material

f - Friction factor

g - Acceleration due to gravity (m/s^2)

H - Static supply head

h - Net pumped head

h_c - Convection heat transfer coefficient

h_r - Head loss

h_{eva} - Heat of evaporation

Δh - Head loss feet of the water column

K - Bulk modulus of elasticity of water

K_c - Composite modules of elasticity

K_L - Minor losses coefficients

k_T - Hourly clearness index

N - Number of valve beats/minute

I_b - beam solar radiation

I_d - diffuse solar radiation

I_H - Global radiation

I_T - Absorbed solar radiation

I_β - Hourly global solar radiation on an inclined surface

$I_{\beta,b}$ - Hourly direct beam solar radiation on an inclined surface

$I_{\beta,d}$ - Hourly diffuse solar radiation on an inclined surface

I_r - Hourly ground reflected radiation on an inclined surface

I_o - Hourly extraterrestrial radiation on a horizontal surface

L - Length of the drive pipe

m - Mass

M - Head loss factors in drive pipe and waste valve

$\dot{m}_{i,a}$ - Inlet mass flow rate of air

$\dot{m}_{o,a}$ - Outlet mass flow rate of air

$\dot{m}_{i,l}$ - Inlet mass flow rate of liquid water

$\dot{m}_{o,l}$ - Outlet mass flow rate of liquid water

$\dot{m}_{i,v}$ - Inlet mass flow rate of vapor

$\dot{m}_{o,v}$ - Outlet mass flow rate of vapor

P - Pressure

Q_u - Useful energy

Q_s - Supply flow to the pump

Q_w - Wasted flow rate

R - Gas constant

R(s) - Friction head loss factor of waste valve

S - Absorbed solar radiation

T - Temperature

T_m - Mean temperature of heat transferring fluid

V - Velocity

V_o - Valve closing velocity

$\forall$ - Volume

v - Specific volume

x - Quality

Greek Letters

α_s - Solar altitude angle

β - Surface inclination

γ - Azimuth angle

δ - Declination angle

ω - Hour angle

θ - The angle of incidence

θ_z - Zenith angle:

γ_s - Solar azimuth angle

ϕ - Latitude

κ - Specific heat ratio

Φ - Relative humidity

ρ - Density of air

$\tau\alpha$ - Average transmittance-absorptance

η_0 - Collector peak efficiency

Subscript and Superscript

a - Air

b - Beam

d - Diffuse

f - Final state

g - Gas

H - Horizontal

i - Initial state

l - Liquid

p - Constant pressure

s - Surface

v - Constant volume

w - Water

sc - Solar constant

cv - Control volume

con - Condensation

eva - Evaporation

max - Maximum

tot -Total

List of Figures

List of Tables

Chapter 1: Introduction

Water hammer is a hydraulic shock caused by often unintentionally induced pressure or wave surge as a result of a fluid in motion being forced to stop or change direction suddenly. Water hammer can be induced intentionally for various applications. A pressure can be created using a water hammer and is commonly used to pump liquid, or in mining, practices to break through rocks. Thus hydraulic ram pump, aka hydram, is a water lifting water hammer device that utilizes the available kinetic energy from water flow dropping an elevation. The water hammer effect of hydram generated by the cyclic opening and closing of two check valves (i.e., waste and delivery valves) [1], [2]. Without the need of another external source of energy, the hydraulic ram pump will work continuously as long as there is a continuous flow of water [3].

Hydraulic ram pump was invented by J. Whitehurst in 1772, which was capable of lifting the water to a height of 4.9m [2]. It was not self-propelled; rather controlled manually. This first generation of hydram was modified and revised as a self-operating ram pump by Montgolfier in 1797, [3]. Pierce (1816) improved the automatic pump further by introducing air through the snifter valve to overcome the air dissolved in water and it was reported that his pump 300 mm in diameter lifted water at a rate of 1700 liters per minute to 48m height [2].

The simplicity of the ram pump, ease of operation, dependability, economy, maintenance, and ruggedness provided formidable acclaim for the device for the past two centuries worldwide. Its popularity increased specifically in Europe and the USA at the beginning of 20 century. The secret behind its popularity during this time was the self-powering capability. It can be installed on any site with at least a fall of 1 meter from the source to the ram, and a flow rate of at the source greater than 5 liters per minute [4]–[7]. There was a case of ram installation on which the valves had not been examined for more than a quarter of a century [8]. Therefore, the durability and cost of hydraulic ram pumps are impressive.

Hydraulic ram pump have many applications where it can be handy. It can be used to pump drinking water, water for agriculture and livestock from sources like rivers, channels, dams, or other sources for [9]. The utilization of a ram pump is appropriate for thinly populated rural areas and undeveloped countries where the installation of the normal municipal water supply system is prohibitively

expensive. Furthermore, the overflow water from the hydram can be recycled back into the reservoir with some energy input, effectively creating zero wastage of water" [10]. Some literature shows that the operating principles behind hydraulic rams can be adopted to provide energy by substituting the pressurized water delivery system for an energy conversion mechanism [11].

Despite the fact that hydram wastes overflow water which hinders its popularity [7], it has numerous advantages. Apart from those mentioned above, the advantages also include:

- Contain few moving parts, i.e., waste and delivery valves. This makes it very simple and cheap to maintain and operate.
- The efficiency of well-designed and constructed hydram is as high as 60 to 70%, pumping water to a height of up to 30 times the supply head [12].
- It can be manufactured using simple workshop equipment and operates for a long period.

Although many researchers in Ethiopia like T. Abiy Awoke and others done researches on hydraulic ram pump, the application of this device in the country is rare [13]. But it is employed in Arusha, Tanzania providing enough water for the irrigation of the local coffee farm, livestock, domestic needs and supply of water to some villagers [14]. The traditional ram pumps are still running in Europe and USA (e.g. in Seattle, the Maple Leaf Pumping Station had two 305mm rams which pump up to 4921m^3/d, sufficient for a population of 28,000). Lighter versions of those pumps are widely produced in Japan, Taiwan, Thailand, and other southeast Asia [14], [15]. Locally produced ram pump was tested successfully in Swabi, Pakistan for irrigation purposes [16]. In addition, the application of the hydraulic ram pump has been exhibited by some charity organizations in the UK, the Philippines, and China [7]. In general, devices that are not driven by fossil fuel benefit either from design improvements, material discovery, or process understanding, despite their simple construction, ram pumps have evaded research attention for so long, and the design changes influencing their costs and performance have been modest [17].

1.1 Components and Working Principle of Ram Pump

Figure 1.1, illustrates a typical installation of a hydraulic ram pump with its components and the working cycle [8].

An inclined tube called drive pipe is the ‘engine’ of the machine in which the potential energy of the source water is primarily converted into kinetic energy and then to the potential energy of water delivered. Owing to the phenomena of water hammer, the waste (impulse) valve close rapidly and the delivery valve is forced to open. The air chamber prevents the water hammer from reaching the delivery (discharge) pipe. The water contained in the drive pipe recoils and backflows towards the supply tank, which removes pressure on the impulse valve, and again allow the escape of water. The recoil causes the snifter valve to open, admitting a small amount of air into the air chamber.

The energy to pump water in hydram comes from the sudden closure of the impulse (waste) valve resulting from the stoppage of flow in the pipe that creates a water hammer effect or pressure surge. If there is a sudden change in momentum of the fluid, which is moving inside the pipe, a phenomenon called water hammer will occur. Thus water hammer is a pressure surge or wave that happens when the motion of the fluid is abruptly forced to stop or to change direction within its confined passage. Assuming the pipe is inelastic, the theoretical pressure rise that can be obtained when the flow stopped instantaneously estimated as [18].

$$\Delta H = -\frac{cV}{g} \tag{1.1}$$

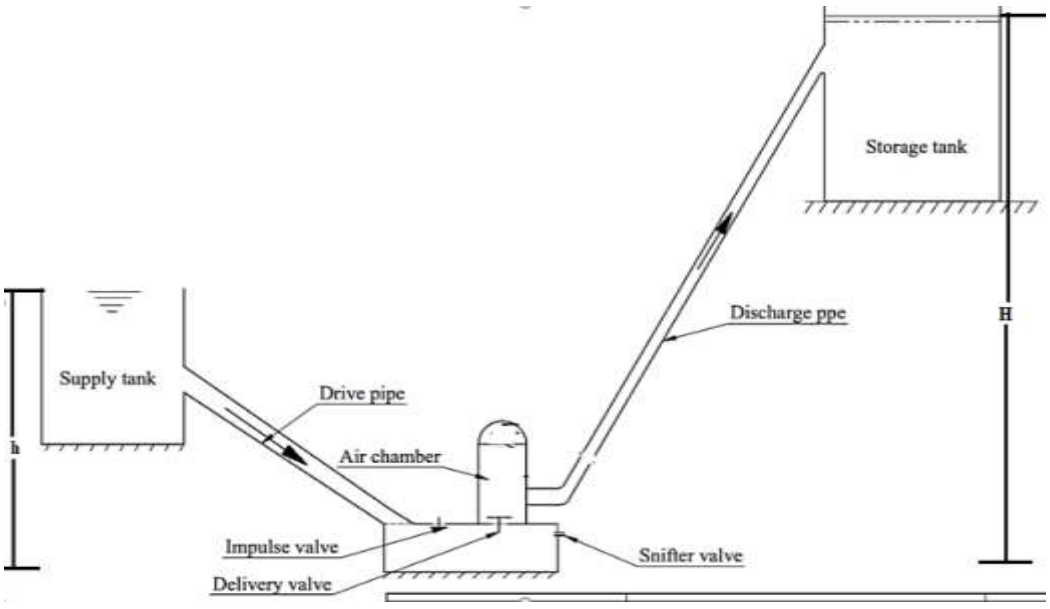

Figure 1.1Schematic illustration of a typical hydraulic ram pump water supply system installation

Customarily, the size of hydraulic ram is represented by the nominal diameter of the drive pipe which depends on the quantity of water captured. The smallest difference in the level of source of water supply and waste valve should be 91.4mm. The minimum delivery head is near twice the supply head. [8]. Cleverdon in 1937 figured out a delivery head equivalent to 30 times the available supply head is a maximum for most rams. The following table lists the typical size of hydraulic ram pump sizes and the approximate pumping characteristics.

Table 1.1 Typical size of a hydraulic ram pump and the approximate pumping characteristics [19]

Hydraulic ram preliminary sizing			
Pipe diameter (mm)		Flow rate (liter per minute)	
Drive pipe	Delivery pipe	Source (minimum)	Delivery (maximum)
19.05	12.7	7.57	2.65
25.4	12.7	22.71	5.26
38.1	19.05	53.0	10.6
50.8	24.5	94.6	18.5
63.5	31.75	132.5	26.1
76.2	38.1	227.1	52.6
152.4	76.2	567.8	189.3

1.2 Problem Statement

In developing countries, population growth results increasing but sparsely spread rural settlement, often above the water source lines. This accompanied by the intensification of agriculture through irrigation [17]. Both of them increase the demand for powered pumping. In most sub-Saharan and East African countries including Ethiopia, energy use and electrification levels are below 1% [14]. In Pakistan there is a gap between agriculture and technology due to energy crisis[16].

“About 1.4 million farmers in Ethiopia are engaged in small-scale irrigated agriculture, between 210,000 to 400,000 of whom use motor pumps” [20]. Ethiopia’s imports of irrigation equipment have trended upwards since 2006. According to Mendes and Paglietti (2015) report the annual value

of imported motor pumps in Ethiopia in 2012 to be USD 10 million [21]. Research report 172 by international water management institute (IWMI) predicted that this value could increase tenfold if Ethiopia achieves its 2020 targets for irrigated agriculture.

Even though Ethiopia is aiming to develop the agricultural sector through irrigation, since the country has an ample amount of water resources and solar potential, limited access to electricity is a key constraint to expanded irrigation. Furthermore, not more than 14% of the population has access to the electricity grid due to poor grid coverage and the dispersed nature of settlements in rural areas [20]. When electricity is available in rural or poor urban areas, it is usually too costly to connect or buy, so it is practically inaccessible. For this reasons, the Ethiopian government strategy is to shift existing motor pump users to distributed energy sources and introducing a new affordable source of energy for irrigation purposes [20]. The plan of the Clean Development Mechanism (CDM) program is also to extend the use of solar irrigation pumps to enhance farming productivity while enabling savings from fuel costs of using diesel irrigation pumps, and as well as offsetting carbon emissions.

This work attempts to address these challenges by further advancing some aspects of hydraulic ram pumps, to benefit small scale users where access to water is rampant. The novel aspect of this research was that coupling of the ram effect with solar-induced heating, since the country have water and solar potential, to boost the pumping pressure. Solar insolation of Addis Ababa is used as a case study to examine a hydrams performance in terms of pumping head and efficiency for the regular ram pump.

1.3 Literature Review

The study into the working principles of thermos-fluid device can be categorized into empirical, theoretical, and rational methods [3], [8]. Many **empirical** studies have been conducted for the ram pump. The leading researches include Eytelwein, d'Aubuisson, Morin, Tresca, Carpenter, Richards, Church, Clarck, Andeson and Clavert [3], [7], [8]. However, empirical methods need validation with theoretical models. Significant results on the theoretical analysis have been provided by Bergeron, Iversen, Montgolfier, Venturoli, Weisbech, Rankine, Lorenz and Navier [3], [8]. Validated research depend on both analytical and experimental approaches has been performed by Harza, Gosline and O'Brien, Lansford and Dugan, J. Krol, Calvert, and Schiller and Kahangire and X. Guo *et al* [3], [7].

A much earlier work of Harza in 1908 [3], shows attempts to combine experimental data with theoretical analyses for the first time and he was successful to obtain some agreement between experimental and theoretical results. There are other, more recent analytical works with experimental validation of hydraulic ram pumps, Glover, 1994, [22]. A comparison was made between the results of earlier and recent analyses and significantly differ with the assumptions considered for the theoretical computation [23].

Attempts to explaining analytically hydraulic ram pump concepts have been based on assumptions of the water velocity-time relationship as depicted in Figure 1.2 below. The period of the ram cycle was subdivided differently by various scholars from two to seven distinct phases increases the difficulties of obtaining a solution for the increased number of phases [4], [24].

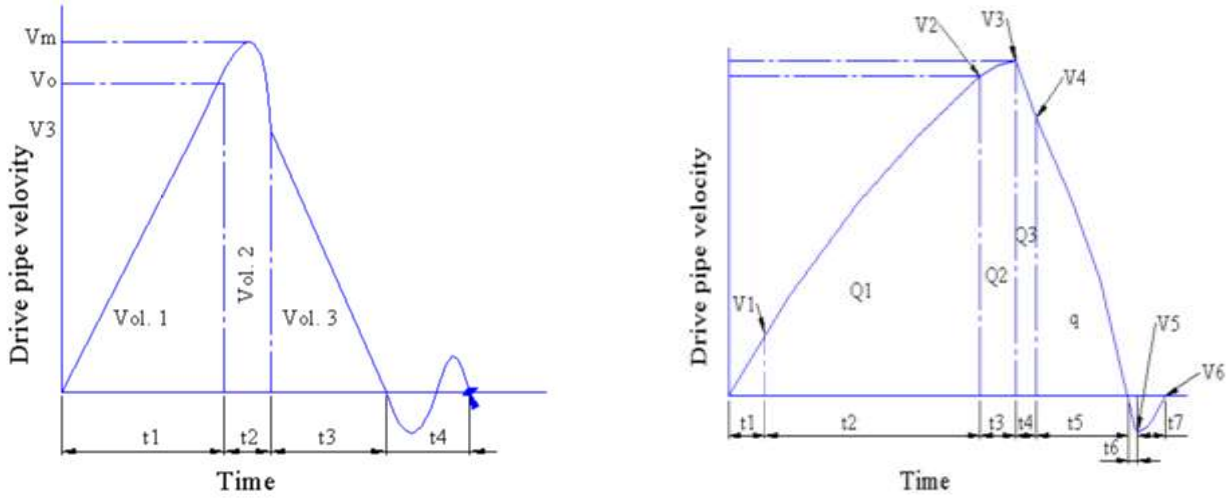

(a) (b)

Figure 1.2 (a) Schematic representation of the time-velocity variation subdivided into four periods, during one pumping cycle [3]. (b) The total pumping period T classified into seven periods [8]

At the early beginning of the 19th century, a small hydraulic ram was transported to Prussia from Paris, and professor Eytelwein made experimental tests with it. After his work, the knowledge of the device is well known in Europe but nothing has been done in America until 1847 [25]. Noise and vibrations of old hydraulic ram pumps are objected but in modern rams, this is eliminated. H.W.

Dickinson reported that the cycle of hydraulic ram can be repeated some 40 to 200 times per minute to give a continuous discharge by the provision of suitable valves and an air vessel/chamber.

1.3.1 Theoretical Principles

Water hammer occurs as a consequence of a rapid change in the momentum of the fluid moving inside a pipe. The hammer generates a pressure surge with waves when the motion of the fluid is abruptly forced to stop or change in direction. Thus, the most common cause of this change in momentum is a sudden closure of the valve, to stop or reduce the flow in the pipe.

Weisbach and Herrmann in their 1897 work give a simple theoretical operation of a hydraulic ram disregarding all forms of friction losses and water hammer effects. This crude derivation is nonetheless no mean accomplishment for a complex phenomenon under consideration. By and large, the theory relies on empirical parameters to get any realistic output [3]. In 1928, Bergeron presented an all-encompassing theoretical model by classifying the cycle into four parts. The author concluded that the maximum theoretical velocity is never attained in the drive pipe. He also suggested that better pump efficiency is obtained with low velocity in the drive pipe during valve closure [30]. Furthermore, Bergeron derived equations for the determination of the minimum length of the drive pipe as a function of head ratio, time for waste valve closure, and theoretical maximum velocity in the drive pipe. Building on the accomplishments of Herrmann, in 1933 Mead [3] proposed hydram efficiency,

$$L \geq \frac{h}{H} \times T\sqrt{2gH} \tag{1.2}$$

Wallace and Lansford's analytical study intended to make a rational mathematical analysis for the operation of automatic hydraulic rams and to compare the result with the experimental values [26]. In the study, the influence of elasticity of waste valve disk was given due attention. The authors attempted to find the relationship between velocity and resident time for the water column in the drive pipe by dividing the cycle into six sections and from that relation, the amount of water wasted and pumped per cycle was determined. The cycle time also calculated. The comparison of the result tells that the amount pumped and wasted can be predicted with an error of less than ten percent.

J. Krol [8], presents his theory for the hydraulic ram and validated it to the specially designed experimental hydram. One of J. Krol's experiments was conducted with an air chamber made of a standard pipe having an inside diameter of 152.4 mm. The height of this chamber was 304.8mm and the level of the water observed employing glass water gauge. On top of the air chamber, a pressure gauge was attached. The air chamber was kept isothermal. He assumed that friction losses in the drive pipe remain constant and the maximum and valve closing flow velocity were equal. Nevertheless, the weakness of this finding was the effect of the air chamber was not considered, despite the cycle divided into six periods. Based on his analysis and experimental investigation the author concluded that it is possible to predict the behavior of any self-operated hydraulic ram, provided that the four main characteristics - such as drive pipe head loss factor, waste valve head loss factor, the drag coefficient of the waste valve, and head-loss during the period of retardation, are determined separately by experiment. It is clear that Krol went further than previous investigators and come up with theoretical expressions for the quantity of water delivered and wasted, efficiency and power. In addition he concluded that efficiency is not the only important operating criterion.

C. Verspuy and A. S. Tijsseling in 1993, presented a simple mathematical model describing the operation of a hydraulic ram. The model results were compared with measurements. That simplified model gave a fair concurrence. The hydraulic ram was modeled as an instantaneous opening and closing of two massless valves and it was analyzed by taking into account the pressure waves occurring in the drive pipe [27].

L.C. Rennie and E.A. Bunt investigate the retardation period more fully than in any prior known works by subdividing the cycle into four main periods. In this work, it was determined that it is better to start by analyzing the delivery period with valves having zero inertia and putting infinitely close to each other [23]. In the case of the idealized valve gear, the solution for the delivery period was an exact solution of the not-simplified mathematical model. The authors designed an experimental investigation to confirm the theoretical analysis and compare the results.

In the Raseta pump, containing 4 springs within the waste and delivery valves, [28], has ballooned in place of the air chamber. The model of the pump was developed and coded MatLab. The results show the parameter that influences the quantity of pumped and lost water and efficiency was similar to those of the former researches conducted on the hydraulic ram pumps.

In 1999, a numerical model for the analysis of wave in hydraulic ram was developed, modeling all components - including the air chamber and the delivery pipe [4]. The model accounts for all possible states of flow in the ram. The numerical model was validated against the experimental data obtained from various test setups. There were variations between numerical and experimental tests while a noteworthy agreement registered when validating the analytical approach [4].

One limitation for researchers was the difficulty of examining the performance of a higher output hydraulic ram pump and becoming more and more complex [25], [29]. By taking into consideration the comparative advantage of computational fluid dynamics (CFD) over experimental and analytical approaches, P. B. Shende et al., on their study used computational fluid dynamics (CFD) to analysis the existing model and enhanced one. Although both experimental and numerical approaches have been reported to the understanding of flow interactions that occur in a hydram, the research showed CFD techniques are very useful tools for the design and analysis of hydraulic ram pump [29].

Based on different researches and their report, the performance of a hydraulic ram pump system dominantly affected by the waste valve design parameters such as valve orifice and disc diameter, valve mass, and valve stroke [1], [7]. Thus procedures were proposed in determining waste valve diameter and stroke and simple formula for estimating optimal mass that can deliver the best performance [1]. The author states that "the optimal diameter of the valve orifice is 0.68 times the pump body diameter, or about 1.35 times the drive pipe diameter if the pump body diameter is twice the diameter of the drive pipe. In addition, the optimal valve stroke can be approximated about one-third thousand (0.00033) of the headwater source."

M. N. Harith et al. tried to modify the hydraulic ram pump by making a threaded waste valve system to control the opening and closing of the valve and conduct simulation to justify the improved design [10]. The result revealed that the water loss at the waste valve reducing about 20-30% compared to the existing design. The paper reported by B. W. Young, show how a ram pump system may be designed through the application of two simple formulas together with empirical factors dependent upon ram size, delivery head, material and wall thickness of the drive pipe and relative position of impulse valve [24].

Three main phases such as the acceleration, delivery, and recoil of a ram pump cycle have been modeled using equations of manageable simplicity giving stress on the application of algebraic modeling to solve common problems of system design and tuning [17]. M. Basfeld and E. A. Müller prepared a simplified theory from Newton's equations of motion, taking into consideration of different loss factors and boundary conditions [30]. Results obtained from this theory compared with measurements found from the experiment as a function of various parameters and the agreement was good.

S. B. Watt [6], provides brief information for field workers on the design and construction of a simple ram pump from commercial pipefittings, selection of a suitable site for the ram, installation, and adjustments and maintenance requirements of the pump throughout its lifetime. Also, the manual also describes in detail the range of operation of ram pumps and the different materials that have been used to build them. Between 1985 and 1997, a series of projects were designed and tested, named S1, S2, P90, etc. [7]

1.3.2 Experimental Work

The principles involved in the hydraulic machine were understood intuitively, designed, and built by J. Whitehurst in 1772. Report of early years of the hydraulic ram by H.W. Dickinson describes, the first constructed ram raised water somewhat above its source with supply head of 4.88m through drive pipe length of nearly 182.88m and 0.038m diameter. The great achievement made by him was putting an air chamber between the draw-off cock and delivery main [25].

The other ram which was built in 1913 was actuated by the opening and shutting of a cock supplied from a reservoir of around 6.1m above the ram level [25]. The self-acting apparatus that we use today, consisting of valves of different construction instead of using cocks, is the invention and modification by J.D Montgolfier. J.D Montigolfier constructed a hydraulic ram in the garden of his house in Paris with an artificial fall of 2.3m for the expenditure of 315 liters of water 30 liters were raised 15.24m to the top of the house, with an efficiency of 64% [25]. He experienced troublesome in building up large hydrams due to the absorption of air in the air vessel and then he got over it by introducing sniffling valves close up to the air vessel.

Gosline and O'Brien carried out an interesting study with emphasis on the retardation period. In their experiments the researchers used 25.4mm commercial hydram with a rigid waste valve and the air chamber was charged by a compressor [3]. The authors concluded that with basic hydraulic constants, the complete operating characteristics of the ram could be predicted with less than 15% error [3], [22].

An investigator, Richards, experimented with commercial hydram for five years concluded that the major energy losses in the ram come from pipe friction, resistance in the delivery valve, and vibration of the pressure wave [3]. We can deduce that from his finding as a result of such losses, the performance of hydraulic ram will diminish. Richards recommends that to reduce the losses the waste valve weight should be adjusted about the supply head and valve stroke. From experimental investigation, Anderson ends up with better pump efficiency was obtained with light waste valves except for few scenarios [3].

In another case, E. J. Schiller and P. O. Kahangire tested five different hydrams to understand hydram operating characteristics and identify the major factors in its design and installation. An improved locally produced pump was tested and its operating characteristics were identified and compared with to that of other hydrams. A simple theoretical model was developed and tested against experimental data of the tested models. It was shown that the new, simple model was superior to the existing models, but less accurate than the more detailed one [3].

Utahara carried out an experimental study of the pressure variations on various components of hydram with respect to waste valve movement and noted that when the delivery head is low, pressure in the air chamber has a significant effect on the hydram system. But his result does not agree with the earlier results of Gosline and O'Brien and Lansford and Wallace [3].

H.W. Iverson attempted to identify the features of the ram, by reducing the variables to simple dimensionless ratios from which the ram performance can be identified [31]. Comparisons of the analysis with the experimental results provide a numerical correlation of the heads and flows. The performance of the ram was analyzed by considering only the time-dependent effects caused by the average drive head and the average discharge head. The result of the analysis was compared with O'Brien and Gosline [26] test reports. It shows that the ram head versus discharge data is very well

predicted by this approximate analysis. However, prediction of the ram efficiency and cyclic frequency versus discharge data was less accurate, despite a general agreement in the trends.

L.C. Rennie and E.A. Bunt's experimental research used Black's hydram by interposing various modifications to this ram. The result shows that the performance can be predicted with complementary relationships and reasonable accuracy having only the physical dimensions of the ram installation, the waste valve lift coefficient, and static friction, and various hydraulic loss coefficients [23].

X. Guo *et al.*, develop a method for optimal design and performance analysis with numerical simulation to shorten the number of prototypes and the physical experiment was presented. They develop high-performance products [7]. The proposed evaluation indexes include the head loss coefficient, drag coefficient, the eccentric distance of pressure, and velocity distribution uniformity. Two types of structures, named front-enlargement and back-enlargement, were initially designed. According to the numerical simulation, the back-enlargement design has a lower head loss coefficient and drag coefficient, a larger eccentric distance of pressure and higher velocity distribution uniformity and was adopted in the novel hydraulic ram pump [2], [7]. Experiments were carried out for the delivery heads of 2.0m and 2.7m and comparisons were conducted with other products. The results show that, when the delivery head is less than 50 m, the efficiency of the new product ranges from 50% to 70% while the delivery flow is the largest. Another researcher fabricated a hydraulic ram pump with standard components and achieved an efficiency of 57.3% [7]

The quiet ram pump patented by Green in 1898 worked with supply heads as low as 30 cm works very well [15]. D. F. Maratos states that the use of parabolic focusing tends to increase the wave height up to 3 times.

D. Sarma et al. investigates the effect of the waste valve and pressure chamber height on the output flow rate and to optimize them for the hydram. The author found that the height of the waste valve and pressure chamber have a significant effect on the discharge of the pump and correlation recorded data is provided with a curve fit below [32].

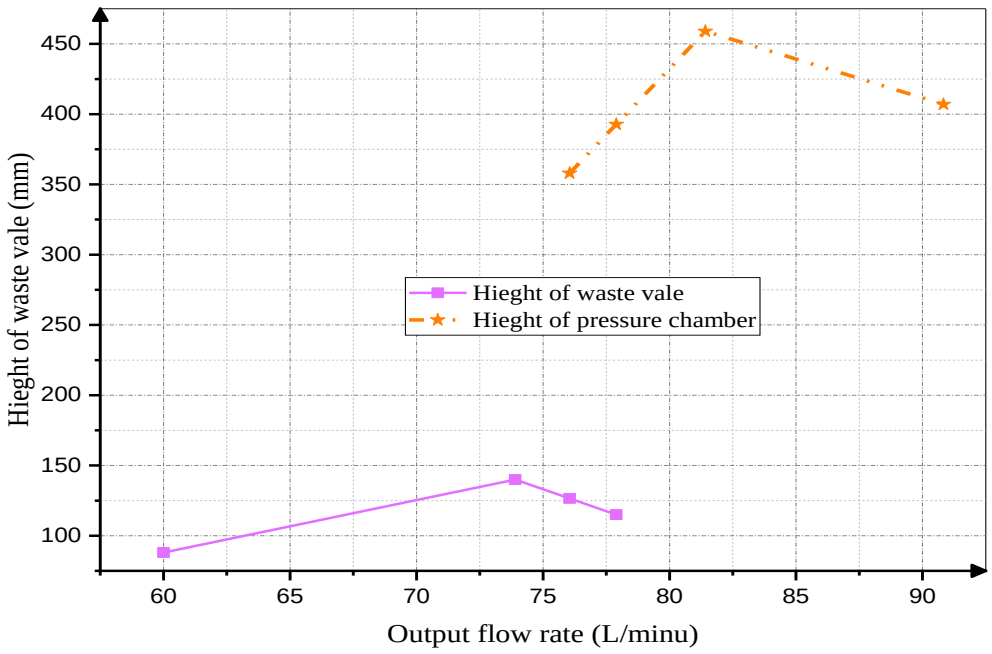

Figure 1.3 Effects of the height of the waste valve and height of the pressure chamber on the output flow [27]

A series of experiments were conducted on hydraulic ram pump showed that geometric parameters and material properties affect its operating efficiency. The researchers reported that impulse and delivery valve displacements were observed utilizing high-speed processing camera video recordings showing a good agreement with theoretical modeling proposed by J. Krol [8]. The impulse valve friction coefficient was driven by processing a set of video records and its effect is pronounced when the valve is almost closed [33].

Experiments were also conducted to come up with the optimum size of the hydram pump by varying the supply heads, delivery heads, and stroke frequency of the waste valve. Although the performance of the hydram is dependent on the drive head, optimum weights for the maximum discharge were noted at the maximum frequency. Besides the use of recycled aluminum was said to suppress noise [34].

One of the most recent researches [35] claims that conventional studies have not described the hydraulic ram pump performance in terms of head and flow rate. According to this report, former researches focused on understanding the basic hydrodynamic characteristics of water hammer pumps

and on experimentally investigating how the characters were affected by the inner diameter of the dive and lift pipes and inclination of the drive pipe. The researchers studied the effect of the air volume in the air chamber, giving little attention yet, to what affects the hydrodynamic feature and the operating condition of the pump [35]. The main finding of the investigation was:

- The pump efficiency generally increases as the volume of air in the air chamber rises.
- The peak pressures in the valve and air chamber vary depending on the pump head.
- The effect of air volume in the air chamber on the pressure holding time during pumping operation in the valve is more significant at lower heads.

Another article evaluates models to examine energy and power change of the hydraulic ram pump. The results indicate that mountainous area has the potential to generate mechanical energy to be converted to electricity from water hammer [36].

1.3.3 Originality

A few modifications to the original simple 2-valve design have been proposed, K. Yang [2] suggests a novel design for the hydram shell cancels the inlet diffuser a necessary component in the traditional hydram and incorporates a short cambered diffuser in between the elbow and the waste valve. Because of this modification, the novel design becomes more compact in structure, lighter in weight (decreased by 29.3%), and less in composite resistance coefficient. With a supply head of 2 m to 2.2m and the waste flow (Q) of 3.8 l/s to 2 l/s, the results of this novel design provided a delivery head (h) increase ranging from 5.6m to 101.1m in efficiency ranges of 63.9% to 29.6%. The maximum efficiency of 63.86% matches a delivery head of 15.51m and a supply head of 2.03m.

International Development Research Centre (IDRC), 1986 [18], emphasizes the need to conduct more research on the technical, social, and economic potential of hydrams. Due to the increased interest in renewable energy technology, there are some centers where the hydram pump has attracted modest interest in research has three main areas of research focus suggested by IDRC include:

i. Existing hydram designs, with a goal of affordability to make them accessible in developing countries. Economic evaluations were mentioned as necessary to increase

accessibility and to determine true hydram costs, spread over the lifetime of the equipment.

ii. Design, manufacturing and field-testing of models

iii. Incorporating a computerized hydram model to develop and produce efficiency hydrams. This would enable rapid comparisons to be made of existing hydrants. It would also be a useful tool in future design modifications.

In another simplified approach, B. W. Young [37], assumes constant friction loss in the drive pipe during acceleration and concentrates on a scenario with back-flow towards the supply tank at which the optimum pump performance occurs. The paper proposes the use of four conservative design formulae. In general, this paper focuses on optimum system operation by following a conservative design assumption for the critical velocity in the drive pipe and the effect of system losses.

W. M. Lansford and W.G. Dugan [26] conducted a rational mathematical analysis of the operation of a single-acting automatic hydraulic ram and compared the results of their model analysis with those found from the experimental investigation. The objective of their analysis was to determine the rate of pumping i.e., reduction of wastage for varying conditions of operation, having previously obtained the physical dimensions and the experimental constants of the apparatus for the noted operation conditions. Their results show that the effects of elasticity of the resilient waste valve disc were often more marked than the effects of the elasticity of the water.

X. Guo et al., [7], introduced a method for the optimal design and performance analysis of a hydraulic ram pump system with numerical simulation and physical experiment, with the intent to improve the performance of the pump. Experiments were carried out for the delivery heads of 2.0 m and 2.7 m and comparisons were conducted with other design alternatives. The results show that, when the delivery head is less than 50 m, the efficiency of their product ranges from 50% to 70% while the delivery flow is the largest.

B. W Young [24], offers a cogent design procedure, which is derived from theoretical and empirical considerations, that enables all relevant system parameters to be determined for the design process. The procedure was tested against existing and new experimental results.

A new type of hydraulic ram pump called Raseta pump A. Rajaonison [28], carries improvements over the traditional pump in that it has a spring on each of the waste and delivery valves. Besides, a balloon with four springs replaces the usual air chamber. Based on the report of this paper the behavior of Raseta pump equipped with a system of springs was studied theoretically. The prominent parameters are nearly the same as those found in previous works. However, under this investigation stiffness of the spring in the waste valve, modulus of elasticity, and waste valve disk radius were found as critical parameters for optimum operations of the device. No techno-economic investigation conducted.

All the authors listed above proposed a design variation of the hydram by combining with different features and conducting research on the improvement of optimum system operation, structural modification, and limited numerical simulation for optimum design. Some recommend topics for future research on the technical, social, and economic potential of hydrams. Besides, robust mathematical modeling of the operation of single-acting automatic hydraulic ram has been developed for an existing hydraulic ram pump. To put it this in perspective the development of the device since its invention followed improvements in mechanical design and research into the principle of its operation [12]. In its design improvement, successes were noted in obtaining a variation of the ram owing to distinctive make-ups such as [8], [15], [25]:

- Regular ram pump combined with a siphon
- Regular ram pump combined with a suction pump
- Mimicking of the air compressor in the cylinder
- Fitting of the mechanically operated waste valve
- Design without a valve or hydro-pulsator, and
- Design for use of tidal power.

In this work, "**Solar Assisted Hydraulic Ram Pump**" a novel approach, will be addressed that has not been addressed yet. Its distinct feature is the air chamber will be heated locally with solar energy. The induced **solar energy** can increase the temperature of the gas and evaporate a fraction of water at the **air-water boundary.** This phenomena can increase the pressure in the chamber corresponding with increase of temperature and formation of vapor. Together the hammer and variation of

temperature result increase of pumping elevation. The focus of this work is analyzing and interpreting of variation of temperature on water hammer pressure.

1.4 Objectives

The general objective of this research is to design and build hydram from affordable, locally available pipe fitting components without greatly affecting its functionality, durability, and experimentally test as a thermally assisted device.

The specific objectives are:

- Development of mathematical modeling for water hammer and designing regular ram pump and supper imposing water hammer effect with thermal signature.
- A test-bed for the hydraulic ram pump will be constructed from locally available pipe fitting components.
- Thermal simulation with ANSYS Fluent for combined water hammer and thermal effect
- Experimentally test the hydram by heating the chamber with electrical energy correlating the equivalent solar radiation of Addis Ababa.

1.5 Significance of the Study

Droughts occur frequently in Ethiopia. If properly managed, surface and groundwater are sufficient to meet most domestic and irrigation needs of the country to lessen the damages of drought. Nevertheless, the lack of installed water infrastructure imposes a serious constraint on domestic usage and irrigation development [20]. As stated above the construction of hydram is quite simple and affordable. The main parts and components of the system are available in market. It can be useful and transformational for rural parts of the country where no power is available for pumping. The use of solar-assisted technologies for residence and irrigation pumps to enhance farming productivity, enables saving from fuel costs for diesel irrigation pumps and offsetting carbon emissions.

This mature technology has found multiple applications across the world, before the advent of fossil fuels. Nonetheless, the discovery was suppressed by power-driven pumps. With sufficient research,

we believe the role of the hydram can be revitalized again, boosting the water supply for drinking and irrigation. By doing so the electric power cost rising from fossil fuel can be saved.

Some works indicate that the operating principles behind hydraulic rams can be adopted to provide energy by substituting the pressurized water delivery system for an energy conversion mechanism [11]. The combination of analytical and experimental models examine the energy balance and power production of the hydraulic ram pump. The results indicate that mountainous area has the potential to generate mechanical energy to be converted to electricity from water hammer [36]. The superposition of water hammer with solar energy may create harvestable energy for electricity, despite the idea requires much more research.

The research can be considered an important step towards improving the performance of a hydraulic ram pump by adopting structural modifications towards promoting green energy resources.

Governing Equations

1.6 Pressure, Velocity and Time History

With the rapid action of opening and closing of valves pressure fluctuations produce compression wave and superimposed velocity changes with propagation at the sonic velocity. If all effects are considered the detailed analysis becomes more complex. Thus an approximate analysis may be made by assuming that pressure and velocity fluctuation produce an average effect [31].

Theoretically, the water in the drive pipe accelerates according to [8], [38]

$$H-\left(1+\sum h_L+f\frac{L}{D}+R(s)\right)\frac{V^2}{2g}=\frac{L}{g}\frac{dV}{dt} \tag{0.1}$$

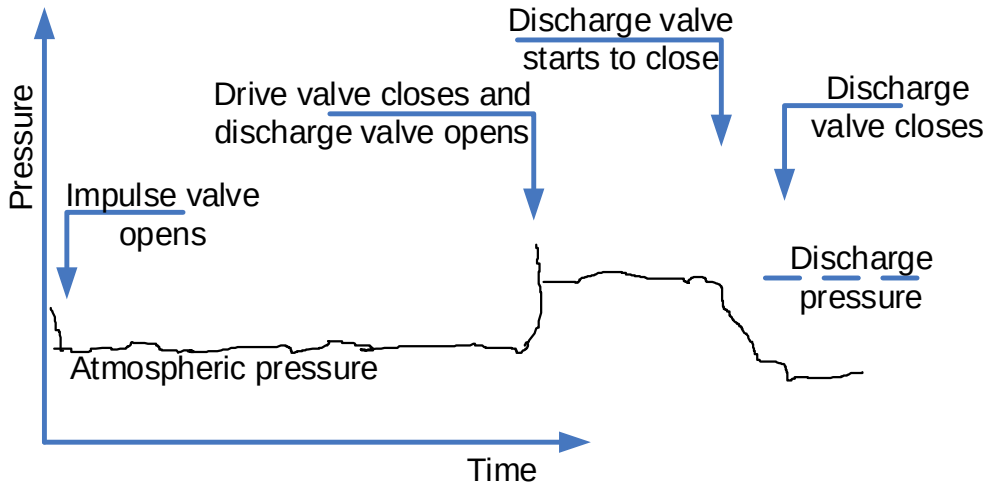

Figure 0.1 Typical measured pressure-time history before the drive valve closed [32]

In the drive pipe, the velocity of water is reduced in proportion to the pressure head ($h+h_r$) generated from the static supply head, H. According to the water hammer theory for an instantaneous valve closure in an elastic pipe, the one-dimensional wave equation to explain observed water hammer effects was made by Joukowski in 1898 [39]. Joukowski correctly predicted the maximum line

pressures and disturbance propagation in a water distribution system in which sudden valve closures occurred. Joukowski equation is expressed as:

$$\Delta P = -\rho c \Delta V \tag{0.2}$$

The change in pressure head in the drive pipe due to water hammer can also be written as [8], [18], [38]

$$\Delta h = -\Delta V \frac{c}{g} \tag{0.3}$$

The speed of an acoustic wave or wave celerity c, in an elastic medium, is given by

$$c = \sqrt{\frac{K_c}{\rho}} \tag{0.4}$$

According to Joukowski suggestion [3], the composite modules of elasticity of water and pipe material is given by

$$K_c = \frac{1}{\left(\frac{1}{K} + \frac{D}{Et_p}\right)} \tag{0.5}$$

In actual practice steel, wrought iron and cast iron are materials most commonly used for ram construction [8]. Besides, if other qualifications are the same, the material of the drive pipe and its radius to thickness ratio affects the performance of the ram.

1.6.1 Drive Pipe

Since the drive pipe is the necessary component of pumping action it should be treated carefully. The range of length to diameter ratio $\frac{L}{D}$ for good hydram operation is given by [3],

$$150 \le \frac{L}{D} \le 1000 \tag{0.6}$$

Again, the drive pipe length needs to be in between the ranges of

$$6H \le L \le 12H \tag{0.7}$$

The Russians researcher [3], developed an empirical relationship for drive pipe length of the form,

$$L = [\frac{900}{N^2}][\frac{H}{D}] \tag{0.8}$$

1.6.2 Velocity in the Drive Pipe

The theoretical maximum steady flow velocity V_{max} in the drive pipe is

$$V_{\max} = \sqrt{2gH} \tag{0.9}$$

Due to losses from pipe friction, resistance in the delivery pipe and concussion (shock) of the high-pressure wave, the maximum theoretical velocity never achieved.

Bergeron in 1928 concluded that better pump efficiency was obtained with low velocities in the drive pipe during waste valve closure. i.e., [40]

$$V_o \le 0.4\sqrt{2gH} \tag{0.10}$$

The velocity ratio from Bergeron's relation:

$$m' = \frac{V_o}{\sqrt{2gH}} \tag{0.11}$$

Rankine efficiency of hydram is expressed as

$$\eta(Rankine) = \frac{qh}{QH} \tag{0.12}$$

1.7 Experimental Loss Factors

The resistance of experimental apparatus [8] that are essential to compare theory with experiments under any stated conditions of the operation for the automatic hydraulic ram pump is presented in a condensed form as follows.

1. Loss of head in the drive pipe such as loss due to velocity head, loss due to bends, elbows, change of cross-section and friction inside the drive pipe.
2. Head loss due to waste valve turbulence
3. Drag force coefficient of the waste valve
4. Head loss during the period of retardation

Mathematical Modeling

1.8 Methodology

This study was conducted by reviewing the scientific literature followed by analytical calculation and CFD simulation. Then it was tested experimentally with the thermal energy. The solar insolation of Addis Ababa will be investigated for the thermal effect simulation. This is because the traditional irrigation based farming is the main source of vegetables for the market of Addis Ababa. However, for the experimental test, the solar radiation will be mapped to an equivalent electrical heat source. Also, the numerical simulation will be carried out to validate the mathematical modeling and the experiment.

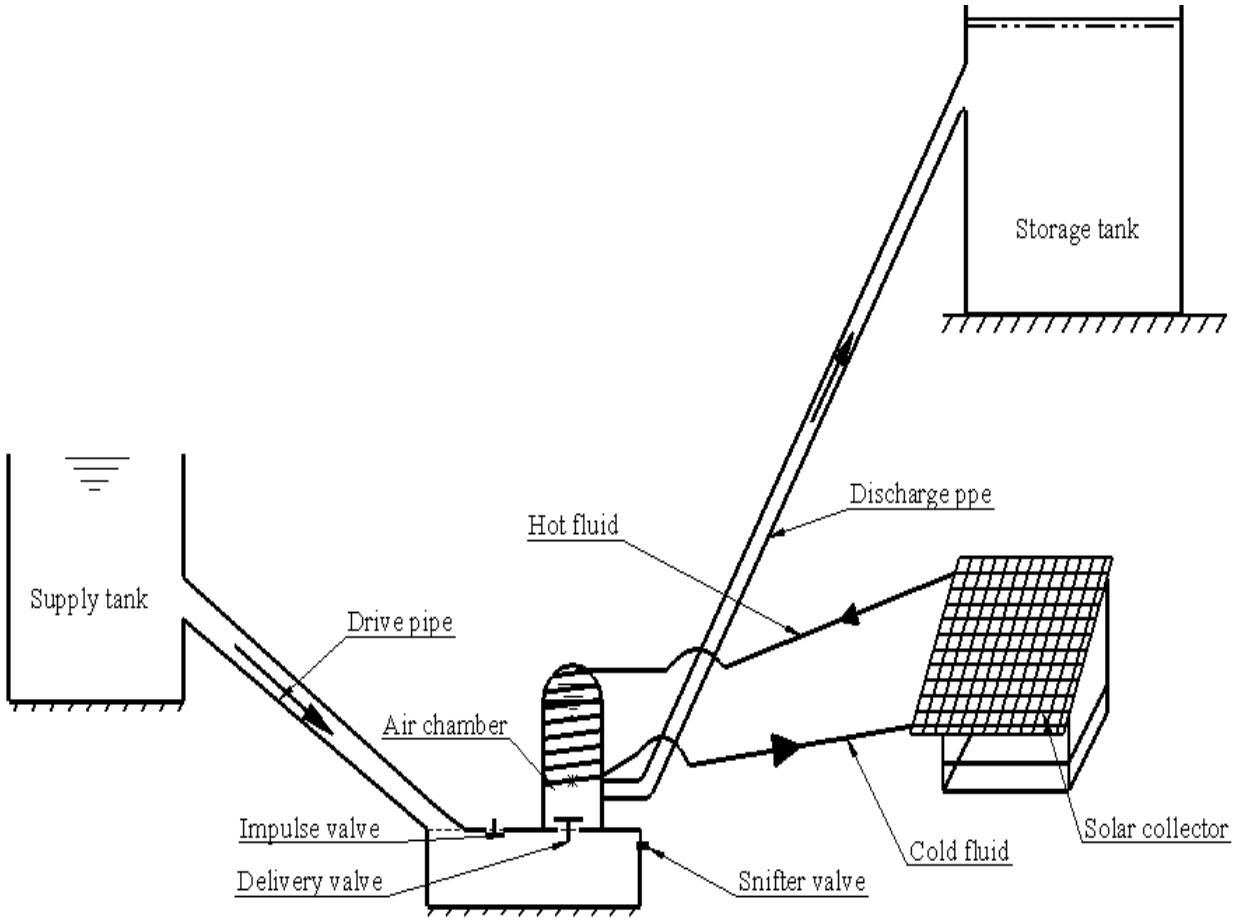

Figure 0.1 Simple schematic diagram of solar-assisted hydram

The main activities of this research work are described in the flow diagram given in the next page.

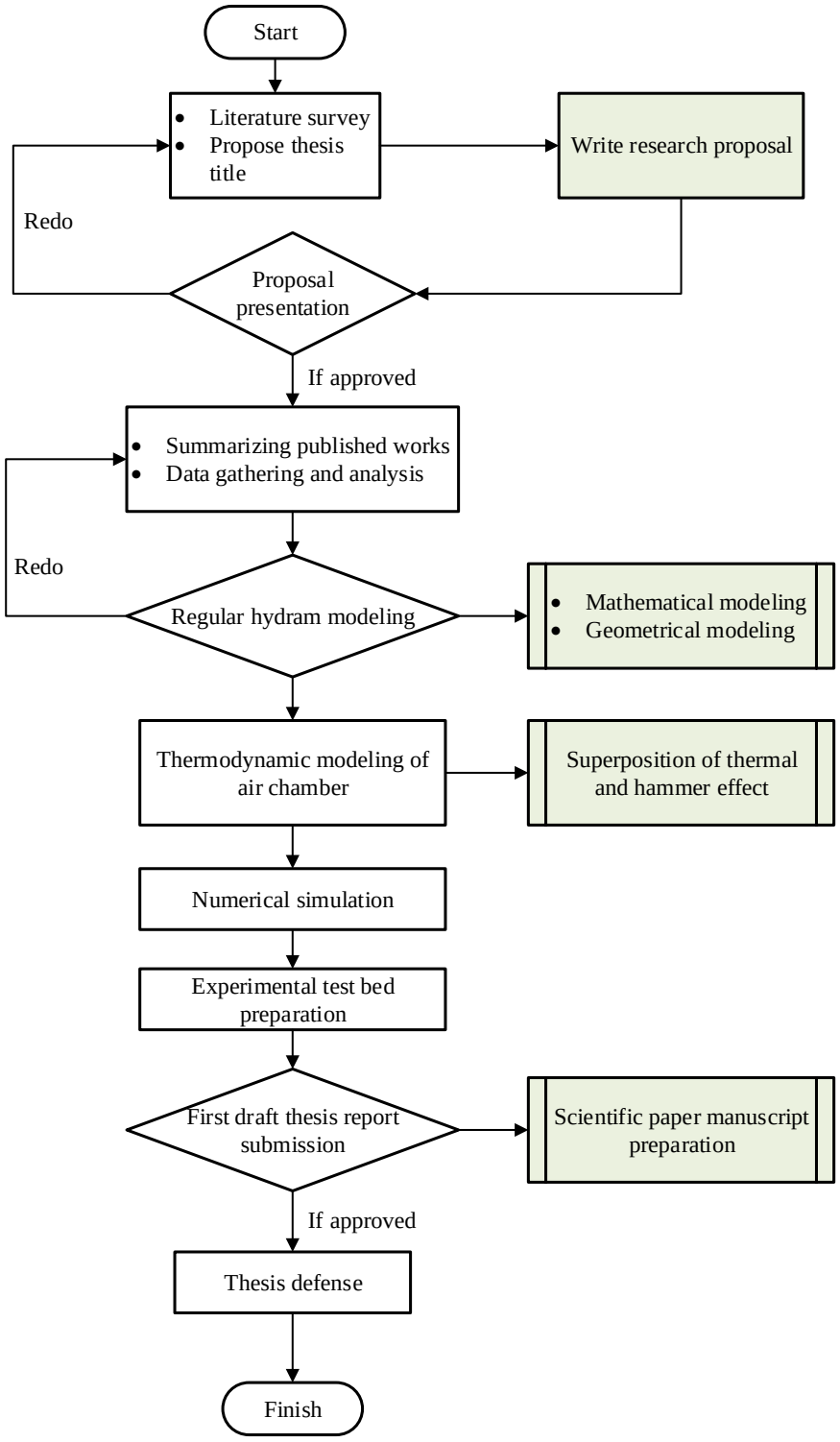

Figure 0.2 Methodology and progressive steps of research work

The construction of the pump was from PVC-pipes and necessary fittings. A swing check valve will be used as an impulse valve oriented in the reverse direction so that the clap is initially open due to its weight and is pushed to close by the moving water column. Teflon tape is used as a sealing component for the threads of pipes and fittings.

The air chamber was constructed from copper. However, using copper as a pressure chamber limits the applied temperature around the chamber up to 150 ^{o}C. At the top of the inverted bottle made from copper plate **resistor of the electrical heater** winded around it.

A detailed description of the theory of hydraulic ram pump presented by some researchers results in many complex equations and some of them are too complex for practical applications [8], [26]. The mathematical model used in this regular hydram analysis is adopted from E. J. Schiller and P. O. Kahangire [3]. This model is practical less complex than J. Krol's [8] but more comprehenssive than H. W. Iversen's [31] which is rather oversimplified.

The following are assumed as the base case study of a hydraulic ram pump.

- The cycle of pump operation is sub-divided into four periods, given in Figure 2.1 (a), depending on waste valve position and time-velocity variation in the drive pipe such as:
    1. The waste valve is fully open and water flows through the waste valve until the critical velocity is attained and the impulse valve starts to close
    2. The waste valve starts to close and continues until fully closed
    3. The waste valve remains closed and the delivery valve opens so that pumping takes place, and
    4. The delivery valve closes, recoil takes place, impulse valve opens and pressure in the drive pipe drops to static supply pressure.
- The friction losses factors during the acceleration and discharge (pumping) periods are determined from manufacturer catalog and material properties
- Water flowing to waste before the valve begins to close is regarded as the useful drive power for hydram operation.
- The friction losses in the drive pipe are included in the analysis of the pumping period together with friction losses through the delivery valve.

1.9 Sizing the Ram

1.9.1 Design Specification

An elementary ram pump constructed from commercial pipe fittings requires a source flow of at least 5 liters every minute [6]. Since most rivers in Ethiopia can supply the minimum source flow for smaller hydrams and those fittings are available from the market, therefore the following specifications are selected.

- The diameter of the drive pipe, $D = 0.027m$
- Supply head, $H = 2m$

1.9.2 Drive Pipe Length

From Eq. (2.6), the minimum and maximum length of the drive pipe with 0.027m nominal diameter lies in the range of 4.05 and 27m. The design length of the drive pipe is selected as 5m.

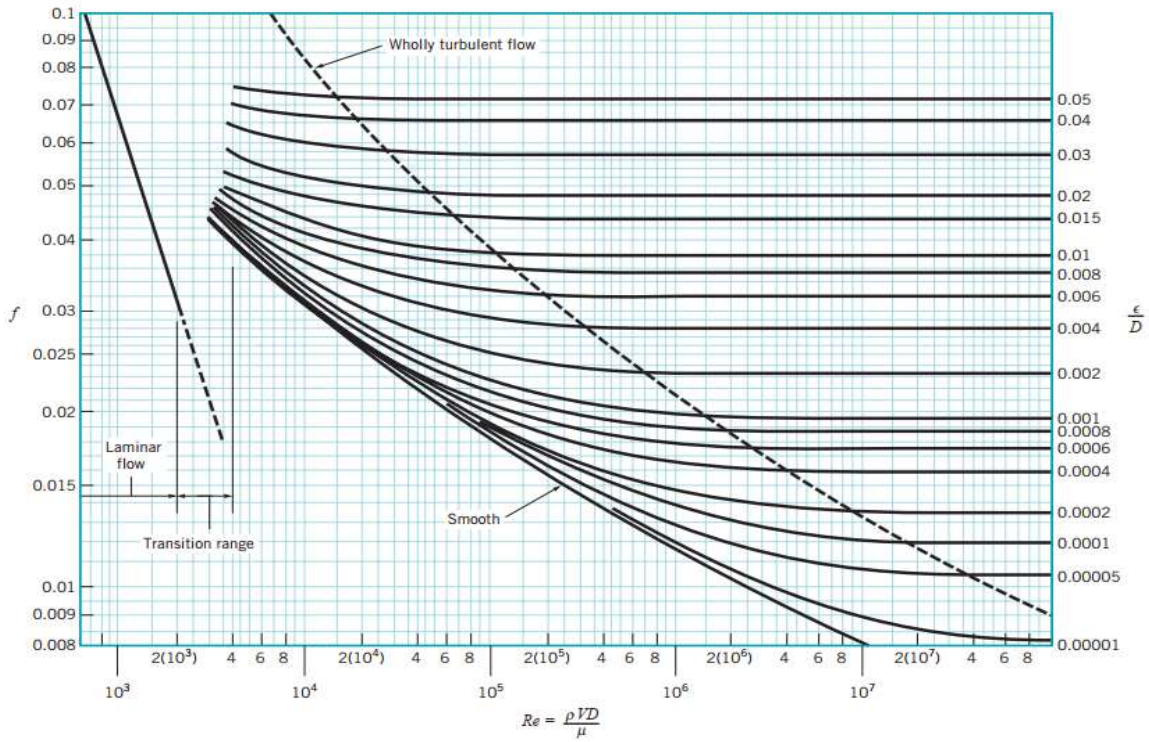

Figure 0.3 Friction factor and relative roughness for round pipes – the Moody chart [41]

Theoretically, the water in the drive pipe accelerates according to the Eq.(3.1)

$$H-\left(1+\sum K_L+f\frac{L}{D}+R(s)\right)\frac{V^2}{2g}=\frac{L}{g}\frac{dV}{dt} \tag{0.1}$$

Substituting head loss factors in drive pipe and impulse (waste) valve by M to the above equation then it simplifies:

$$H-M\frac{V^2}{2g}=\frac{L}{g}\frac{dV}{dt} \tag{0.2}$$

Where

$$M=\left(1+\sum K_L+f\frac{L}{D}+R(s)\right) \tag{0.3}$$

From the above Eq.(3.3) 1 refers to loss due to velocity head.

The water continues to accelerate until it reaches a critical velocity at which the impulse valve begins to close. The closing characteristics of the swing check valve were studied and it is reported as 0.61m/s and at this velocity closing effect of a swing check valve is sever [42]. The minimum valve closing velocity is assumed $V_o=0.61 m/s$ as described in Appendix A-3.

To characterize the flow in the drive pipe, Reynold's number is determined first.

$$\mathrm{Re}=\frac{\rho V_o D}{\mu} \tag{0.4}$$

$$\mathrm{Re}=\frac{1000\times 0.61\times 0.027}{10^{-3}}=16,470$$

From the Moody chart given before the friction factor of the smooth drive plastic pipe (PVC) is $f=0.026$. Applying Eq. (3.3) friction head loss factor due to the drive pipe and fittings

$$M = \left(1 + \sum K_L + f\frac{L}{D} + R(s)\right)$$

$$M = \left(1 + (1 + 0.15 + 0.7 + 0.9 + 3 \times 0.08) + 0.026 \times \frac{5}{0.03} + 2\right) = 10.49$$

1.9.3 Swing Check Valve as an Impulse (Waste) Valve

A swing check valve consists of a circular disk that dances about a pivot point beyond the boundary of the disk. The amount that the disk swings depend upon the upstream flow rate [43]. The characteristics of the waste valve (swing check valve) are affected by parameters such as the orifice diameter of valve sitting, the diameter of the valve disc, the stroke length, and the weight of the valve as well as the discharge and head of water supply to drive the hydraulic ram pump [44].

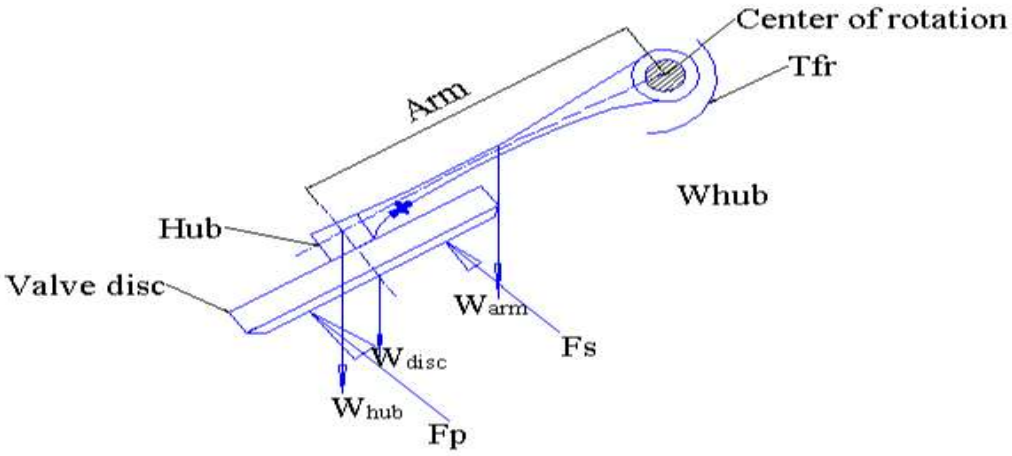

Figure 0.4 Force diagram for the swing check valve

The minimum valve closing velocity for different check valves are given in appendix-A: 3.

Swing check valves are preferable for this research because they are readily available, low cost, and have low head loss characteristics when fully open. The disc location contributes greatly to the closure of the valves. If the disc moves or pivots out of the flow stream when open, it will be difficult for the flow to rapidly close the valve. However, in the case of Swing Check Valves, they all have the closure member in the flow stream that will assist for rapid closure. A related geometric feature of the valve is the length of the stroke. It only makes sense that the further the disc must travel, the longer it will

take to close. Of the Swing Check Valves, the Resilient Hinge Check Valve has the shortest stroke (35 degrees) and the traditional Swing Check the longest (60 to 90 degrees) [44].

From conex|Banninger valves an IBP Group company manufacturer of a swing check valve nominal size of 1 inch, nominal diameter of 25 mm, stroke of 59 degrees and weight of 0.64 Kg is given attention in the modeling.

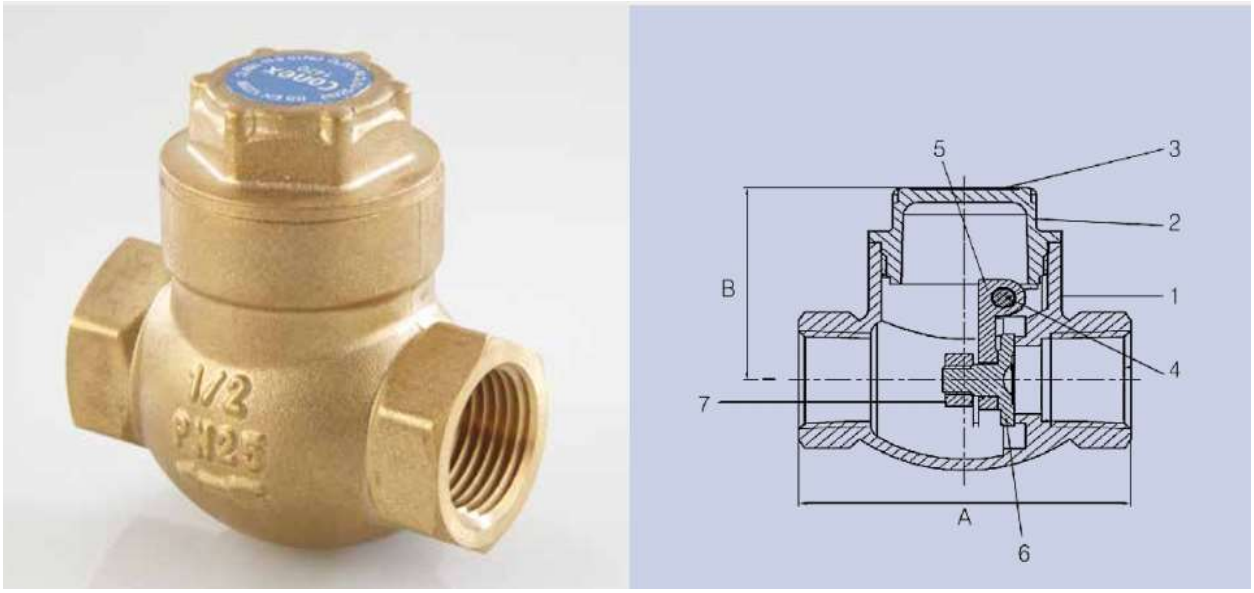

Figure 0.5 Swing check valve

The manufacturer characteristic of a swing check valve is given in Appendix A-4.

1.10 Analysis of the Ram Pump Cycle

1.10.1 Period 1

The maximum possible theoretical velocity achieved from a 2 meter source tank is $6.26\,{}^{m}\!/_{s}$ estimated by applying Eq. (2.9).

Putting $\frac{dV}{dt}=0$ and evaluating Eq. (3.2) provides a steady-state velocity for the accelerating water.

$$V_s = \sqrt{\frac{2gH}{M}} \tag{0.5}$$

The steady state velocity is $1.93 \, m/s$.

If the valve does not close until steady-state velocity reaches, the impulse valve will not close at all and the waste becomes infinity. Therefore, it follows that the velocity ratio should less than unity.

$$m = \frac{V_o}{V_s} = \frac{V_1}{V_s} \leq 1 \tag{0.6}$$

The ratio of valve closing velocity and steady-state velocity, $m = 0.313 \leq 1$ satisfy the condition stated above in Eq. (3.6).

Now integrating the governing equation of flow within the drive pipe in the limits of $V = 0$ to $V_1 = V_0 = 0.61 \, m/s$ the duration of the first cycle will be

$$\int_0^{t_1} dt = 2L \int_0^{V_1} \frac{dV}{\left(2gH - MV^2\right)} \tag{0.7}$$

$$t_1 = \left(\frac{L^2}{2gHM} \right)^{0.5} \ln \left[\frac{\sqrt{V_s} + V_1}{\sqrt{V_s} - V_1} \right] \tag{0.8}$$

$$t_1 = \left(\frac{5^2}{2 \times 9.81 \times 2 \times 10.49} \right)^{0.5} \ln \left[\frac{\sqrt{1.93} + 0.61}{\sqrt{1.93} - 0.61} \right] = 0.232 \, \text{sec}.$$

The elapsed time to complete the first period is 0.232sec.

The **volume of water**, flowing to waste during period 1 is derived by integrating the product of the area of drive pipe, velocity and time.

$$\overline{V} = \int_0^{t_1} AVdt = 2L\int_0^{V_1} \frac{dV}{\left(2gH - MV^2\right)} \tag{0.9}$$

The integration of Eq.(3.9) provides the following equation.

$$\overline{V_1} = \frac{LA}{M}\left[\ln\left(\frac{1}{1-\frac{V_1^2}{V_s^2}}\right)\right] \tag{0.10}$$

$$\overline{V_1} = \frac{5\times\pi\times 0.027^2}{10.49\times 4}\left[\ln\left(\frac{1}{1-\frac{0.61^2}{1.93^2}}\right)\right] = 2.873\times 10^{-5} m^3$$

The quantity of water wasted during period 1 is considered a useful drive power for the hydram.

1.10.2 Period 2

Period 2 is separated from period 1 because it is assumed that the quantity of water escaping after the valves start to close is wasted and the energy is also wasted. The force and torque acting on the underside of the impulse valve are greater than the weight and torque due to the weight of the disc, the velocity of water is now leading to the closing of the valve. The impulse valve begins to close and is completely closed at the end of the period. Details of the analysis are complicated since by the fact that both water and the impulse valve are in motion.

Because of the short duration of the time, it is certain that this velocity does not vary greatly from its initial value and for all practical purposes, it can be assumed that $V_1 = V_2$. Many pieces of evidence supported that the maximum velocity V_m significantly does not differ from V_1. Since V_1 is assumed as the same with the maximum velocity there is no acceleration during this period. The duration of period 2 is estimated by assuming an instantaneous valve closure

$$t_2 = \frac{2L}{c} \tag{0.11}$$

Where c is wave celerity is given by Eq. (2.4)

The bulk modulus of water at atmospheric pressure is 2.2 x 10^9 Pa and Young's modulus of PVC rigid pipe is 2.4 x 10^9 Pa. Composite modules of elasticity of water and pipe material from Eq.(2.5)

$$K_c = \frac{1}{\left(\frac{1}{2.2\times10^9} + \frac{0.027}{2.4\times10^9 \times 0.0024}\right)} = 1.94\times10^8$$

The wave celerity of the drive pipe can be predicted as follows.

$$c = \sqrt{\frac{1.94\times10^8}{1000}} = 441 \, m/\text{sec}$$

Duration of period 2 is now

$$t_2 = \frac{2\times5}{440.4} = 0.023\text{sec}$$

Quantity of water escaping to waste during period 2 is given by the equation

$$V_2 = AV_2t_2 \qquad (0.12)$$

$$V_2 = \frac{\pi\times0.027^2}{4}\times0.61\times0.023 = 8.03\times10^{-6} m^3$$

1.10.3 Period 3

At the end of period 2, the impulse valve is completely closed, and abrupt retardation takes place causing the delivery valve to open, whilst at the same time the velocity in the drive pipe is reduced in proportion to the pressure head ($h+h_r$) generated in excess of the static head H.

If V_3 is the maximum velocity of water in the drive pipe during period 3, then change in pressure head due to water hammer

$$\Delta h = h + h_r = -\left(V_3 - V_2\right)\frac{c}{g} \tag{0.13}$$

h is delivery head measured above the supply source

The maximum theoretical pressure that the hydram can develop is obtained when $V_3 = h_r = 0$

$$h_{\max} = V_2 \frac{c}{g} \tag{0.14}$$

$$h_{\max} = 0.61 \times \frac{441}{9.81} = 27.4m$$

This value refers the maximum pressure can be achieved from the hammer is 269 kPa.

For the drive pipe of the 27 mm nominal diameter, a 13.5 mm nominal diameter of delivery pipe is suggested [13]. Thus 18.5 mm outside diameter with a wall thickness of 2.82 mm was used for the delivery pipe. Now the head loss through the drive pipe, delivery valve, and a delivery pipe is estimated for the average maximum delivery head as follows.

$$h_r = h_{r,drive\_pipe} + h_{r,delivery\_valve} + h_{r,delivery\_pipe} \tag{0.15}$$

From the above equation head lost, h_r during the retardation period is in the drive pipe, delivery valve, and delivery pipe by considering maximum delivery head of 15 m.

$$h_r = \left[\left(1 + \sum K_L + f\frac{L}{D}\right) + R(s) + \left(1 + 0.15 + 0.08 + f\frac{h}{D}\right)\right]\frac{V_0^2}{2g} \tag{0.16}$$

$$h_r = \left(10.49 + \left(1.23 + 0.032 \times \frac{15}{0.0185}\right)\right)\frac{0.61^2}{2 \times 9.81} = 0.71m$$

This head loss value is a more conservative estimation.

From Eq.(3.13) the maximum velocity during period three is

$$V_3 = V_2 - (h + h_r)\frac{g}{c} = 0.61 - (15 - 1 + 0.71)\frac{9.81}{440.4} = 0.282\, m/s$$

Discharge continues at the rate governed by the equation

$$-h - \frac{NV^2}{2g} = \frac{L}{g}\frac{dV}{dt} \tag{0.17}$$

Where N is the total head loss factor for the drive pipe and delivery valve

$$N = 2 + \left(1.23 + f \times \frac{h}{d}\right)$$

Duration of period 3

Discharge continues until the velocity becomes zero and the delivery valve starts to close. The duration of period 3 is obtained by integrating the above equation for the limits $V = V_3 = 0$

$$\int_c^d dt = -2L\int_{V_3}^{0} \frac{dV}{\left(2gH - NV^2\right)} \tag{0.18}$$

Time integration of the above equation gives the following simplified equation.

$$t_3 = \left(\frac{2L^2}{ghN}\right)^{0.5} \tan^{-1}\left(\frac{NV_3^{\,2}}{2gh}\right)^{0.5} \tag{0.19}$$

Evaluating Eq.(3.19) by substituting all the known parameters and constants duration of period 3 is 0.011sec.

$$t_3 = \left(\frac{2\times 5^2}{9.81\times 15\times 29.2}\right)^{0.5} \tan^{-1}\left(\frac{29.2\times 0.324^2}{2\times 9.81\times 15}\right)^{0.5} = 0.011\text{sec}$$

Quantity of water discharged during period 3

The quantity of water discharged during period 3 is expressed by the following integral form of an equation.

$$\overline{V_3} = \int_{t_2}^{t_3} AVdt = \int_{V_3}^{0} \frac{AVL}{g}\left(\frac{dV}{h+\frac{NV^2}{2g}}\right) \tag{0.20}$$

Simplifying the above equation results in the following.

$$\overline{V_3} = \frac{LA}{N}\left[\ln\left(1+\frac{NV_3^2}{2gh}\right)\right] = \frac{LA}{N}\left[\ln\left(\frac{N}{M}\frac{H}{h}\frac{V_3^2}{V_s^2}+1\right)\right] \tag{0.21}$$

Pumping continuous until the kinetic energy in the drive pipe ceases and the velocity becomes zero and then pumping stops and the delivery valve closes.

1.10.4 Period 4

At this period, the delivery valve is completely closed. Near to the delivery valve the water is under the pressure head ($H + h + h_r$) while at the other end of the drive pipe the pressure is due to the static supply head, H. The pressure difference and elasticity of water and pipe material causes the water to recoil towards the supply tank [3],[8]. The recoil causes a reduction of pressure in the hydram to below atmospheric pressure causing a small quantity of air to be sucked into the hydram through the snifter valve.

The waste valve opens by the force and torque due to its own weight and results in a reduction of pressure in the hydram. The opening of the hydram is assumed instantaneous so that the pressure in the drive pipe returns to the static supply pressure and gets ready for the next cycle of operation [3]. Thus the duration of period 4 can be estimated as the time for complete reflection of an acoustic wave.

$$t_4 = \frac{2L}{c} = 0.023\text{sec}$$

Now duration of the pumping cycle is summation of time of the four periods.

$$T = t_1 + t_2 + t_3 + t_4 = 0.454 \text{ second}$$

1.10.5 Summary of Operating Characteristics

A brief summary of the operating characteristic of the pump is stated below.

1. Duration of the pumping cycle

   $T=t_1+t_2+t_3+t_4$

However, most researchers found period T is one of the most difficult parameters to determine reliably.

2. Average pumped flow per second, (Liters per second)

$$q=\frac{\cancel{V}_3}{T}\ \left[\mathrm{L}/\mathrm{min}\right]$$

3. Total wasted flow in liters per second

$$Q_w=\frac{\cancel{V}_1}{T}+\frac{\cancel{V}_2}{T}\ \left[\mathrm{Liters}/\mathrm{sec}\right]$$

4. Flow ratio

$$FR=\frac{Q}{Q_w}=\frac{\cancel{V}_3}{\cancel{V}_1+\cancel{V}_2}$$

5. Rankine pump efficiency,

$$\eta=\frac{qh}{QH}\ [\%]$$

6. Pump power,

   $P=q\gamma h$ [watt]

7. Valve beat frequency, (beats per minute)

$$n=\frac{60}{T}\ \left[\mathrm{beats}/\mathrm{minute}\right]$$

8. Total supply flow to the pump Q_s to the pump liters per second

   $Q_s=Q_w+q\ [\mathrm{L}/\mathrm{min}]$

1.11 Air Chamber Design

About the size of the air chamber, the University of Warwick United Kingdom, recommended that it should have a minimum volume of 20 times the expected delivery flow per cycle of the hydram, with 50 times the expected delivery being a better selection. A larger air chamber needs a little more time to initially start the pump [13].

For this design scenario, the average delivery flow at the pump efficiency of 60% is considered. The delivery flow per cycle at this efficiency was calculated and its value is $1.352\times10^{-5}m^3$. Now the volume of the air chamber is

$$V_{ac} = 50\times1.352\times10^{-5} = 6.76\times10^{-4}m^3$$

The pressure chamber diameter is a critical point to increase water pressure. The smaller the pressure chamber diameter, the greater the water pressure will be [45]. For size of drive pipe diameter of the air chamber is within the range of 50.8 – 76.2 mm[13]. If 76.2 mm diameter of air chamber is assumed the height will be.

$$V_{ac} = \frac{\pi D_{ac}^2}{4} h_{ac} \tag{0.22}$$

$$h_{ac} = \frac{4V_{ac}}{\pi D_{ac}^2} = \frac{4\times6.76\times10^{-4}m^3}{\pi\times(0.0762)^2 m^2} = 0.148m$$

The height of the pressure chamber is 148mm

Experiments with the larger air chamber resulted in a consistent increase of approximately 10% in the efficiency and power developed. As explained, this is due to the additional potential energy available for pumping, formed by water temporarily stored in the air chamber during the period of retardation. The additional potential energy due to the effect of the air chamber is small compared with the kinetic energy developed in the drive pipe so it is ignored in the theory [8].

If q is the quantity of water delivered during a single cycle, the duration of which is T, then the average rate of flow through the delivery pipe is the ratio of quantity of water delivered to its duration. However, the time of actual pumping much shorter than the total time T, and the air chamber receives water at a much quicker rate q/t_3. Since water is delivered at the average flow rate which is smaller than water received by the chamber, excess water temporarily stored in the air chamber during t_3 is

$$q_{ac} = q\left(1 - \frac{t_3}{T}\right) \tag{0.23}$$

q_{ac} - The Quantity of water temporarily stored in the air chamber

Temporarily stored water in the air chamber is

$$q_{ac} = 0.167\, Liter/\min ute\left(1 - \frac{0.011}{0.454}\right) = 0.163\, Liter/\min ute$$

1.12 Snifter Valve

The purpose of this valve is to supply air for the air chamber to keep the content of the air within it [46]. It is a small valve opening inwards into the body of the ram usually located just below the delivery valve.

Air Chamber Heat Transfer Analysis

As discussed in chapter 3 section 3.4, the total volume of the air chamber is $6.76\times10^{-4}m^3$. From this volume $1.63\times10^{-4}m^3$ is occupied by water each minute, which is temporarily stored in the air chamber during the period of retardation. The air will contain the rest of the air chamber volume, which is $5.13\times10^{-4}m^3$ per minute.

The average atmospheric pressure of Addis Ababa located at an altitude of 2355 m above sea level is 76.2 kPa [47] having an average ambient temperature of 17 ^{o}C. The saturation temperature of water at this pressure is 92 ^{o}C.

1.13 Basic Assumptions for Modeling

1. The chamber is insulated so heat loss to the surrounding will be minimized
2. Vapor and air are in thermodynamic equilibrium to each other all the time
3. Kinetic and potential energy are neglected
4. Presence of air does not affect the thermodynamic properties of vapor
5. Liquid phase is separated from the mixture and located at the bottom of the vessel
6. In this case, water vapor can be approximated as an ideal gas because the specific heat of an ideal gas is a lower limit for the real gas specific heat constant [48].

In this part of thermodynamics and heat transfer modeling, the focus is on getting an expanding air-vapor mixture to do useful work by enlarging and contracting the control volume, i.e., by pushing the liquid water under the pressurized air-vapor mixture.

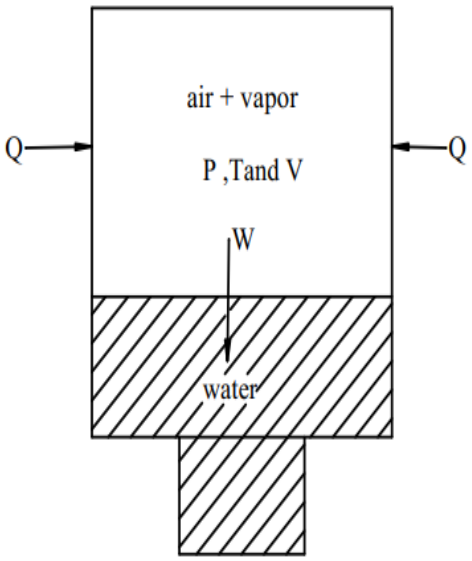

Figure 0.1 An overview of the interaction of heat and work transfer in the closed system

1.14 Conservation of mass

The mass conservation equation for the phases depicted in the picture above is stated as follows

1.14.1 Mass of air

$$d\dot{m}_a = \dot{m}_{i,a} - \dot{m}_{o,a} \tag{0.1}$$

If the mass of air leaving or entering the control volume is ignored, integrating the above equation for the cycle gives

$$\dot{m}_a = \rho_a \cdot V_a \tag{0.2}$$

1.14.2 Mass of liquid water

When no condensation happens in the process the amount of liquid water temporarily stored in the chamber is

$$d\dot{m}_{l,cv} = \dot{m}_{i,l} - \dot{m}_{o,l} - d\dot{m}_{eva} \tag{0.3}$$

1.14.3 Mass of evaporated water

The amount of water vapor coexist with air at the top of the chamber is stated as

$$d\dot{m}_{v} = \dot{m}_{i,v} - \dot{m}_{o,v} - d\dot{m}_{cond} + d\dot{m}_{eva} \tag{0.4}$$

No steam is entering or leaving the control mass and condensation has not occurred.

$$d\dot{m}_{v} = d\dot{m}_{eva} \tag{0.5}$$

1.15 Energy Balance

The mixture of vapor and air in the air chamber is surrounded by the walls of the cylinder at the top and side while the bottomed is covered by liquid water. So the system can be treated as a closed system. Because the major energy transferring mechanisms are work and heat. [49].

It is assumed that the control mas (closed system) of the mixture of air and vapor changes quasi-statically, typically because of rising and falling of the water level due to the hammer pressure in the chamber. Therefore, the internal energy of the mixture of the gases is given by

$$dU = dQ + dW \tag{0.6}$$

1.15.1 Moving Boundary Work

The moving boundary work for the quasi-static process, the process during which the system proceeds nearly equilibrium all the time, is the product of the absolute pressure and the differential change in volume [50]. In this case, the water bounding the gas at the bottom is assumed as a moving piston. Thus the boundary work is positive during pushing the water and negative while compressing the gas.

$$dW = P \cdot dV \tag{0.7}$$

This moving boundary work of the hammer effect will be taken in to account during the superposition of water hammer and thermal effect.

$$dU = dQ \tag{0.8}$$

1.15.2 Perfect Gas Characteristic

A perfect gas is a gas whose temperature, pressure and volume are related by:

$$P \cdot V = mRT \tag{0.9}$$

$$R = c_p - c_v \tag{0.10}$$

By assuming constant specific heat with respect to temperature, the ratio of the specific heat is given by

$$\kappa = \frac{c_p}{c_v} \tag{0.11}$$

The internal energy of an ideal gas is the function of temperature only. i.e.

$$dU = c_v m dT \tag{0.12}$$

For the gas constant R in Eq. (4.10) remaining constants during expansion and contraction, the ideal gas equation can be expressed as

$$\frac{P_f v_f}{T_f} = \frac{P_i v_i}{T_i} \tag{0.13}$$

The above equation can be written as by rearranging volume and temperature terms

$$P_f = P_i \frac{T_f}{T_i} \left(\frac{v_i}{v_f} \right)_{spec} \tag{0.14}$$

Specific volume is the ratio of volume to mass of the gases at the specified state.

$$v_{spe} = \frac{V}{m} \tag{0.15}$$

1.15.3 Heat Transferred to the Chamber

Two different models explain the amount of heat transferred to the chamber [49], [51], [52]. These are the empirical polytropic (EP) and rational heat transfer (RHT) models.

An empirical polytropic model is a standard approach, which approximates the state of the gases within the chamber uses the polytropic thermodynamic model stated below.

$$PV^n = C \tag{0.16}$$

Where n is a polytropic factor ranges from an isothermal (n=1) to adiabatic (n=1.4) condition. In this model, the heat inflow is generally inspected by favor of a change in pressure and volume variables.

The second rational heat transfer model proposed by Graze, considers heat transfer modes of conduction, convection, and radiation simultaneously typically for one-dimensional temperature distribution. This method postulated that the rate of heat inflow for quasi-steady state is [52]

$$\frac{dQ}{dt} = 0.19 A_s \left(T_s - T_{g,i} \right)^{4/3} \tag{0.17}$$

This equation is an oversimplified equation that ignores conduction through pipe wall and radiation since they are small compared with the turbulent free convection coefficient for a semi-infinite vertical flat plate.

$$h_c = 0.19\left(T_s - T_{g,i}\right)^{1/3} \tag{0.18}$$

From the basics of heat transfer concept, if phase-change is undergoing and constant specific heats are assumed, heat energy transferred to the chamber is the sum of heat gained by gas mixture and heat of evaporation (the latent heat of vaporization).

$$Q_{tot} = \left[\left(mc\right)_a + \left(mc\right)_v\right]\left(T_{g,f} - T_{g,i}\right) + h_{eva} \cdot m_v \tag{0.19}$$

1.15.4 Heat Transfer Surface Area

It is assumed that the heat transferring surface area of the chamber is the original surface area of the chamber which has direct contact with the air inside the vessel. Thus the surface area can be calculated by the equation given below.

$$A_s = \pi Dh \tag{0.20}$$

The cross-sectional area of the chamber is $D = 76.2mm$ and height $h = 112mm$. Now the heat transferring area become $A_s = 0.027m^2$

1.15.5 Surface Temperature of Chamber

The outside surface temperature of the chamber can be obtained by balancing heat energy from Eq.(4.17) and (4.19).

$$T_s = T_{g,i} + \left\{\frac{\left(mc\right)_a + \left(mc\right)_v \cdot \left(T_{g,f} - T_{g,i}\right) + h_{eva} \cdot m_v}{0.19A_s\Delta t}\right\}^{\frac{3}{4}} \tag{0.21}$$

1.16 Total Pressure Change

Eq.(4.16) is applicable for both vapor and air since they are treated as a perfect gas. The total pressure inside the chamber is the summation of the partial pressure of each gas contained in the chamber. Thus the total pressure is

$$P = P_a + P_v \tag{0.22}$$

Now the total pressure obtained from the heat transfer is

$$P_{tot} = \left(P_i \frac{v_i}{v_f} \frac{T_f}{T_i} \right)_{air} + \left(P_i \frac{v_i}{v_f} \frac{T_f}{T_i} \right)_{vapor} \tag{0.23}$$

The gross head of the gas volume in a meter of water by assuming a constant density of water is estimated by

$$h = \frac{P_{tot}}{\rho_w g} \tag{0.24}$$

1.17 Vapor Formation

1.17.1 Heat of Vaporization

The process of evaporation occurs whenever the temperature of the surface of the liquid exceeds the saturation temperature corresponding to the fluid pressure. The process is characterized by the formation of vapor bubbles, which grow and detach from the surface. When the temperature of the liquid slightly exceeds the saturation temperature then the evaporation is called saturated boiling.

Inside the air chamber, heat is transferred through free convection as a result of minor density variation within the different layers of a gas mixture from the center to the wall. Since the surface of the water is in touch with the hot gas there is heat transfer by convection at the surface and through conduction for tentatively stored water. Therefore, the content of vapor in the air will change due to evaporation at the interface.

The amount of water evaporated from the surface of liquid water is

$$Q_{eva} = h_{eva} \cdot m_v \tag{0.25}$$

h_{eva} is the heat of evaporation per unit mass of water and its value is 2256.4 kJ/kg at the saturation temperature and pressure. During the vaporization process, a substance coexists as part liquid and part vapor. The proportion of the mixture is defined by quality x as the ratio of vapor and total mass.

$$m_v = x \cdot m_{tot} \tag{0.26}$$

1.17.2 Relative Humidity of Ambient Air

Relative humidity specifies the amount of water vapor in the air. The amount of vapor in the air can be expressed as

$$m_{v,ath} = m_a \frac{0.622 \Phi P_g}{P - \Phi P_g} \tag{0.27}$$

Where $P_g = P_{sat@T}$

The dry mass of air in the chamber can be determined by

$$m_{dry\_air} = \frac{P_a \cdot V}{R_a \cdot T} \tag{0.28}$$

The relative humidity of the ambient is 59%. Saturation pressure at the mean ambient temperature of 17^{o}C is 2.022 kPa. From this, the partial pressure of the vapor in the ambient air is 1.193 kPa. The partial pressure of air in the ambient is 75.015 kPa and

Total mass of vapor in the air chamber is the sum of evaporated water and moisture in the ambient air.

$$m_{v,tot} = m_v + m_{v,ath} \tag{0.29}$$

$$m_{v,tot} = x \cdot m_{tot} + m_a \frac{0.622 \Phi P_g}{P - \Phi P_g} \tag{0.30}$$

1.18 Initial and Boundary Conditions

Initially the chamber was at a temperature of 17 ^{o}C and at the ambient pressure. The boundary conditions are heating wall, and velocity inlet. The interface of gas mixture and liquid water is characterized by the existence of constant temperature at the surface.

1.19 Superimposing Water Hammer and Thermal Infusion

In this part of this chapter, head gained from the water hammer effect is going to be superimposed with the head which is obtained from the thermal effect. To that end combining Eq.(3.13) with Eq.(4.24) finally yields head in the following form.

$$\Delta h = \left(V_2 - V_3\right)\frac{c}{g} + \frac{P_{tot}}{\rho_w g} - h_r \tag{0.31}$$

$$\Delta h = \left(V_2 - V_3\right)\frac{c}{g} + \frac{1}{\rho_w g}\left[\left(P_i \frac{v_i}{v_f}\frac{T_f}{T_i}\right)_{air} + \left(P_i \frac{v_i}{v_f}\frac{T_f}{T_i}\right)_{vapor}\right] - h_r \tag{0.32}$$

Solar Thermal Analysis for Addis Ababa

Solar thermal technologies collect the sun's thermal energy and transfer to heat transferring medium for various purposes. They can satisfy the substantial amount of heat required for both industrial and agricultural processes in any country. The solar thermal system can supply hot air, hot water, or steam in a temperature range of up to 400 ^{0}C [53]. The group of those technologies that are useful for heat supply is solar air heater, solar water heater, and solar concentrators.

Currently, engineering systems are becoming hybrids such as a hybrid solar water heater and ice-making system, a hybrid car, and a combined solar hydrothermal system [53], [54]. Because of ecological problems and continuous energy crises, solar energy become the most attractive for the development of hybrid sustainable energy systems for various applications. This section focus on an investigation of the solar potential of Addis Ababa for base hydraulic ram pump application.

1.20 Summary of Solar Thermal Collectors

In general, there are three different categories of solar thermal collectors such as solar air collectors, solar water heater, and solar concentrator. Small-scale industrial applications require a temperature range of 150 to 400 ^{0}C. This medium range of temperature could be generated through the design and installation of advanced flat plate collector with ultra-high vacuums or parabolic solar dishes [55], [56]. The table given below gives a summary of technologies together with their characteristics and applications.

Table 0.1 Overview of solar thermal technology applications and characteristics [57]

Technology	**Characteristics**			**Applications**				
	Max. tem.	Diffused light	Adaptable integration	Pool heating	Domestic water heating	Space building heating and cooling	Industrial process	Electricity
FPC	100	Yes	Flat plate	Yes	Yes	Unfeasible	Up to 100 ^{o}C	Unfeasible
EFPC	180	Yes	Flat plate	Yes	Yes	Yes	Up to 180 ^{o}C	Unfeasible
ETC	300	No	Flat plate possible	Not customary	Yes	Yes	Up to 300 ^{o}C	Unfeasible
PTC	550	No	Flat plate	Not customary	Not customary	Yes	Up to 500 ^{o}C	Yes
UHVFPC	400	Yes	Flat plate	Feasible	Feasible	Feasible	Feasible	feasible

Yes – there are currently applications using this technology
Not customary – not found yet

For hybrid solar-assisted hydraulic ram pump, a solar thermal collector of generating temperature in the range of 150 to 400 ^{o}C is selected.

1.20.1 Components of UHV flat pale collector

The main components of ultra-high vacuum flat plate solar thermal collectors are absorber plate, selective plate coating material, transparent cover glass, none evaporable getter pump, metal frame, and insulation material.

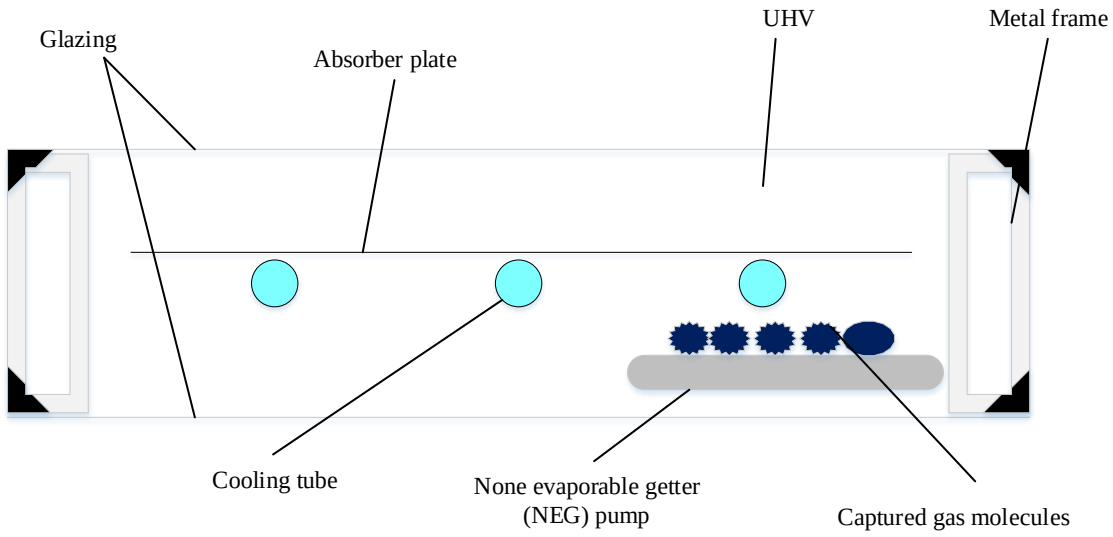

Figure 0.1 Cross-section of the solar thermal UHV collector (representation)

Getter pump

The main component of this technology is none evaporable getter (NEG) pump. The adaptive integration of getter material to maintain a vacuum inside the flat plat collector enhance the performance of the collector. Getters are materials with the ability to react with free gases and form chemical compounds at their surface. In this sense, a getter acts as a gas "pump" capturing the surrounded gas molecules to create thermal insulation inside the collector [58].

Absorber and Glass

The absorbers of the solar thermal UHV collector are characterized by a selective coating of black chrome with high absorbance (92%) and low emissivity (3.5%) of visible and infrared radiation, respectively [58], [59]. A special surface treatment for the absorber of the collector should be realized for capturing maximum sunlight radiation.

Heat Transferring Fluid

Due to availability and low-cost water is the most widely used heat transferring fluid for the solar thermal process. However, additional pressure is required for the hydraulic system to maintain the water in a liquid state at temperatures above 100˚C. By using thermal oils as a heat transferring fluid,

high temperature can be achieved, by maintaining the operation pressure of the circuit much lower compared to water.

1.21 Site Information and Radiation Data

The selected site, Addis Ababa the capital city of Ethiopia, is located at Latitude 9.0^0 N, and Longitude 38.75^0 E. The nearest weather station branch located at Addis Ababa is the National Metrology office. From the station, only global solar radiation and temperature data were obtained. Such data were collected recorded with an interval of fifteen minutes for years 2013 to 2019. The rest of the radiation components were evaluated using empirical relations.

Global solar radiation data was obtained from the National Metrological Agency at Bole automatic recording station. Using the raw data obtained from the station the daily average solar radiation was calculated for the day time of 9:00: 00 AM to 4:00: 00 PM or (3:00:00 to 10:00:00 local time). From the daily average, the average monthly global solar power was determined and given in the figures below.

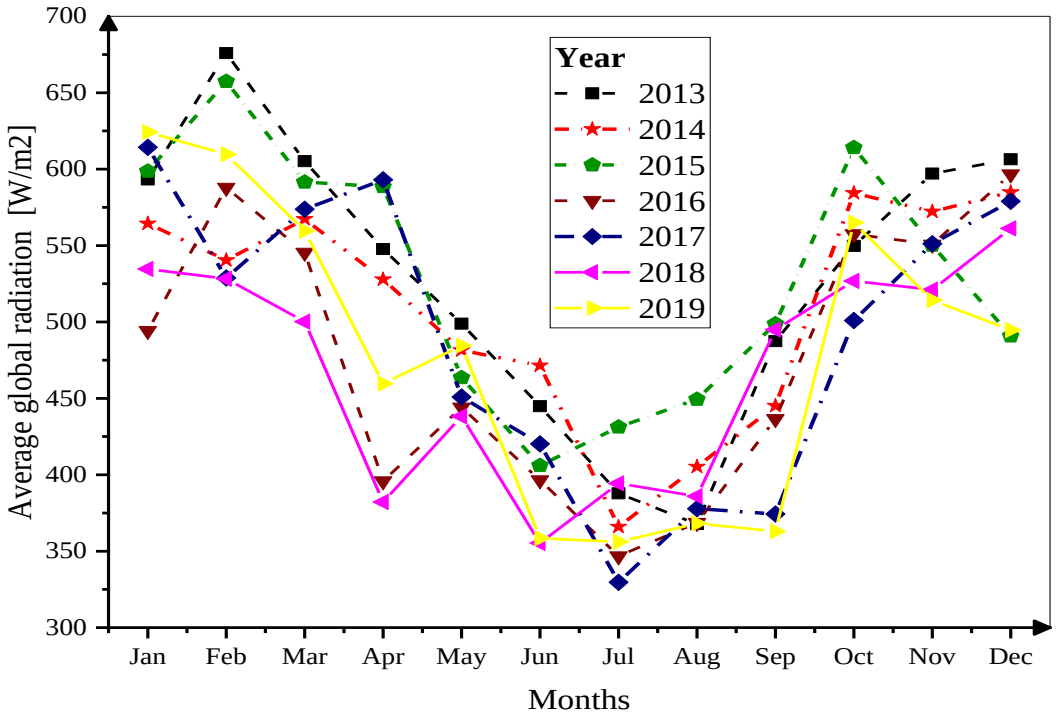

Figure 0.2 Average monthly global solar radiation (W/m^2) of Addis Ababa

The following graph demonstrates the yearly average global solar radiation on a horizontal surface.

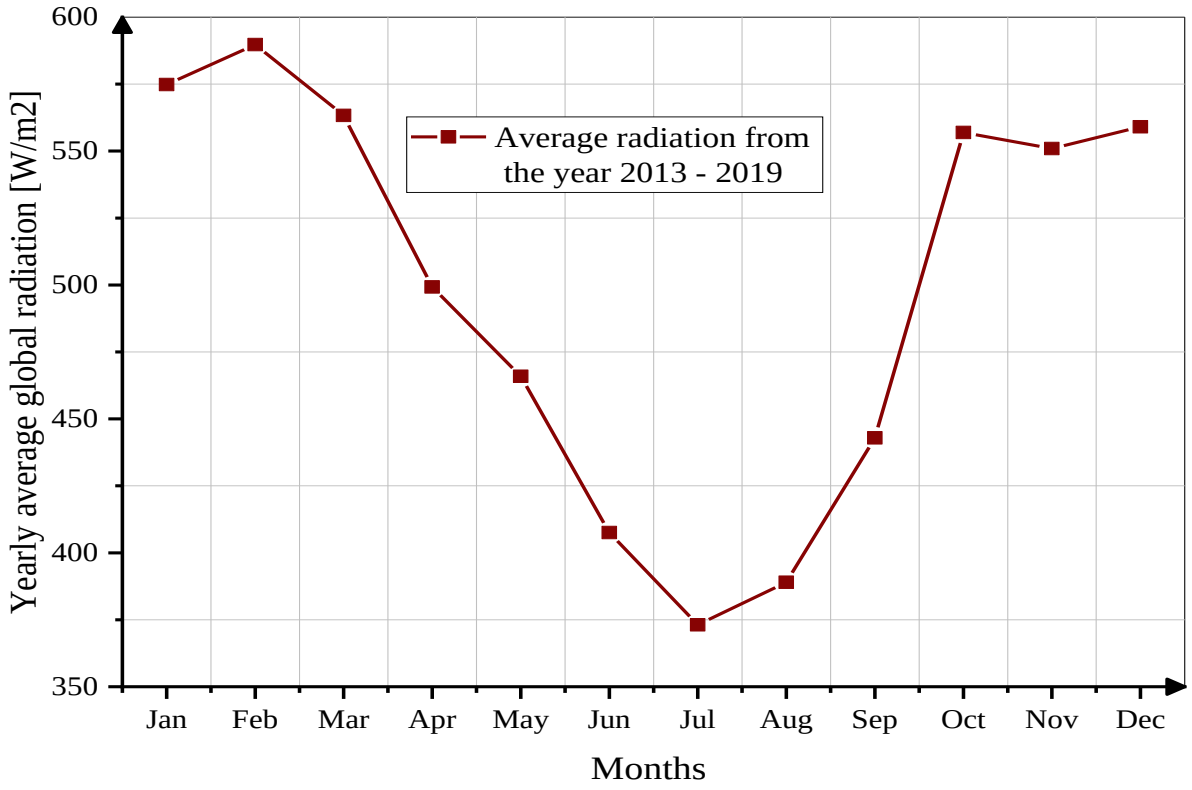

Figure 0.3 Average global solar radiation of Addis Ababa from the year 2013 to 2019.

1.22 Sun-Earth Angles

Latitude (ϕ): The latitude of a certain location is its position north or south of the equator, taking north as positive. The latitude of the site is 9.03° to North.

Surface inclination (β): surface inclination is the angle between the plane of the surface and the horizontal. Mounting at an angle equal to the latitude (ϕ) works best for year-round energy demand.

Azimuth angle (γ): The angular displacement from the south of the beam radiation projection on the horizontal plane. It is zero due south, east negative, and west positive. A collector located in the Northern hemisphere best operates when facing to the south.

Declination angle (δ): The angular position of the sun north or south from the earth's equator, north positive. The declination δ can be found from Cooper approximate equation

$$\delta = 23.45 \sin\left(360 \frac{284+n}{365}\right) \tag{0.1}$$

Where *n* is an average representative days of the month.

Hour angle (ω): The angular displacement of the sun east or west of the local meridian.

$$\omega = (12 - ST) \times 15^{\circ} \tag{0.2}$$

ST is local solar time.

The angle of incidence (θ): The angle between the beam radiation on a surface and the normal to that surface. For the south or north-facing surface, the surface azimuth angle (γ) is zero.

$$\cos\theta = \sin\delta\sin\phi\cos\beta - \sin\delta\cos\phi\sin\beta\cos\gamma + \cos\delta\cos\phi\cos\beta\cos\omega + \cos\delta\sin\phi\sin\beta\cos\gamma\cos\omega + \cos\delta\sin\beta\sin\gamma\sin\omega \tag{0.3}$$

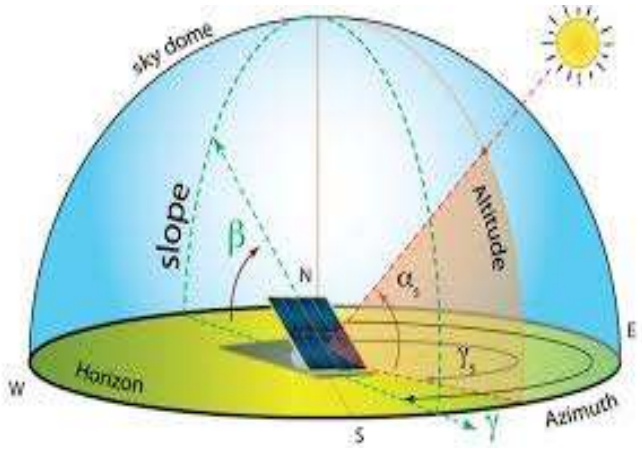

Figure 0.4 An overview of flat plate solar thermal collector and sun-earth angle [60]

Zenith angle (θ_z)**:** Angle between the incidence of beam radiation on a horizontal surface and vertical to the surface.

$$\cos\theta_z = \cos\phi\cos\delta\cos\omega + \sin\phi\sin\delta \tag{0.4}$$

Solar altitude angle (α_s)**:** The angle between the horizontal and the line to the sun, that is, the complement of the zenith angle.

Solar azimuth angle (γ_s)**:** Angular displacement from south of the projection of beam radiation on the horizontal plane. Displacements east of south are negative and west of south are positive.

1.23 Absorbed Solar Radiation

1.23.1 Extraterrestrial Radiation

From the total incoming solar constant, the only fraction of the extraterrestrial solar radiation is reaching the surface of the earth due to various motives. Solar radiation outside of the atmosphere on a horizontal surface is

$$I_o = \frac{12\times 3600}{\pi} G_{sc}\left(1+0.033\cos\frac{360n}{365}\right)\times\left[\cos\phi\cos\delta\left(\sin\omega_2-\sin\omega_1\right)+\frac{\pi\left(\omega_2-\omega_1\right)}{180}\sin\phi\sin\delta\right] \tag{0.5}$$

Part of the incoming solar radiation received by a surface without having been scattered by the atmosphere. Whereas diffuse radiation is the rest, which has been scattered by the atmosphere either reflected space or reaches to the ground. Liu and Jordan calculated fractions on a horizontal surface at ground level [61]. In their study, they have computed factors called atmospheric transmittance for direct radiation, diffuse radiation, and total radiation.

1.23.2 Solar Radiation on Surfaces

Global solar radiation on a horizontal surface can be measured with the help of a pyrometer. The data from the Metrological Agency is global solar radiation on a horizontal surface. The global solar radiation on a horizontal surface is beam (I_b) and diffuse (I_d) solar radiation only.

$$I_H = I_b + I_d \tag{0.6}$$

Total solar radiation is the sum of the beam, diffuse, and reflected solar radiations to the surface of the collector that is generally oriented at a certain inclined angle (β). Models to estimate diffuse radiation for an inclined surface are isotropic and anisotropic [62], [63]. The isotropic model assumes that uniform distribution of radiation from the sky but anisotropic model considers circumsolar diffuse and horizon brightening in addition to isotropic distribution.

The isotropic model for diffuse radiation is relatively easy to understand and its conservativeness makes the estimation of radiation on the inclined surface simple. Among the isotropic models, Liu and Jordan's model found to be the most accurate [62].

$$I_T = I_b R_b + I_d \left(\frac{1+\cos\beta}{2} \right) + I_H \rho_g \left(\frac{1-\cos\beta}{2} \right) \tag{0.7}$$

Beam radiation geometric factor (R_b) is the ratio of beam radiation on the tilted surface to that on a horizontal surface at any time given by:

$$R_b = \frac{\cos\theta}{\cos\theta_z} \tag{0.8}$$

The most widely used correlation to estimate diffuse radiation for practical purpose is the Orgill and Hollands relation

$$\frac{I_d}{I_H} = \begin{cases} 1 - 0.249k_T & for \;\; 0 \le k_T \le 0.35 \\ 1.557 - 1.84k_T & for \;\; 0.35 \le k_T \le 0.75 \\ 0.177 & for \;\; k_T > 0.75 \end{cases} \tag{0.9}$$

Hourly clearness index is defined as:

$$k_T = \frac{I_H}{I_o} \tag{0.10}$$

The ground reflectance $\left(\rho_g\right)$ is often estimated at a constant 0.2 value [62].

1.24 Useful Energy Gain of Collector

1.24.1 Heat Loss Coefficients

Total energy absorbed depends on the transmissivity-absorptivity product (τα), the area of the collector A_c, and the incident solar radiation intensity. In steady-state operating conditions, the total energy absorbed by the collector with area A_c is stated by the absorbed solar radiation equation.

$$Q = 0.96 \times (\tau\alpha) I_T \times A_c \tag{0.11}$$

In the UHV flat plat solar thermal collector, there is a vacuum gap inside the solar thermal collector. It is assumed that the space between the glasses and the absorber plate kept as a vacuum by the getter pump. The different heat transfer mechanisms which contribute to the total heat loss to ambient are radiation from the plat to glass and radiation and convection from the first glass to ambient [58], [64].

A space maintained at a vacuum pressure of 10 mTorr (~1.3 Pa) or below is sufficient to effectively eliminate conductive and convective heat losses [65]. Thus, the UHV acts as a perfect insulation, maintaining the generated heat inside the collector. Useful energy accounting heat loss is expressed as

$$Q_u = A_c \left[S - U_L \left(\overline{T_p} - T_a \right) \right] \tag{0.12}$$

$$S = 0.96 \times (\tau\alpha) \times I_T \tag{0.13}$$

1.24.2 Performance of Collector

If conditions are steady, the performance of the collector is given as

$$Q_u = \eta I_T A_c \tag{0.14}$$

It is practical expressing efficiency of the collector using optical parameters of a solar thermal collector (η_0, a_1 and a_2) which are determined by standard EN12975-2 performance tests [58], [63], [66].

$$\eta = \eta_0 - a_1.\frac{\left(T_m - T_a\right)}{I} - a_2.\frac{\left(T_m - T_a\right)^2}{I} \tag{0.15}$$

$$T_m = \frac{T_{i,f} + T_{o,f}}{2} \tag{0.16}$$

Rearranging Eq.(5.15) for the mean temperature gives the following simplified quadratic formula considering the mean temperature difference as a variable.

$$a_2 \times T_m^2 - \left(2a_2T_a - a_1\right) \times T_m + \left[I_T\left(\eta - \eta_0\right) - a_1T_a + a_2T_a^2\right] = 0 \tag{0.17}$$

Solving this quadratic equation gives the mean temperature difference $\left(T_m\right)$ and fluid outlet temperature $\left(T_{o,f}\right)$ in the form of:

$$T_m = \frac{-\left(2a_2T_a - a_1\right) + \sqrt{\left(a_1 + 2a_2T_a\right)^2 - 4a_2\left(I_T\left(\eta - \eta_0\right) - a_1T_a + a_2T_a^2\right)}}{2a_2} \tag{0.18}$$

$$T_{o,f} = 2\frac{-\left(2a_2T_a - a_1\right) + \sqrt{\left(a_1 + 2a_2T_a\right)^2 - 4a_2\left(I_T\left(\eta - \eta_0\right) - a_1T_a + a_2T_a^2\right)}}{2a_2} - T_{i,f} \tag{0.19}$$

1.25 Design Assumption and Collector Specification

The following assumptions are made to model the flat-plate solar collectors:

- The collector operates under a steady-state condition.
- The incoming solar radiation is perpendicular to the plane of the collector.
- Temperature gradient through cover, absorber plate around, and tubes is negligible.
- One-dimensional heat flow through cover, back, and side insulation system.
- The collector has a single cover.
- The area of the absorber is assumed the same as the frontal transparent area.
- Average global solar radiation of each year on a horizontal surface for Addis is above 500 w/m^2.
- The optical performance characteristics of collectors without reflection mirror (η_0, a_1 and, a_2) are given in appendix-A. Those parameters are obtained by a test based on EN12975-2 standard [58].

CFD Simulation

The geometrical model was developed by the design modeler of ANSYS 2019.2. The three-dimensional model is shown in figure 6.1 below. The computational model is a closed cylinder, the upper portion of it filled with air, and the lower part, green highlighted with water. So this CFD simulation studies the three-dimensional physical models of evaporation of water at the interface and its consequence in the closed vessel.

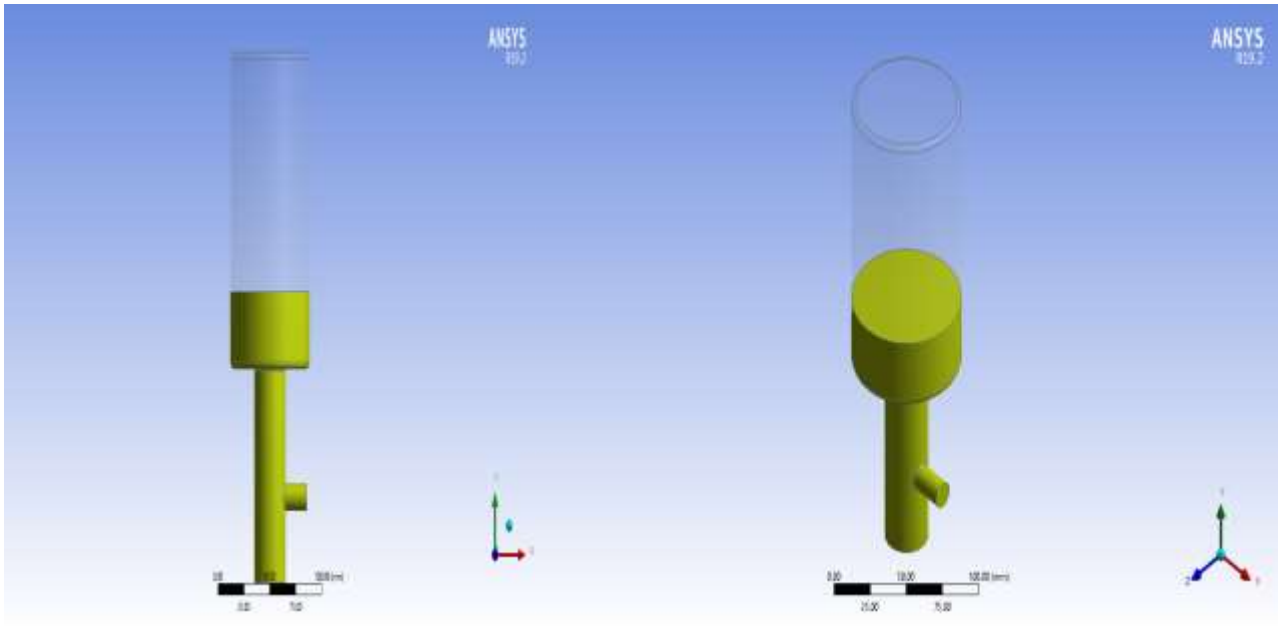

Figure 0.1 The schematic diagram of the simulation model

1.26 Boundary and Initial Conditions

The boundary condition of air chamber exposed to heat is set at a temperature of 200 ^{o}C which is gradually increasing from the ambient initial temperature of 17^{o}C. The inlet surface allows water to enter at a velocity of 1.93 m/s. The boundary condition of the remaining walls is assumed as an insulated. The picture given below demonstrates the boundaries of the chamber and the fluid domain.

Initially the gauge pressure is 0 kPa. The initial temperature is 17 oC and the volume fraction of vapor is also 0.

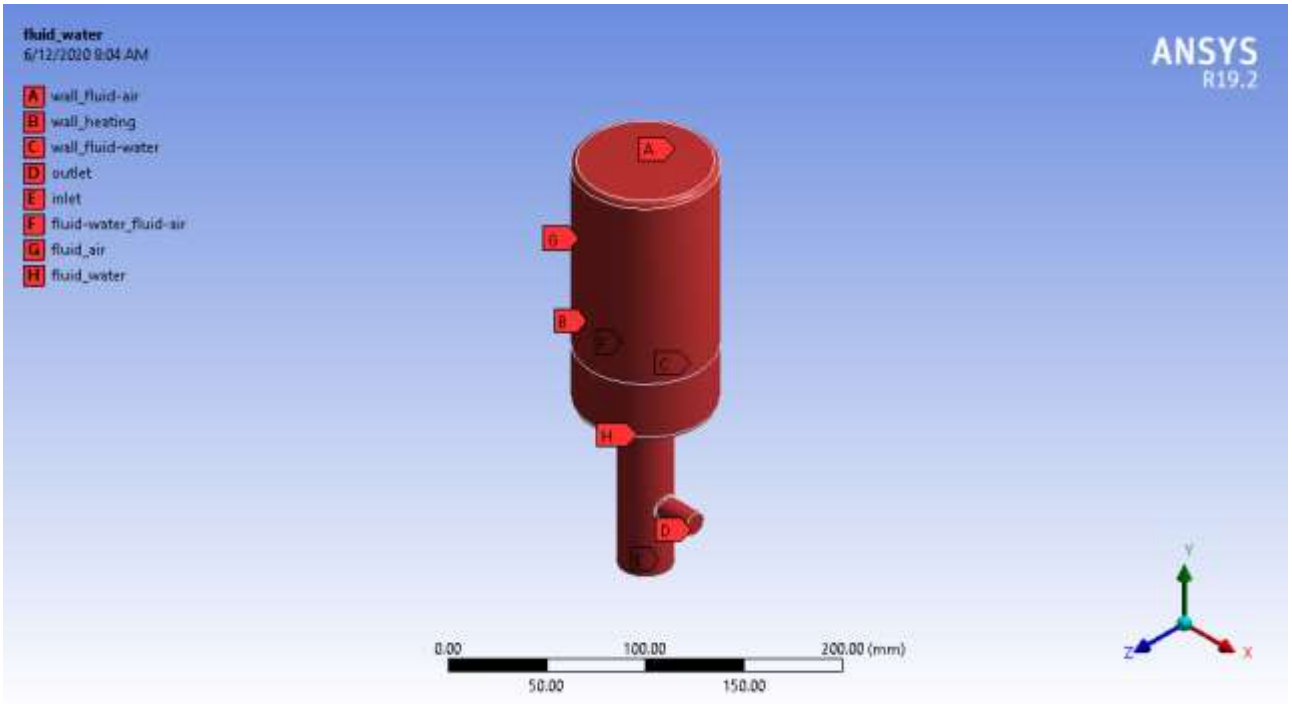

Figure 0.2 Boundaries of simulation domain

The next table summarizes the boundary physics of the fluid domain and type of boundaries.

Table 0.1 Boundary Physics

Domain	Boundaries	
Fluid air	Boundary - fluid air-fluid water	
	Type	Interface
	Boundary - wall heating	
	Type	Wall
	Boundary - wall vessel fluid air	
	Type	wall
Fluid water	Boundary - fluid air-fluid water fluid water	
	Type	Interface

	Boundary - inlet surface	
	Type	Velocity-inlet
	Boundary - outlet surface	
	Type	Pressure-outlet
	Boundary - wall vessel fluid water	
	Type	Wall

1.27 Method and Solving Procedure

All CFD tools analyze a problem based on the fundamental governing equations of fluid dynamics i.e., continuity, momentum, and energy equations. The computational fluid dynamics (CFD) solver of this problem is ANSYS Fluent. The geometry discretized (meshed) with the help of a triangular and quadrilateral cell. About 102,000 number of elements was generated. The following table gives mesh information of each region (water and air) and the whole fluid domain. Mesh check was applied to avoid problems due to incorrect mesh connectivity.

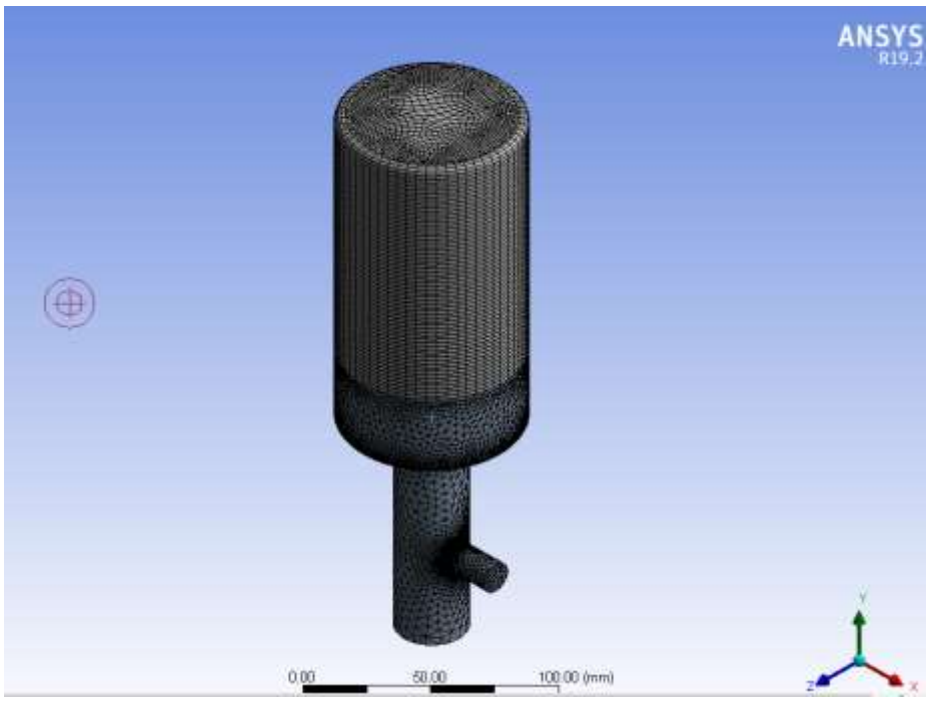

Figure 0.3 Discretization of the physical model

Table 0.2 Mesh Information of the computational domain

Domain	Nodes	Elements
Fluid air	17166	45963
Fluid water	25749	56037
All domains	42915	102000

The numerical simulation of vapor-liquid two-phase flow assisted by heat transfer contains particle tracking techniques that can give the information of the two phases accurately and comprehensively. Thus the mixture model is used for the analysis of the simulation [67]. The solver is set up as explicit pressure-based, time-dependent with gravity taken into consideration. The multiphase model was mixture containing three Eulerian phases. Volume fraction parameters were formulated through explicit time scheme. Sharp/Dispersed type of interface modeling was selected for thee phase interactions. The problem is a multi-phase problem having a phase interaction of water evaporation at a frequency of 0.2/sec.

Air is taken as a primary phase since it was assumed as a compressible ideal gas and the second phase was water since it was patched as the volume fraction of 1 in the portion of the domain [68]. The saturation temperature is 365.15 K at a pressure of 76.2 kPa. The other properties of the fluid domain (liquid-water and air) are given in the appendix part.

To couple the pressure and velocity, the COUPLE algorithm was introduced. Second order upwind scheme was adopted to discrete the momentum and energy equation. To converge the solution satisfactorily the under-relaxation factors used at a value of 1 for density, 1 for body force, 1 for vaporization of mass, 0.5 for volume fraction, 0.8 for turbulence kinetic energy, and 1 for energy. It was assumed that the numerical calculation becomes converged when the residuals of mass, energy, and velocity are less than 0.001.

The time stepping method was set as fixed. For the numerical integration the number of time steps used in the simulation was 30, 000 with the time step size of 0.001. The maximum number of iterations per time step size was 30.

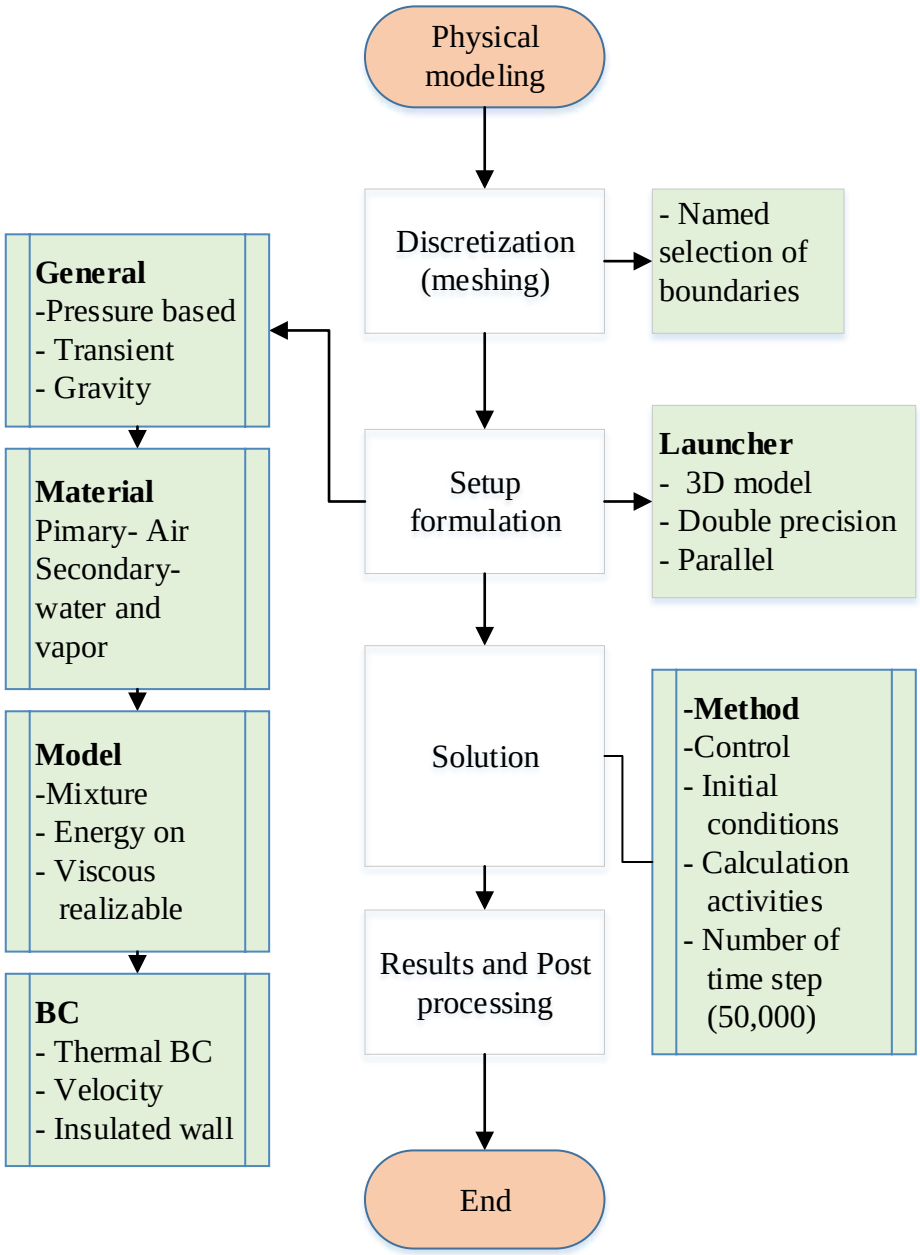

Figure 0.4 Flow diagram of CFD solver

1.28 ANSYS Simulation Result

Based on the numerical simulation the following result was obtained. The figure below gives information about temperature, pressure and vapor distribution in the chamber.

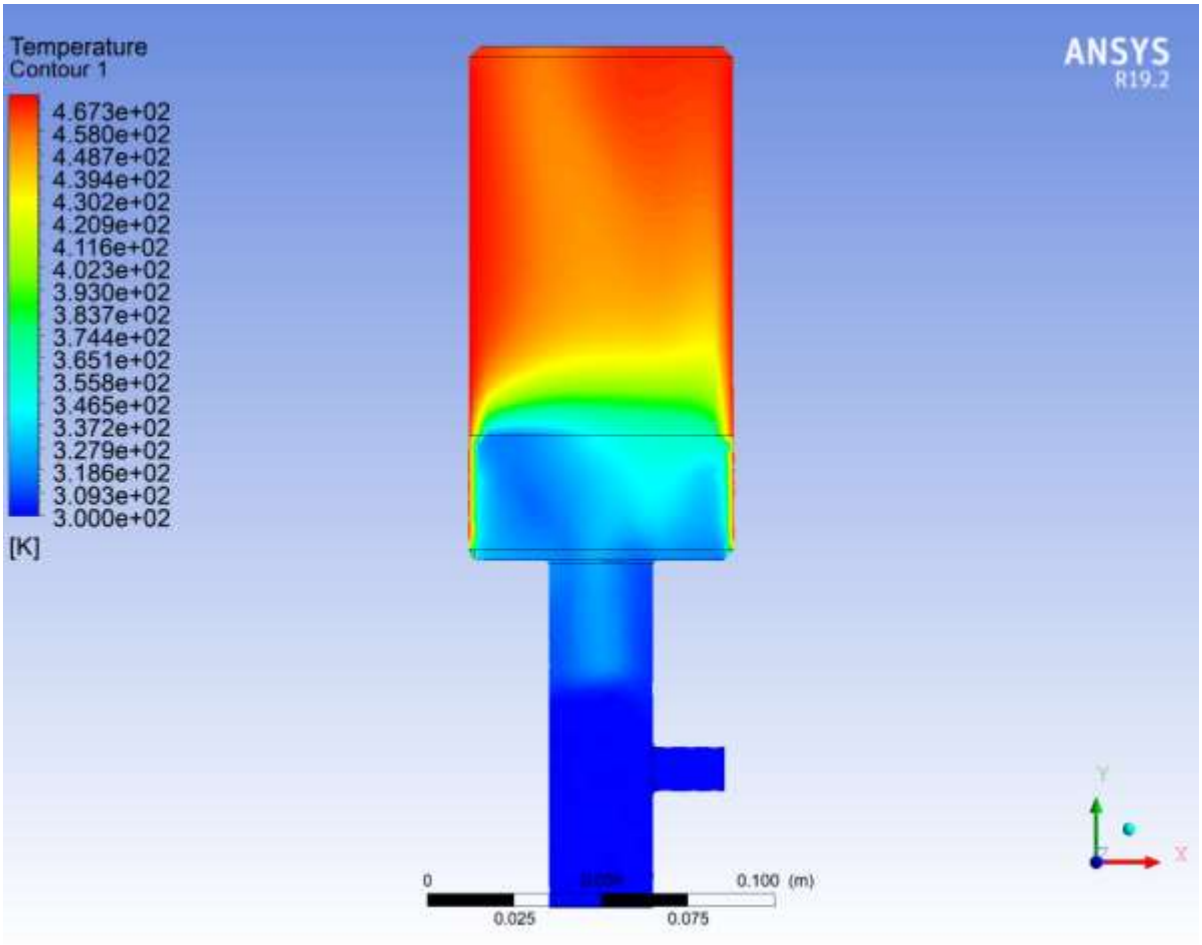

Figure 0.5 Temperature distribution

The contours presented above and next page gives the condition only. This is because the solution is time dependent. The full time history of the solution is described in chapter eight result and discussion part. Temperature contour shows maximum final temperature is in the gas air mixture. At the exit of the chamber the temperature is similar with the ambient. Figure 6.6 demonstrates the pressure inside the chamber increased by 50 kPa in the course of heat addition process. There is also a phase change process around the water air interface. The formation of vapor introduces an increment of pressure in the chamber.

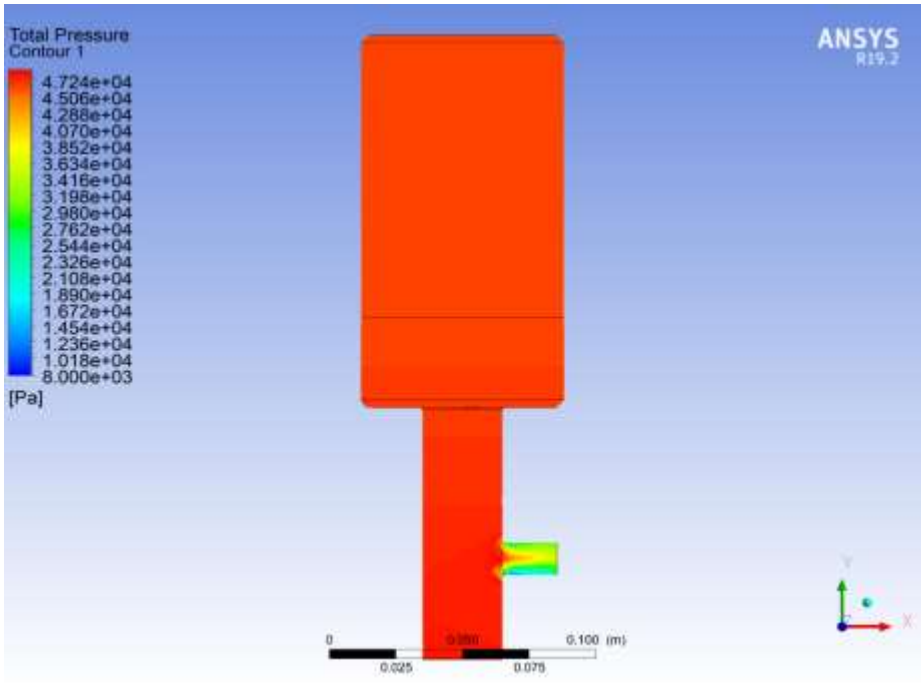

Figure 0.6 Total pressure distribution

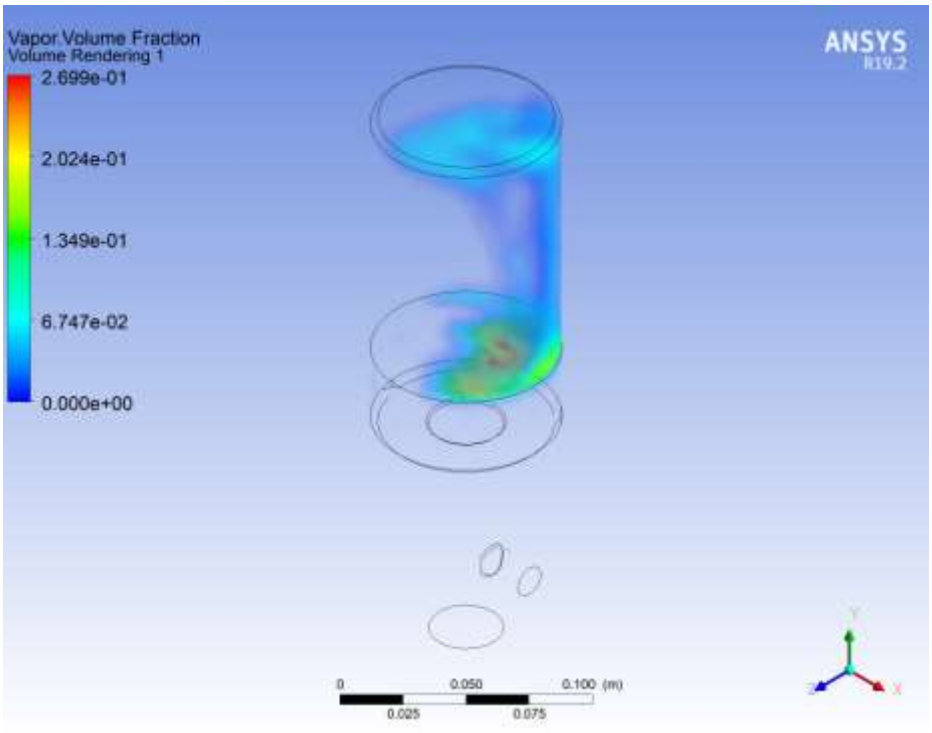

Figure 0.7 Volume fraction of vapor at the water air interface

1.28.1 Grid Independence Test

The following table summarizes thermal simulation results simulated with three different grids.

Table 0.3 Grid independence simulation

Number of grids	Pressure [kPa]	Temperature [^{o}C]	Flow rate [liters per second]
26000	48	145	0.183
56000	50	150	0.18
102,000	63	160	0.19

To simulate this physical problem around 50, 000 number of grid is enough to save time and to obtain good numerical simulation result.

Experimental Test Setup

1.29 System Level Diagram and Fabrication

The source tank located 2.18 m above the pump with a bucket capacity of 18.9 liters to provide a constant volume flow rate of 34 liters per minute for the pump. The flow supplied to the drive pipe is controlled by a gate valve.

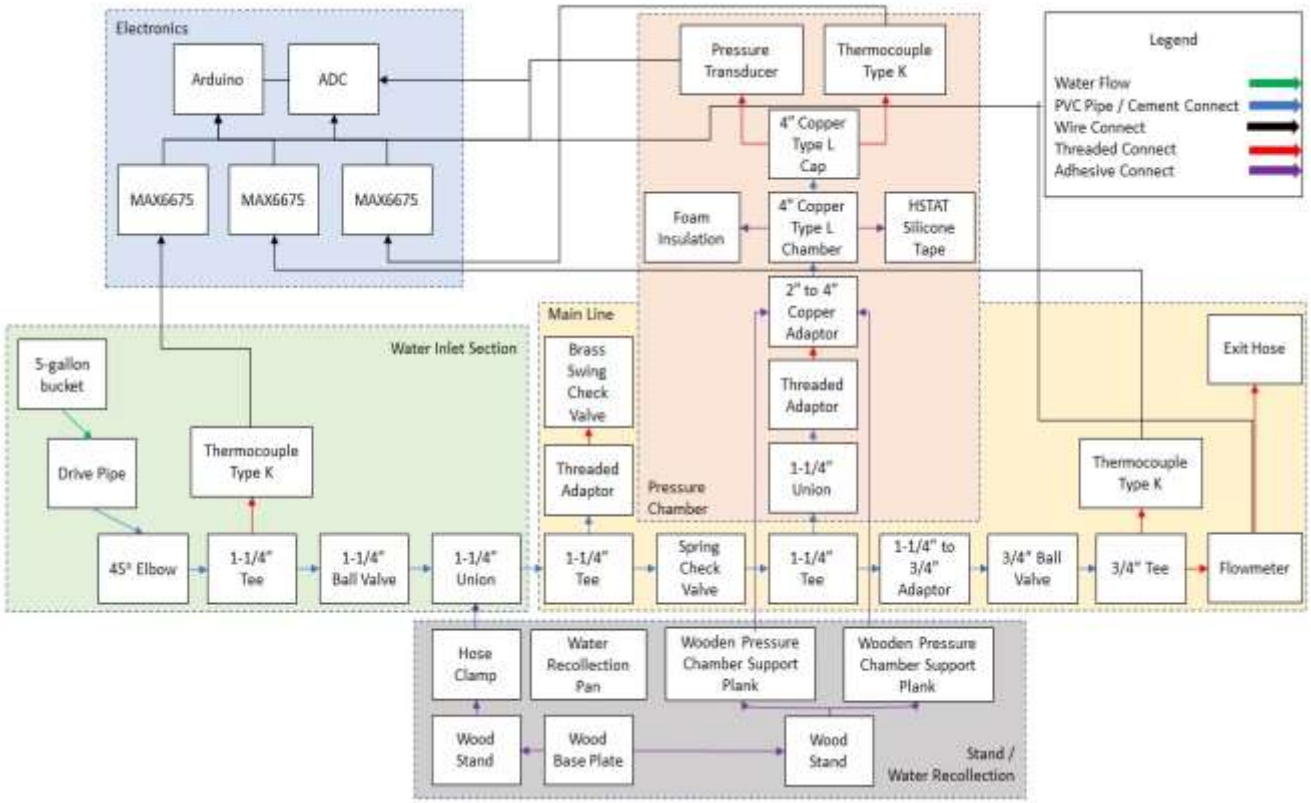

Figure 0.1 System-level diagram

The experimental testbed was built as shown in figure 7.1 to measure the flow rate supplied to the pump, the delivered water, and the delivery head during its operation.

Components:

1) Inlet Drive Pipe
2) Thermocouple
3) Ball Valve

4) Wye with Mesh Filter
5) Swing Check Valve
6) Spring Check Valve
7) Copper Pressure Chamber with Heating Strip
8) Thermocouple
9) Pressure Transducer
10) Ball Valve
11) Thermocouple
12) Flow Meter

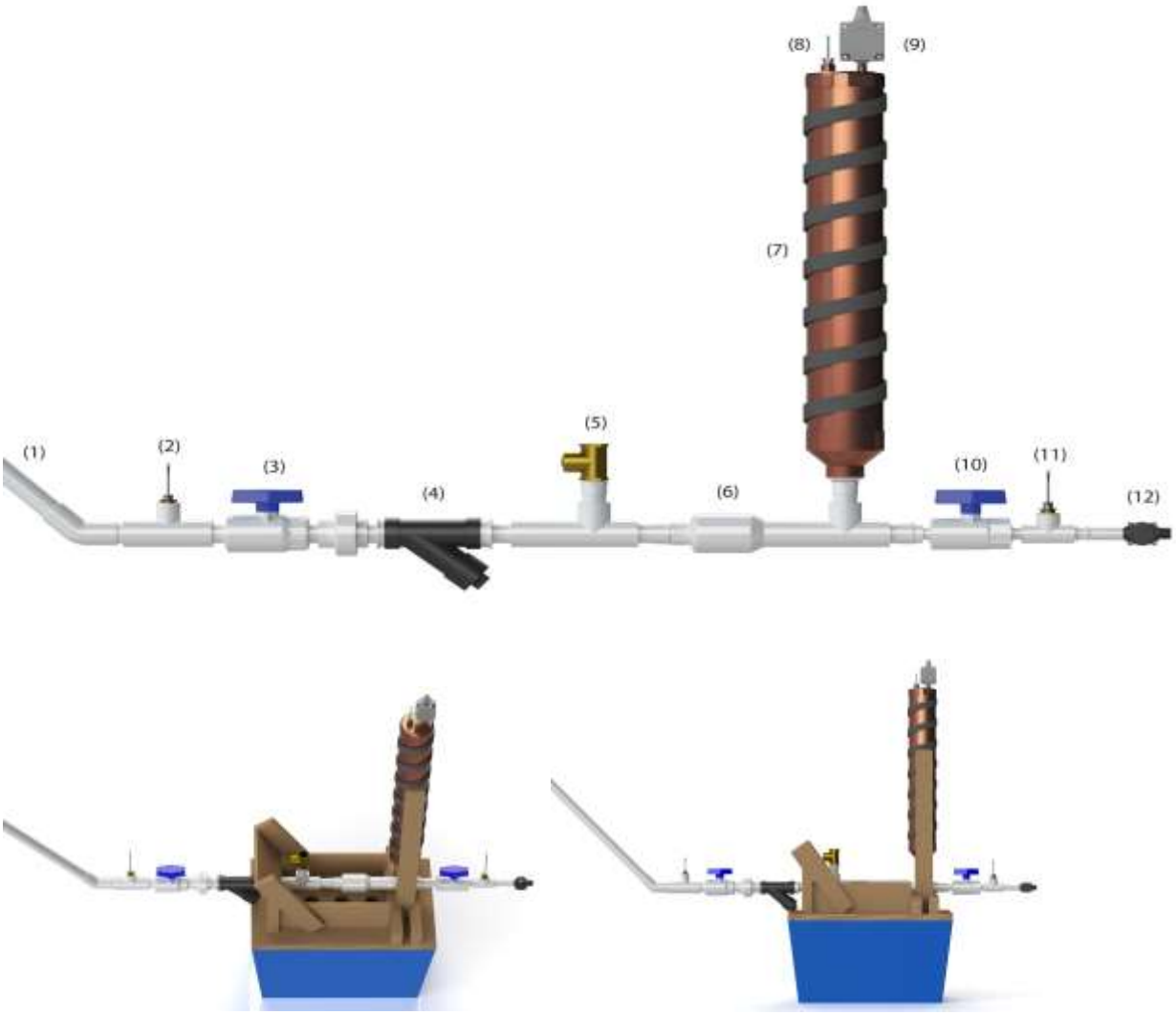

Figure 0.2 Final design of the pump

A PVC Sch 40 drive pipe, copper type L pressure chamber, and support made from wood are assembled with pipe unions as shown below in the level diagram. In the experiment delivery head, delivery flow, total supply flow, surface temperature of the chamber, and temperature of delivered water was measured. The whole system weighs not more than 30 kg and it is transportable via cart.

Figure 0.3 Assembly of the pump with water capturing container

Wastage water was stored on a base plate tub. The base plate tub able to collect more than twice the capacity of water entering from the source tank. The specification of the wastewater collecting container is 1.15 m of total length, 1.14 m total height, 0.38 m total width, and weighs 19 kg.

The final design of the system is modular, using pipe fittings for easy disassembly. Foam insulation wrapped around the copper pressure chamber to ensure no heat loss. The air chamber was supplied with a constant heat source. A controllable heating strip has a maximum temperature of 218 ^{o}C.

1.30 Engineering Specification and System Requirements

The heat source is applied around the pressure chamber. But copper is not heated above 75 ^{o}C. The system must be able to withstand a surrounding operating temperature range of 4.5 to 35 ^{o}C.

Figure 0.4 Heater and suction line strainer with a minimum sediment filter size of 50

Installation of pipe unions incorporates suction line strainer with a minimum sediment filter size of 50 mesh.

Table 0.1 System requirements

Priority Level	User Requirement	Justification	User Requirement Information Sources
1	Must include thermal infusion into the design	The use of thermal infusion is an interest in increasing the efficiency of the Hydram.	The objective of the research
1	Hydram must be kept in an upright position	The Hydram pump must be able to maintain a straight orientation to perform at maximum efficiency.	System Functional Requirement, Safety Requirement

3	Must be reliable	A Hydram with poor reliability will comprise the lifespan of the pump.	System Functional Requirement
3	Must be easy to deploy	Efficient assembly and transportation are essential for the user's convenience.	System Functional Requirement
3	Must be easy to maintain	Sustain a reasonable running cost for the Hydram during long term usage.	System Internal Interface Requirements
2	Reduce wastewater leakage	Increase the water output efficiency of Hydram. A safety hazard for the user and the surrounding area of operation.	System Functional Requirement
1	Safety	Poor safety precautions will greatly increase the chance of the pump's failure and harm to the user.	Safety Requirement

Table 0.2 Requirement verification method

User Requirements	**Engineering Specifications**	**Initial Testing Method**	**Evaluation**
Must include thermal infusion into the design	Copper must not be heated above 71 oC	Infrared thermometer	Verify copper does not exceed system max operating temperature
	Apply heat source that surrounds the pressure chamber	Pressure sensor/ Thermocouple	Verify pressure increase by comparing baseline evaluated pressure to thermally infused evaluated pressure
Must be reliable	Must be able to withstand a surrounding operating temperature of 4.5 to 35 oC	Thermometer/Thermocouple	Test different temperature of water to ensure the system can be used in an open water setting

	Must incorporate suction line strainer with a minimum sediment filter size of 50 mesh	Dilute water with sediment	Place sediment in the water and ensure mesh filter works effectively
Must be easy to deploy	The whole system must not weight more than 30 kg	Luggage scale	Measure overall weight to ensure can be picked up by average human
	Transportable via cart	Cart	Transport system via cart
Reduce wastewater leakage	Create a water recapture system that collects 60% of the wastewater	Measure water volume	Calculate initial water column and pumped water volume to calculate total wastewater, then capture at least 60%
Safety	Achieve an IP certification of IP44	Inspection of a waterproof casing	Create 3d printed waterproof case for electronics, ensure it can take minor water splash
	Not exceeding 1.38 kpa throughout the whole system	Pressure sensor	Monitor system safety through the pressure sensor

Result Analysis and Discussion

1.31 Simulation Results

1.31.1 Performance of regular hydraulic ram pump

Based on the rational design method of the regular hydraulic ram pump the following system performance was obtained for various operating conditions.

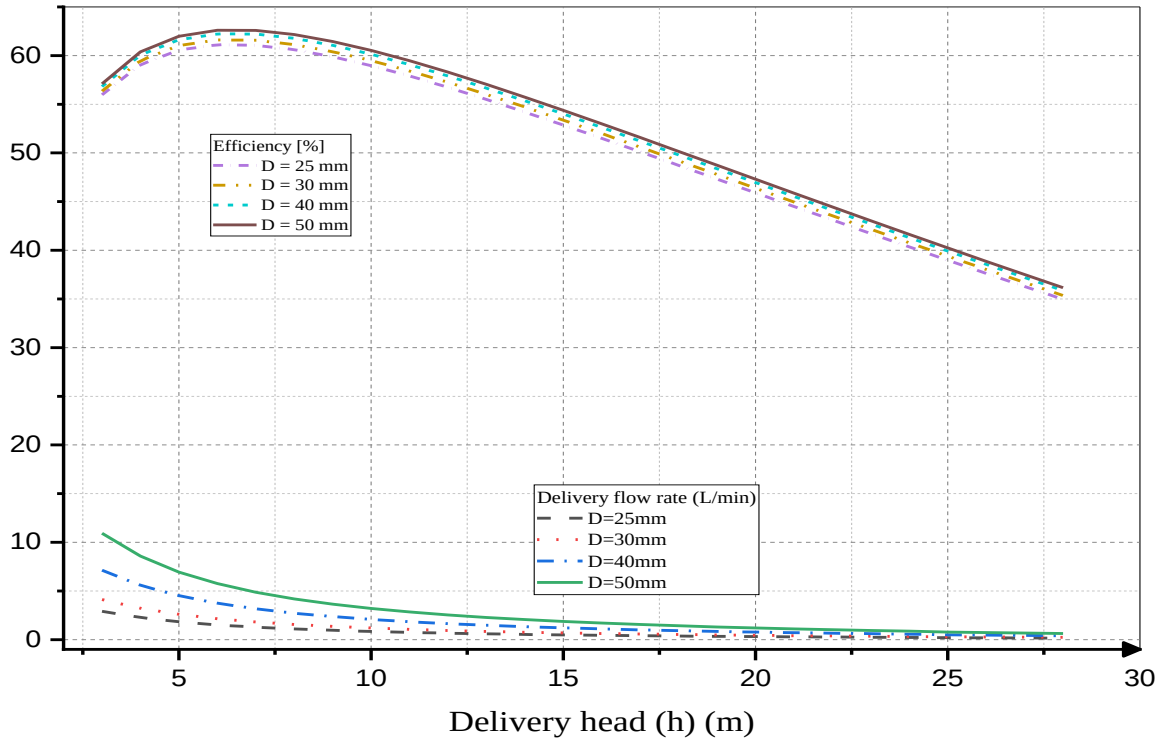

Figure 0.1 Performance of regular hydraulic ram pump at 2m supply head drive pipe length 5 m.

The performance of the pump is optimum when the delivery head is three times of the supply head. From this performance curve, delivery head and delivery flow are inversely related to each other. The figure in the next page follows similar pattern with the performance of the pump illustrated in figure 8.1.

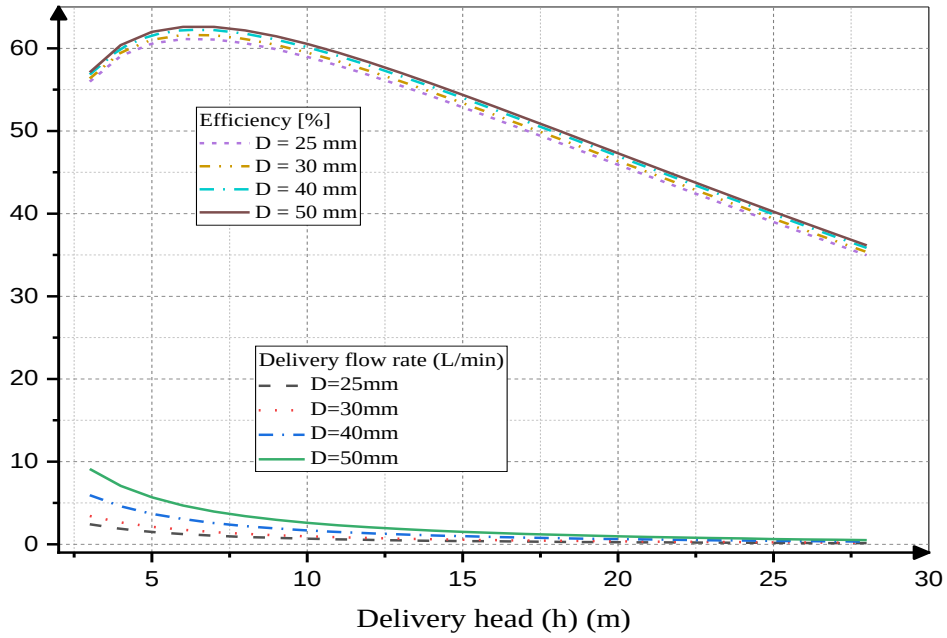

(a)

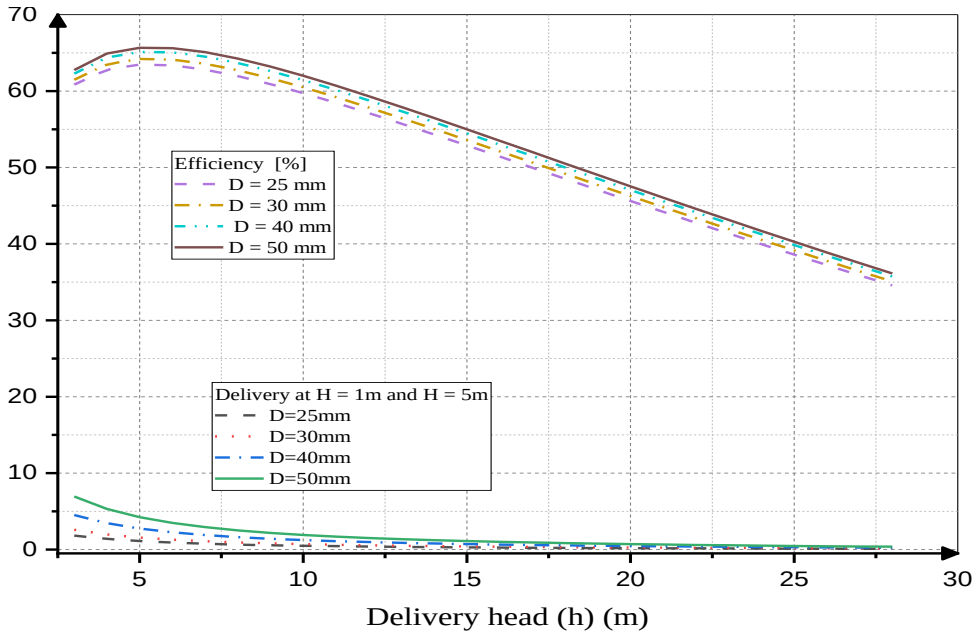

(b)

Figure 0.2 Performance of regular hydraulic ram pump simulated with different diameter of drive pipe (a) at supply head of 1.5m and (b) at supply head of 1m

1.31.2 Analytical Results and CFD Simulation of Thermal Infusion

Analytical and CFD simulation results are presented in this section. Figure 8.3 gives water hammer pressure profile during pumping period (discussed in section 3.2.3) for the pump predicted at a supply head of 2 m above it. The pressure in the chamber increased with time until the delivery valve begins to open. But in short time interval the delivery valve begins to open and impulse valve closed. The opening of the delivery valve allows pumping of water collected in the pressure chamber proportional to pressure gained through water hammer by the air. When the water pushed up the compressed air relaxed and the pressure drop back to the original state. This periodical opening and closing of the valves admit normal functioning of regular ram pump.

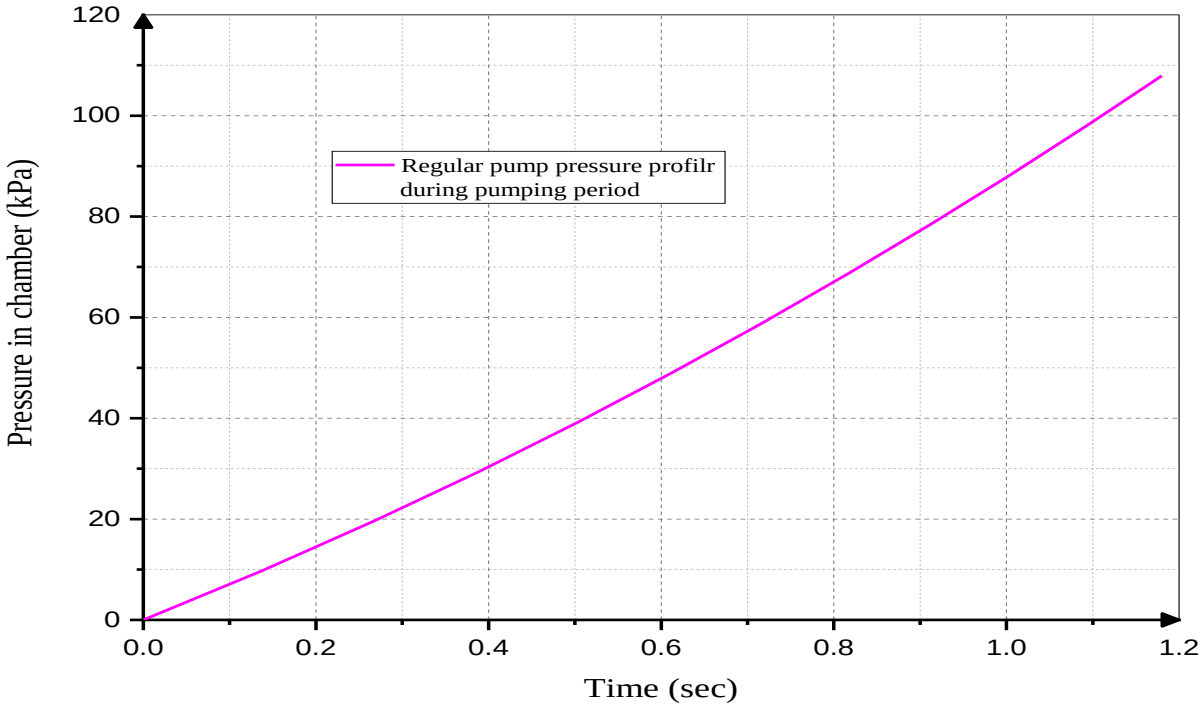

Figure 0.3 Pumping period characteristic of regular pump constructed from drive pipe diameter of 25 mm

The graph shown in figure 8.4 is pressure inside the chamber varies with time. This pressure was gained by temperature difference created in the gases mixture due to heat addition around wall of the chamber. The first section of the graph indicates pressure rise linearly with time during the visible heat addition process. In the beginning of evaporation pressure drop and later increases slowly with time. The pressure drop indicates the specific volume of the gas mixture starts to increase but

gradually the specific volume decrease results increasing of pressure. From this analytical computation, a pressure up to 35 kPa can be achieved by supplying heat source having a temperature 150 ^{o}C around the chamber.

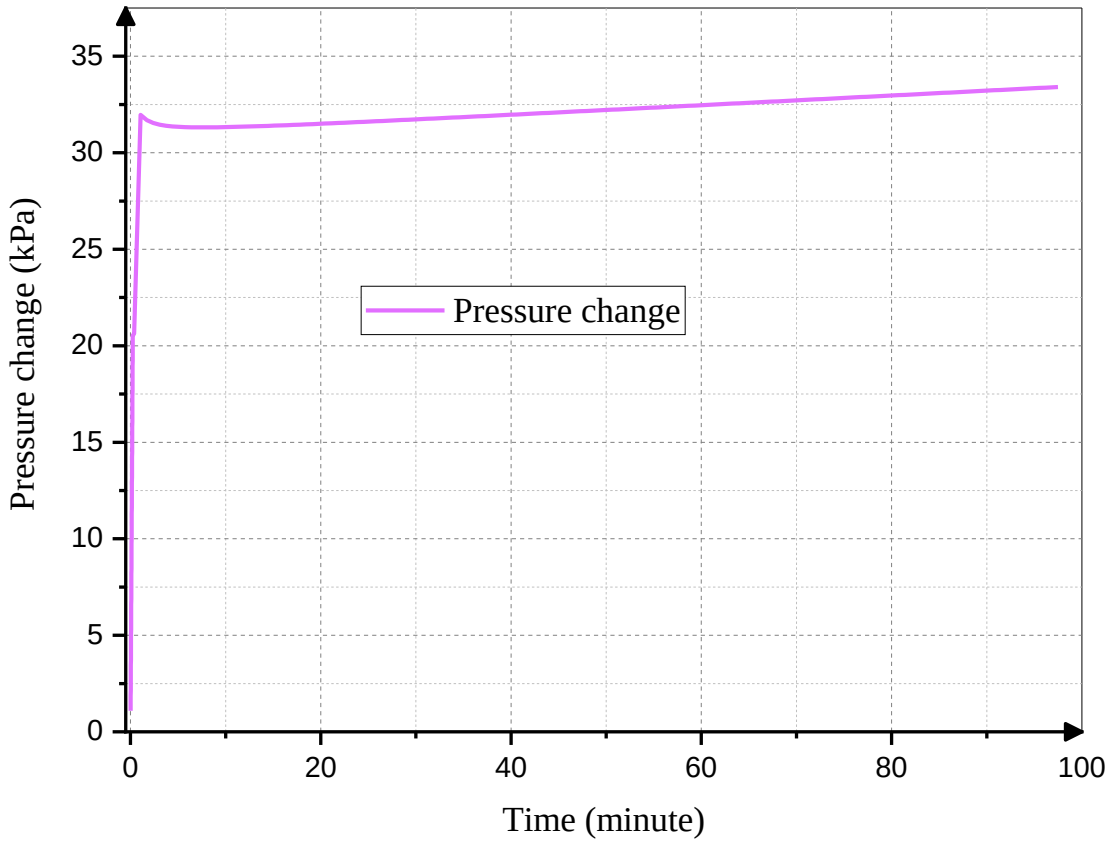

Figure 0.4 Analytical solution of the thermal signature

Computational fluid dynamics (CFD) simulation of the thermal effect provides similar pressure profile with the analytical result. As mentioned before, while the air becomes hot the pressure increased linearly until evaporations starts. When the gases water interface reaches saturation temperature, evaporation process begins at the surface of the water (see figure 6.7). At this point like the analytical result, as shown in figure 8.5 pressure starts to drop in CFD simulation. Unlike the analytical result, in the computational fluid dynamic (CFD) simulation pressure becomes steady with time. The comparison of the pressure obtained by analytical and CFD via heat addition process are presented in figure 8.6.

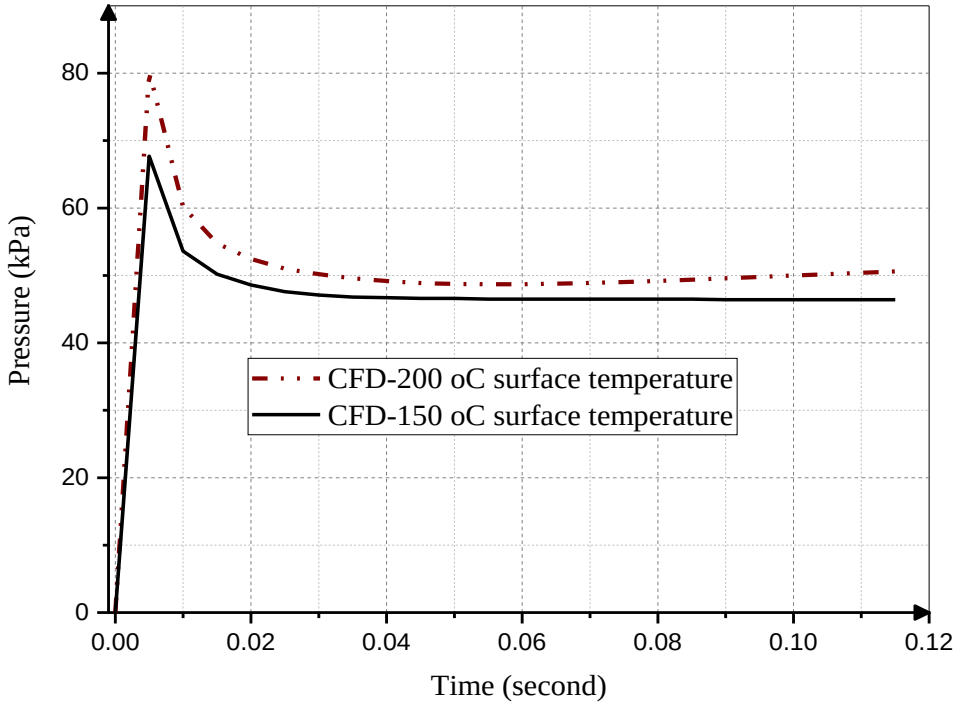

Figure 0.5 CFD simulation result of thermal infusion effect

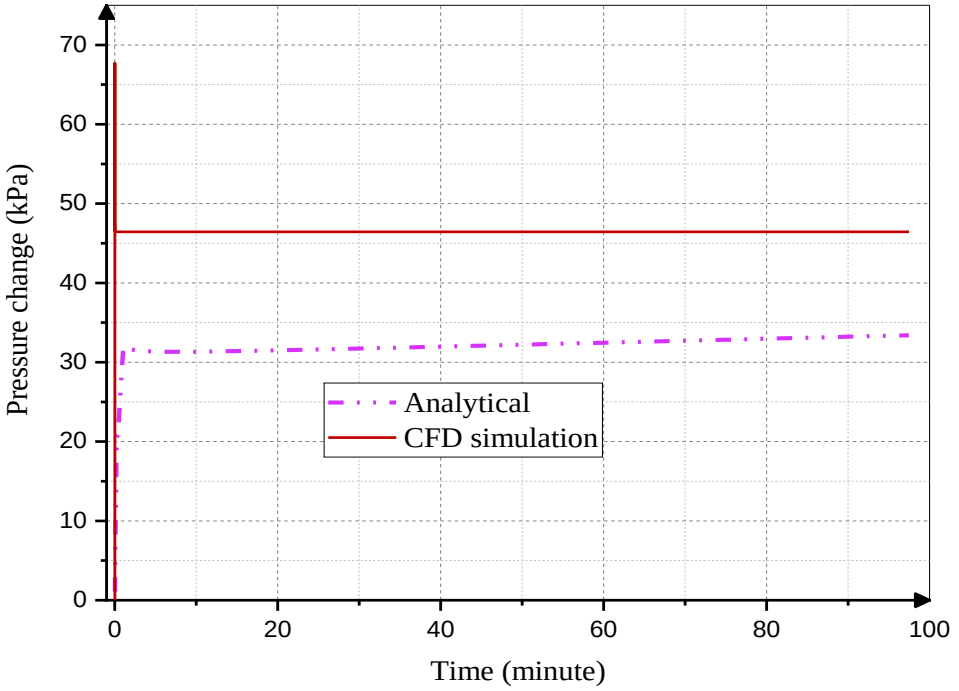

Figure 0.6 Comparison of analytical and CFD simulation

The large difference of pressure between analytical and CFD simulation may arise from the conservative assumption of the specific heat of water vapor as an ideal gas. Because ideal gas is the lower limit properties of a real gas.

1.31.3 Experimental Test Result

The results obtained in the experimental investigation can be summarized as follows. The following chart gives a comparison of two different runs with an approximate inlet flow rate of 34 liters per minute. The results show an amazing effect of temperature on pressure created by hammering within the chamber. By heating the air in the chamber with minor phase change process, pressure was increased from 175 kPa in normal operating condition to above 325kPa. The figure presented below illustrates the non-thermal and thermal infusion test performance of hydram.

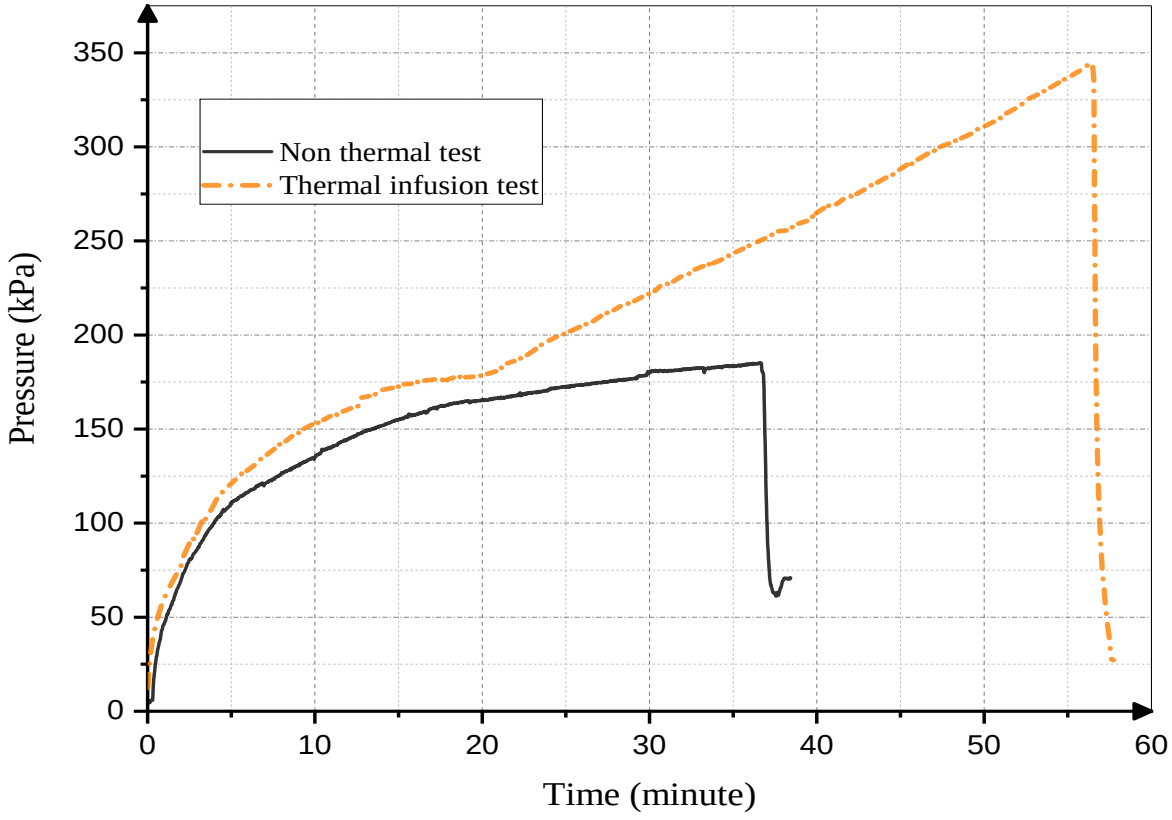

Figure 0.7 Pressure chamber comparison of non-thermal and thermal infusion ram pump performance

Measurement of flow rate at the exit of the ram pump proves that, outlet flow rate reaches 17 liters per minute from maximum flow rate of 11 liters per minute in the normal operating condition. This performance increment of hydram was obtained by simple heat addition process.

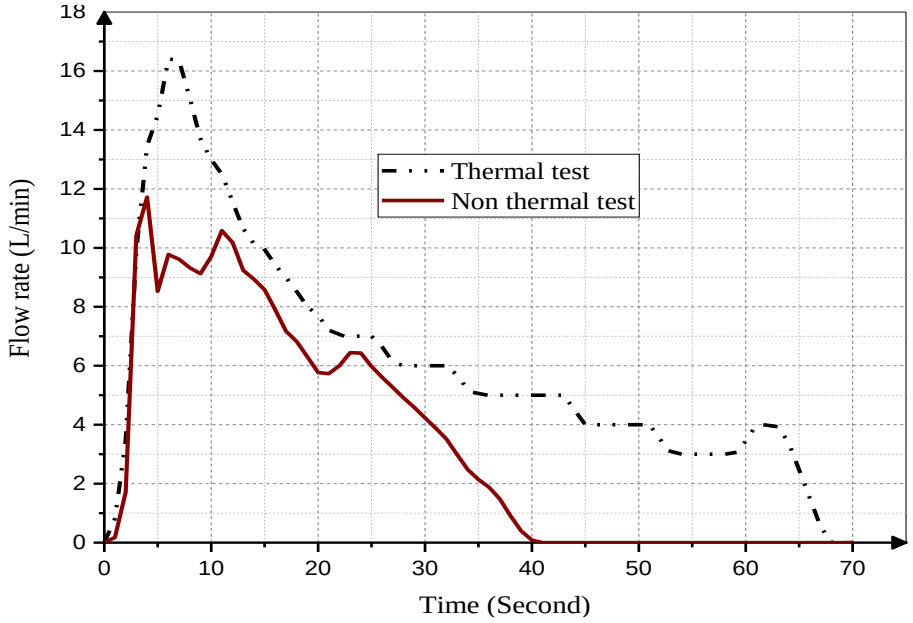

Figure 0.8 Exit flow rate comparison of non-thermal and thermal infusion ram pump

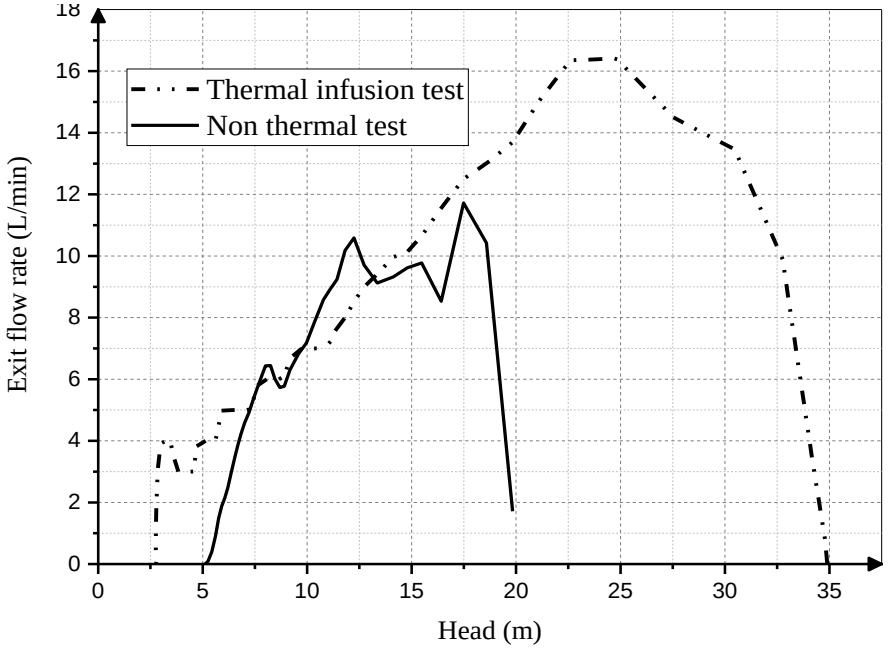

Figure 0.9 Pump capacity comparison of non-thermal and thermal infusion condition

From the chart given in figure 8.9, the maximum outlet flow rate is around 11 liters per minute with possible maximum head of 17 m. However, thermally assisted hydram the exit flow rate reaches to 16 liters per minute with head of about 23 m for similar source flow for the pumps.

1.32 Comparison of Analytical, CFD and Experimental Results

Both analytical and CFD results of the thermal effect combined with the regular pump system performance provide the feature of the solar-assisted hydraulic ram pump. Comparison of the simulation result with the experimental result have almost nearly the same feature. From this research it can be conclude that heating the air inside the chamber by adding a heat source around the chamber increases the performance of the regular pump. The graph of both analytical and CFD simulation in the figure 8.10 was generated by adding maximum hammer pressure predicted by Eq.(2.2) with the pressure obtained by thermal effected given in figure 8.6.

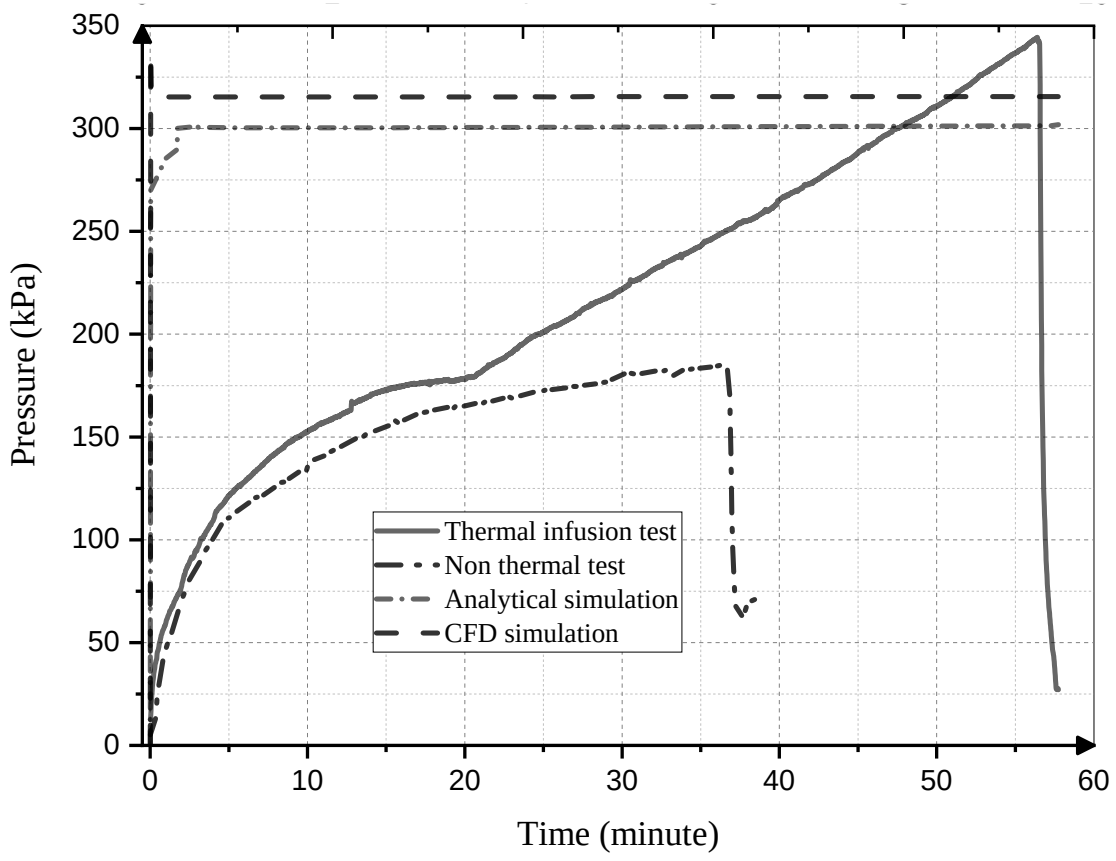

Figure 0.10 Comparison analytical, CFD simulation and experimental results of pump performance

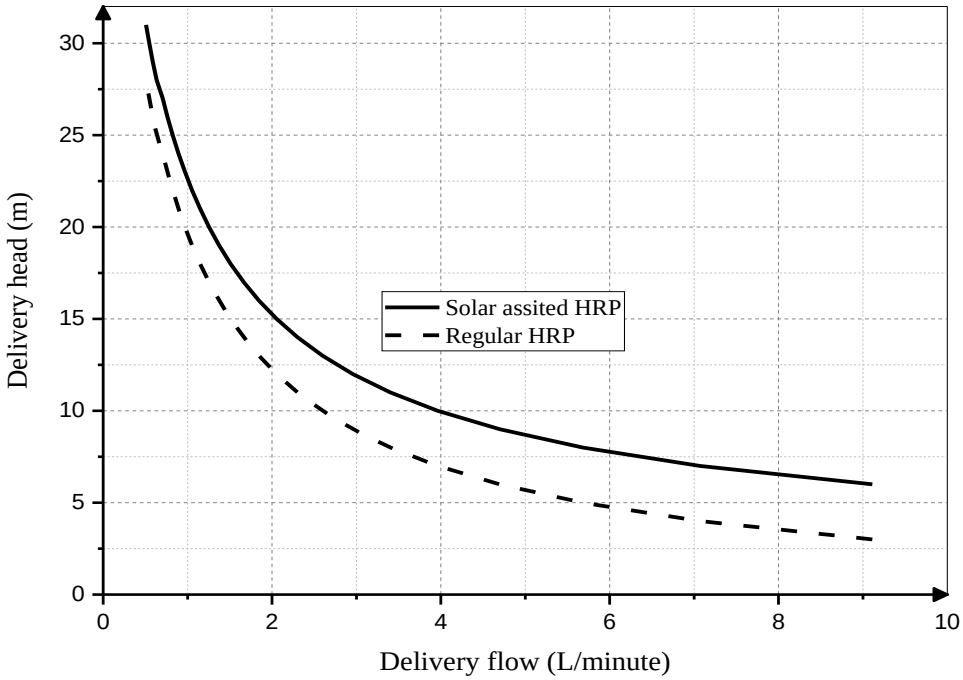

Figure 0.11 Performance comparison of solar assisted and regular HRP

The result presented in Figure 8.11 was obtained by adding the minimum delivery head generated by temperature change. The minimum head is the result obtained from analytical calculation which is 3m. From this study addition of temperature on the gas can improve the delivery head of regular hydraulic ram pump at least by 3m as discussed on Figure 8.11.

1.33 Incident Solar Radiation on the Collector

The average total solar radiation incident on the surface of the collector was estimated based on the above empirical relations and sun-earth angles. As discussed in the previous section, the incident solar radiation on the surface of the collector is the sum of radiation streams including beam, diffuse, and reflected components. The following graph compares the average incident solar radiation on the collector surface $\left(I_T\right)$ and the mean global solar radiation $\left(I_H\right)$.

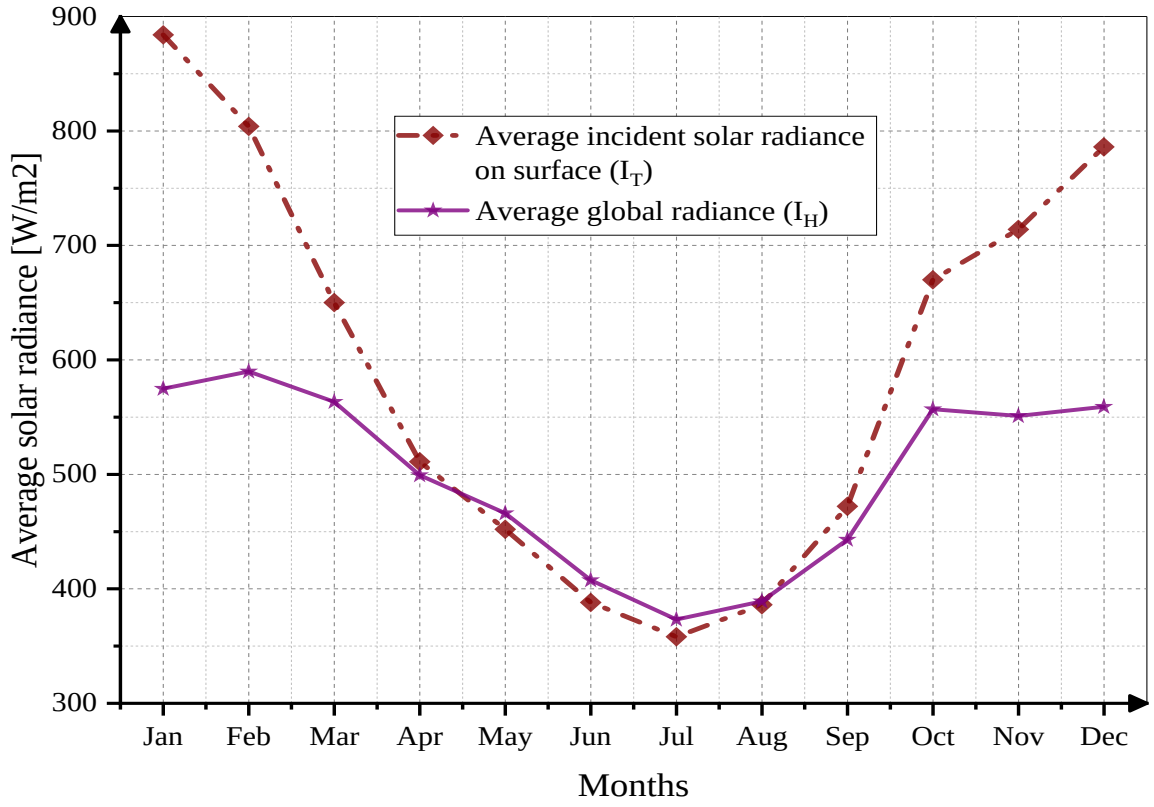

Figure 0.12 Average incident solar radiation (I_T) on the surface of a collector and global solar radiation (I_H)

The above graph depicts solar radiation is very weak during the summer season especially in June, July and August. On the contrary for the rest, the radiation is good to generate the desired temperature to heat the pressure chamber using ultra high vacuum (UHV) solar thermal collectors. The temperature of heat transferring fluid is shown in the following graphs on the next page.

1.33.1 Temperature of Heat Transferring Fluid

As described in Eq. (5.15) the performance of the solar thermal collector is dependent on the mean temperature difference of heat transferring fluid. The mean temperature profile of heat transferring fluid is estimated based on the solar radiation of Addis Ababa. Depending on the efficiency of the collector mean temperature difference is varying. When the efficiency of the collector becomes higher mean temperature difference is getting lower. Although at performance of collector is attractive while the efficiency is 30 – 50%. On this range of efficiency the mean temperature of the heat transferring fluid is on the range of 100 – 200 ^{o}C. This domain of mean temperature range can be used to heat the chamber.

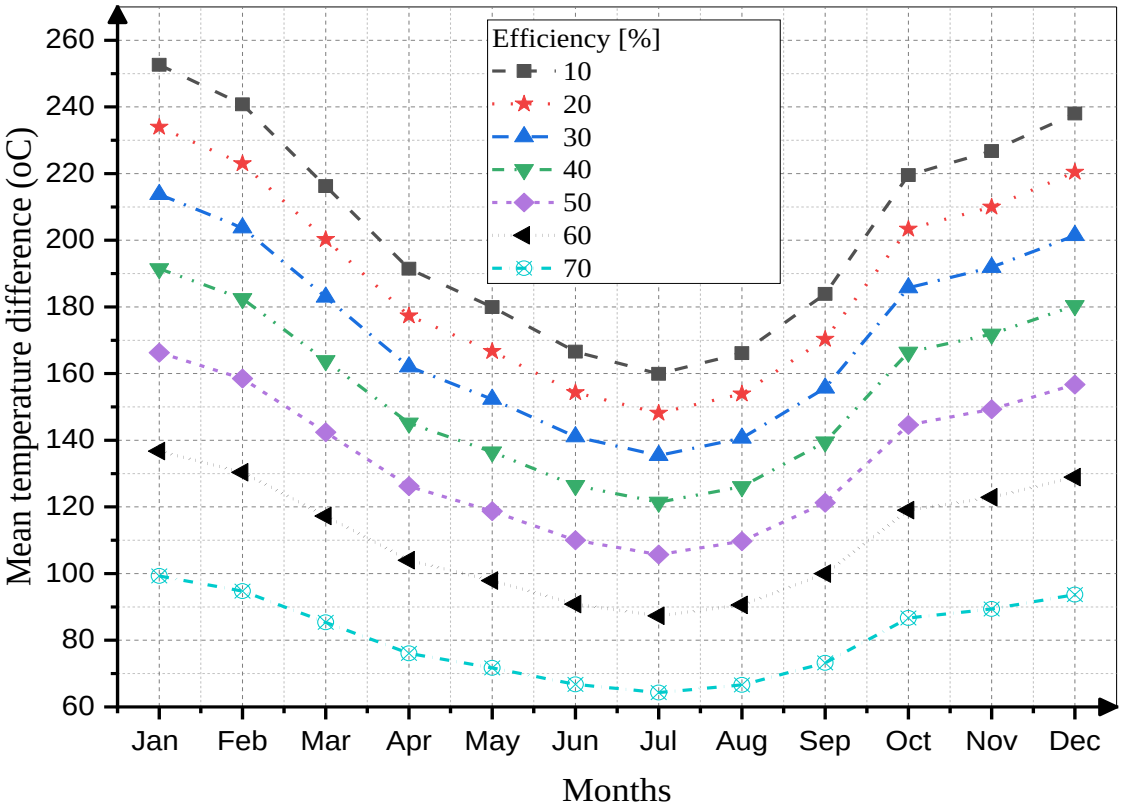

Figure 0.13 Mean temperature difference profile of the collector with various efficiency of the collector

The outlet temperature of heat transferring fluid is plotted in figure 8.12. The profile follow similar pattern with the mean temperature difference. On the selected range of temperature the exit temperature of the fluid can reach up to 300 ^{o}C.

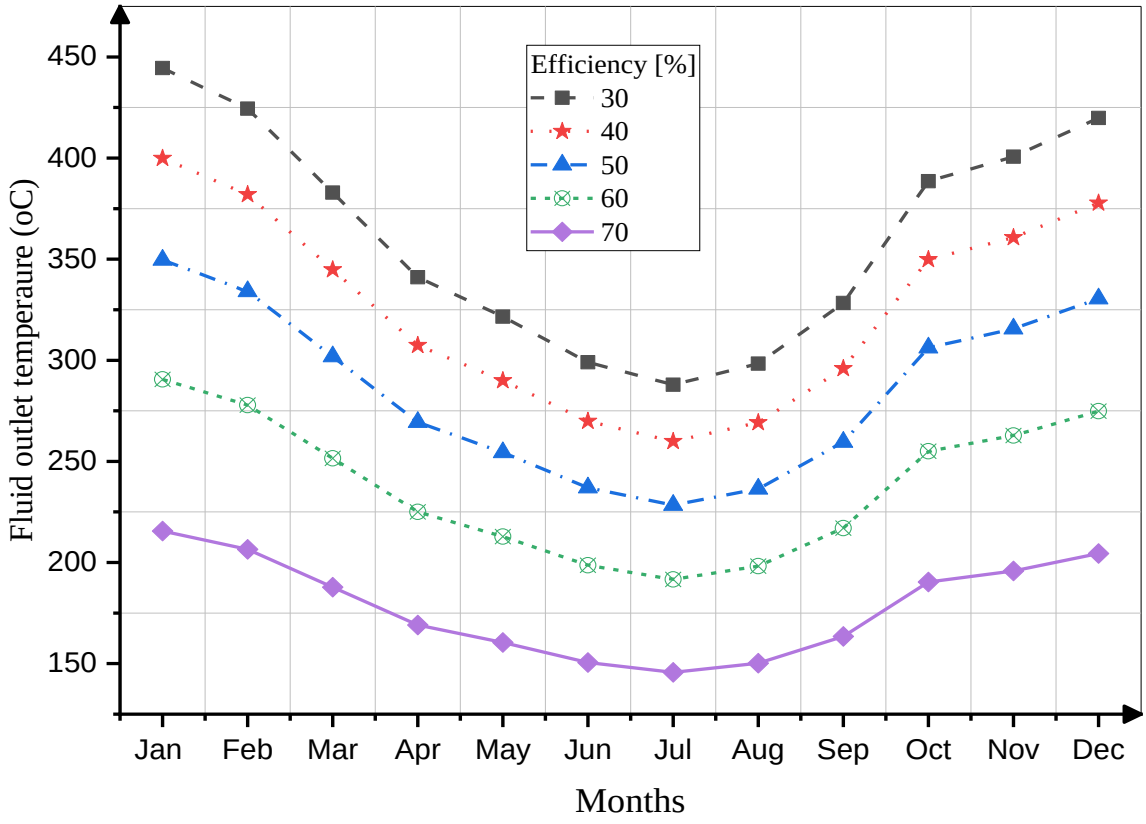

Figure 0.14 Fluid outlet temperature profile at the exit of the collector with various efficiency of a collector

1.34 Electrical Heater Selection

Based on Eq. (5.11) the minimum useful energy obtained from the collector with an efficiency of 50% and an aperture area of 1 m^2 is 179 W. It is estimated that at this operating condition collector has a mean plate temperature of around 158 ^oC. The minimum mean temperature difference of the fluid is about 100 ^oC. Thus controllable heat source that can generate a temperature of about 200 ^oC was selected. This controllable heater is applied on the chamber provided that the properties of wall material limits amount of heat to be applied on the chamber.

Conclusion and Recommendation

1.35 Conclusion

This work deals with the integration of the solar thermal system for the regular hydraulic ram pump to improve its performance. The approach to achieve the objective involves knowing the basic working principle of regular hydram and water hammer effect, data collection, synthesis with understanding of fundamental thermo-fluid and heat transfer principles, development of the mathematical model, CFD simulation of the thermal effect on the pressure chamber and experimental test.

Based on the analytical methodology, the performance of the regular hydraulic ram pump was designed and predicted. The prediction of the regular pump was good compared with the previously published works listed in the review section. The efficiency of well-designed hydram can reach up to 65% delivering around 5 liters per minute with the net head of 6m. The difference of the result is due to the difference of source flow. But if the ratio of the source flow rates for both analytical and experimental is considered, the result is similar. i.e., the ratio of source flow of experimental to analytical is 2.83 and ratio of exit flow rates is 2.48. The error becomes 12.2% by taking source flow rate as a reference.

Table 0.1 Non-thermal results comparison of ram pump

Parameters	Analytical solution	Experimental test
Maximum hammer pressure in the chamber [kPa]	268.4	183.33
Maximum exit flow rate [liters per minute]	4.72	11.72
Source flow [liters per minute]	12	34

The mathematical model gives a pressure change of 33 kPa and CFD predicts 50 kPa pressure raise for the applied constant temperature of 150 ^{o}C on the wall of the pressure chamber. Other parameters are given in table 9.2.

Table 0.2 Results of temperature effect on the chamber

Parameters	Thermal simulation	
	Analytical solution	CFD simulation
Maximum pressure in the chamber [kPa]	33	50
Maximum exit flow rate [liters per minute]	1.35	1.667
Source flow [liters per minute]	12	12
Maximum temperature of chamber [^{o}C]	150	145

The maximum pressure produced by a sudden closure of the impulse valve 268.4 kPa. This value was added with a pressure modeled by heat addition gave the character of a solar-assisted hydraulic ram pump as shown in Figure 8.11. The superposing method results in the maximum pressure inside the chamber is 300 kPa.

The experimental test, conducted at Santiago State University, indicates that the maximum pressure developed in the pressure chamber with thermal infusion was 330 kPa. This value is twice the maximum pressure developed through base hydram working under the ambient temperature. The temperature of the heat source was not more than 140 ^{o}C because the properties of the chamber made from copper limit the maximum temperature under the simulation temperature. The optimal discharge at the exit of the pump was 17 liters per minute for a thermally assisted pump. The discharge at the exit of the pump was increased by more than 5 liters per minute when contrasted with the thermal infusion test.

Table 0.3 Thermal assisted hydraulic ram pump results comparison

Parameters	Thermally assisted ram pump		Experimental test
	Analytical	CFD simulation	
Maximum pressure in the chamber [kPa]	301.4	318.4	342.32
Maximum exit flow rate [liters per minute]	6.07	6.387	16.41
Source flow [liters per minute]	12	12	34
Maximum temperature of chamber [^{o}C]	150	145	106.75
Maximum exit temperature [^{o}C]	17	17	26.00

From this research it can be concluded that, the performance of regular hydram can be increased by integrating with solar thermal system as shown by this work.

The power of solar radiation for Addis Ababa was investigated to know the solar thermal potential of the location. The lowest solar radiation occurs in July and its value is 350 watt per square meter. Ultra-high vacuum (UHV) collector was selected since it can generate mid-range temperature. A minimum means temperature difference of 110 ^{o}C obtained with a collector efficiency of 50%. With the UHV collector fluid outlet temperature, 225 ^{o}C can be produced during July. Therefore based on this thesis, it can be possible to build a novel hydraulic ram pump combining with a solar thermal system to increase the efficiency of the old pump.

1.36 Recommendation and Future Works

This study creates a foundation and should be thought of as a starting point for further investigation and research works. For the future, this combined system needs more attention to commercialize it. Among the research conducted to improve the performance of the regular hydraulic ram pump through combined system this thermal assisted ram pump open a way for future investigation. The following activities are suggested to be done for the future.

- This work identifies the effect of temperature on the performance of regular hydram. It is suggested to study the performance of the pump in detail experimentally.
- Developing better mathematical formulation and numerical model to analyze the performance of the hydram
- Field work study of the solar thermal system by integrating the collector with the base hydram.

References

[1] M. Suarda, A. Ghurri, M. Sucipta, and I. G. B. W. Kusuma, "Investigation on characterization of waste valve to optimize the hydraulic ram pump performance," *AIP Conf. Proc.*, vol. 1984, no. July, 2018, doi: 10.1063/1.5046607.

[2] K. Yang, J. Li, Y. Guo, X. Guo, H. Fu, and T. Wang, "Design and hydraulic performance of a novel hydraulic ram pump," *11th Int. Conf. Hydroinformatics*, p. 10, 2014.

[3] E. J. Schiller and P. O. Kahangire, "An experimental investigation and design of hydraulic ram pump," *Int. J. Dev. Technol.*, vol. 2, no. 3, pp. 173–183, 1984.

[4] H. N. Najm, P. H. Azoury, and M. Piasecki, "Hydraulic ram analysis: a new look at an old classic," *Proc Instn Mech Engrs*, vol. 213 Part A, no. 1, p. 15, 1999, doi: 10.1177/026765838900500102.

[5] B. W. Young, "Generic design of ram pumps," *Proc Instn Mech Engrs*, vol. 212 Part P, no. 2, pp. 117–124, 1998, doi: 10.1243/0957650981536646.

[6] S. B. Watt, "A manual of information on the automatic hydraulic ram for pumping water," National College of Agricultural Engineering, Silsoe, Bedford, MK45 4DT, U.K., 1974.

[7] X. Guo *et al.*, "Optimal design and performance analysis of hydraulic ram pump system," *Proc. Inst. Mech. Eng. J. Power Energy*, vol. 232 Part A, no. 7, pp. 841–855, 2018, doi: 10.1177/0957650918756761.

[8] J. Krol, "The Automatic hydraulic ram," *Proc. Inst. Mech. Eng.*, vol. 165, no. 1, pp. 53–73, 1951, doi: 10.1243/pime_proc_1951_165_011_02.

[9] M. Inthachot, S. Saehaeng, J. F. J. Max, J. Müller, and W. Spreer, "Hydraulic ram pumps for irrigation in Northern Thailand," *Agric. Agric. Sci. Procedia*, vol. 5, pp. 107–114, 2015, doi: 10.1016/j.aaspro.2015.08.015.

[10] M. N. Harith, R. A. Bakar, D. Ramasamy, and M. Quanjin, "A significant effect on flow analysis & simulation study of improve design hydraulic pump," *IOP Conf. Ser. Mater. Sci. Eng.*, vol. 257, no. 1, 2017, doi: 10.1088/1757-899X/257/1/012076.

[11] A. Roberts, B. Thomas, P. Sewell, and E. Hoare, "Generating renewable power from water hammer pressure surges," *Renew. Energy*, vol. 134, pp. 1392–1399, 2019, doi: 10.1016/j.renene.2018.09.006.

[12] J. Tacke and C. Verspuy, "Hydraulic rams," in *Hydraulic rams*, Delft University of

Technology, 1989.

[13] Clemson, “Home-made Hydraulic Ram Pump,” vol. 00. USA, pp. 1–8, 2005.

[14] S. Karekezi *et al.*, “The potential contribution of non-electrical renewable Energy technologies (RETs) to poverty reduction in East Africa,” Nairobi, Kenya, 2005.

[15] D. F. Maratos, “Technical feasibility of wavepower for seawater desalination using the hydro-ram (Hydram),” *ELSEVIER*, vol. 153, no. 1–3, pp. 287–293, 2003, doi: 10.1016/S0011-9164(02)01148-7.

[16] M. Adil, A. Khan, M. A. Arshad, M. S. Aslam, R. Zafar, and Samiullah, “Low cost water pumping for sustainable irrigation using renewable energy based ram pump,” in *5th International Mechanical Engineering Congress*, 2015, p. 6.

[17] T. H. Thomas, “Algebraic modelling of the behaviour of hydraulic ram-pumps,.” Development Technology Unit, Department of Engineering, University of Warwick, Coventry CV4 7AL UK, p. 26, 1994.

[18] E. J. Schiller, “Proceedings of a workshop on hydraulic ram pump (hydram) technology held at Arusha, Tanzania, May 29 - June 1, 1984,” Arusha, Tanzania, 1985.

[19] CA. Foragebeef, “Water-powered water pumping systems for livestock watering,” *Agric. Agro-Food Canada*, pp. 1–5, 2003.

[20] M. Otoo, N. Lefore, P. Schmitter, J. Barron, and G. Gebregziabher, “Business Model Scenarios and Suitability: Smallholder Solar Pump-based Irrigation in Ethiopia,” 2018.

[21] D. M. Machado and L. Paglietti, “Ethiopia Irrigation market brief,” *Food Agric. Organ. United Nations*, 2015.

[22] P. B. M. Glover, “Computer simulation and analysis methods in the development of the hydraulic ram pump,” University of Warwick, 1994.

[23] L. C. Rennie and E. A. Bunt, “The automatic hydraulic ram experimental results,” *Proc. Inst. Mech. Eng. Part A J. Power Energy*, vol. 204, no. 1, pp. 23–31, 2007,

[24] B. W. Young, “Design of hydraulic ram pump systems,” *Proc. Inst. Mech. Eng. Part A J. Power Energy*, vol. 209, no. 4, pp. 313–322, 1995

[25] H. W. Dickinson, “Early years of the hydraulic ram,” *Trans. Newcom. Soc.*, vol. 17, no. 1, pp. 73–83, 1936, doi: 10.1179/tns.1936.005.

[26] W. M. Lansford and W. G. Dugan, “An analytical and experimental study of the hydraulic

ram," *Engineering Experiment Station Bulletin Series*, vol. 38, no. 22. p. 78.

[27] C. Verspuy and A. S. Tijsseling, "Hydraulic ram analysis," *J. Hydraul. Res.*, vol. 31, no. 2, pp. 267–278, 1993, doi: 10.1080/00221689309498849.

[28] A. Rajaonison and H. T. Rakotondramiarana, "Theoretical study of the behavior of a hydraulic ram pump with springs system," *Am. J. Fluid Dyn.*, vol. 9, no. 1, pp. 1–12, 2019, doi: 10.5923/j.ajfd.20190901.01.

[29] P. B. Shende, D. S. K. Choudhary, and A. P. Ninawe, "Analysis and enhancement of hydraulic ram pump using computational fluid dynamics (CFD)," *Int. J. Innov. Res. Sci. Technol.*, vol. 2, no. 3, pp. 109–133, 2015.

[30] M. Basfeld and E. A. Müller, "The hydraulic ram," *Forsch. im Ingenieurwes.*, vol. 50, no. 5, pp. 141–147, 1984, doi: 10.1007/BF02560600.

[31] H. W. Iversen, "An analysis of the hydraulic ram," *J. Fluids Eng.*, vol. 97, no. 2, p. 191, 2010, doi: 10.1115/1.3447251.

[32] D. Sarma, M. Das, B. Brahma, D. Pandwar, S. Rongphar, and M. Rahman, "Investigation and parameter optimization of a hydraulic ram pump using Taguchi method," *J. Inst. Eng. Ser. C*, vol. 97, no. 4, pp. 551–559, 2016, doi: 10.1007/s40032-016-0295-0.

[33] G. Viccione, N. Immediata, R. Cava, and M. Piantedosi, "A preliminary laboratory investigation of a hydraulic ram pump," *Proceedings*, vol. 2, no. 687, p. 7, 2018, doi: 10.3390/proceedings2110687.

[34] R. N. Mbiu, S. M. Maranga, and M. Mwai, "Performance testing of hydraulic ram pump," *Proc. Sustain. Res. Innov. Conf.*, no. May, pp. 6–8, 2015.

[35] S. Saito, M. Takahashi, and Y. Nagata, "Effects of the air volume in the air chamber on the performance of water hammer pump system," *Int. J. Fluid Mach. Syst.*, vol. 4, no. 2, pp. 255–261, 2011, doi: 10.5293/ijfms.2011.4.2.255.

[36] R. Fatahi-Alkouhi, B. Lashkar-Ara, and A. Keramat, "On the measurement of ram-pump power by changing in water hammer pressure wave energy," *Ain Shams Eng. J.*, no. xxxx, pp. 1–13, 2019, doi: 10.1016/j.asej.2019.05.001.

[37] B. W. Young, "Simplified analysis and design of the hydraulic ram pump," *Proc. Inst. Mech. Eng. Part A J. Power Energy*, vol. 210, no. 4, pp. 295–303, 1996,

[38] E. J. Schiller and P. Kahangire, "Analysis and computerized model of the automatic hydraulic

ram pump," *Can. J. Civ. Eng.*, vol. 11, no. 4, pp. 743–750, 1984, doi: 10.1139/l84-093.

[39] T. W. Choon, L. K. Aik, L. E. Aik, and T. T. Hin, "Investigation of water hammer effect through pipeline system," *Int. J. Adv. Sci. Eng. Inf. Technol.*, vol. 2, no. 3, p. 246, 2012, doi: 10.18517/ijaseit.2.3.196.

[40] Bergeron, "Beliers hydrauliques, hydraulics machinery." p. 23, 1928.

[41] B. R.Munson, D. F. Young, T. H. Okiishi, and W. W. Huebsch, *Fundamentals of Fluid Mechanics*, 6th Editio. USA: Don Flowley, 2009.

[42] J. V. Ballun, "A methodology for predicting check valve slam," *J. / Am. Water Work. Assoc.*, vol. 99, no. 3, pp. 60–65, 2007, doi: 10.1002/j.1551-8833.2007.tb07888.x.

[43] B. E. Dallstream, B. A. Fricke, and B. R. Becker, "Swing check valve design criteria and CFD validation," *Int. Conf. Nucl. Eng. Proceedings, ICONE*, vol. 2006, no. July, 2006, doi: 10.1115/ICONE14-89827.

[44] T. Bulletin, "Design and selection of check valves." Val-Matic and Mfg. Corp, p. 17, 2012.

[45] N. S. M. Hussin *et al.*, "Design and analysis of hydraulic ram water pumping system," *J. Phys. Conf. Ser.*, vol. 908, no. 1, 2017, doi: 10.1088/1742-6596/908/1/012052.

[46] E. W. Anderson, "Hydraulic rams," *Inst. Mech. Eng.*, no. 274, pp. 337–355, 1989.

[47] "Air-Pressure-At-Altitude-Calculator @ Www.Mide.Com." .

[48] M. J. Moran, H. N. Shapiro, D. D. Boettner, and M. B. Bailey, *Fundamentals of engineering thermodynamics*, 8th ed. United States of America: Don Flowley, 2014.

[49] H. Yeung, "Mathematical models of air vessels for pressure transient control in water pipelines- A review," no. February, pp. 1–7, 2014.

[50] Y. a. Çengel, "Thermodynamics: An Engineering Approach," *McGraw-Hill*. 2004.

[51] S. Van Der Zwan, M. Toussaint, A. Alidai, I. W. M. Pothof, and P. H. Leruth, "Thermodynamics of surge vessels," in *BHR Group - 12th International Conference on Pressure Surges*, 2016, no. November, pp. 713–727.

[52] H. R. Graze, "A Rational thermodynamic equation for air chamber design," in *Third Australasian Conference on Hydraulics and Fluid Mechanics*, 1968, pp. 57–61.

[53] S. Bertolucci, B. Bressan, F. Caspers, Y. Garb, A. Gross, and S. Pauletta, "CERN-OPEN-2014-054.pdf," in *The BGU/CERN Solar Hydrothermal Reactor*, 2014, pp. 1–6.

[54] R. Z. Wang, M. Li, Y. X. Xu, and J. Y. Wu, "An energy efficient hybrid system of solar

powered water heater and adsorption ice maker," *Sol. Energy*, vol. 68, no. 2, pp. 189–195, 2000, doi: 10.1016/S0038-092X(99)00062-6.

[55] M. Günther and R. Shahbazfar, "Advanced CSP teaching materials," Wilhelmshöher, 2011.

[56] R. Kempener, G. Simbolotti, and G. Tosato, "Solar heat for industrial processes technology brief," *Int. Renew. Energy Agency Energy Technol. Syst. Anal. Program.*, vol. 21, pp. 1–40, 2015.

[57] B. Lande, J. Santos, and J. Nunes, "CERN ' s Ultra High Vacuum Flat Plate Solar Collector (UHVFPC) Markets and Applications," no. November. European Organization for Nuclear Research, 2008.

[58] K. Chatzichristos, "Applicability of the solar thermal Ultra High Vacuum collector for heating , cooling and power generation," Eindhoven University of Technology Stan Ackermans Institute, 2014.

[59] "Solar thermal collectors - Nordic Folkecenter," no. 877. SunMaxx Solar Inc, 15 Catherwood Rd, Ithaca, NY 14850 USA Ph:, pp. 1–56.

[60] Wawan, "Imgres @ Www.Google.Com." [Online]. Available:

[61] L. Merino, E. Antaluca, B. Akinoglu, and B. Beckers, "Solar energy inputs estimation for urban scales applications," in *8th International Conference on System Simulation in Buildings, Liege*, 2010, vol. 1, no. 1, pp. 1–15.

[62] S. A. M. Maleki, H. Hizam, and C. Gomes, "Estimation of hourly, daily and monthly global solar radiation on inclined surfaces: Models re-visited," *Energies*, vol. 10, no. 1, 2017, doi: 10.3390/en10010134.

[63] J. A. Duffie and W. A. Beckman, *Solar engineering of thermal processes*, 4th ed. Solar Energy Laboratory University of Wisconsin-Madison: John Wiley and Sons, Inc.,.

[64] V. Shemelin and T. Matuska, "Detailed Modeling of Flat Plate Solar Collector with Vacuum Glazing," *Int. J. Photoenergy*, vol. 2017, 2017, doi: 10.1155/2017/1587592.

[65] L. R. Arana, S. B. Schaevitz, A. J. Franz, M. A. Schmidt, and K. F. Jensen, "A microfabricated suspended-tube chemical reactor for thermally efficient fuel processing," *J. Microelectromechanical Syst.*, vol. 12, no. 5, pp. 600–612, 2003, doi: 10.1109/JMEMS.2003.817897.

[66] I. Iparraguirre *et al.*, "Solar Thermal Collectors for Medium Temperature Applications: A

Comprehensive Review and Updated Database," *Energy Procedia,* vol. 91, pp. 64–71, 2016, doi: 10.1016/j.egypro.2016.06.173.

[67] H. Song, W. Zhang, Y. Li, Z. Yang, and A. Ming, "Simulation of the vapor-liquid two-phase flow of evaporation and condensation," *Intrnational J. Hrat Technol.*, vol. 34, no. 4, pp. 663–670, 2016, doi: 10.18280/ijht.340416.

[68] "www.afs.enea.it." [Online]. Available: https://www.afs.enea.it

Appendices

Appendix-A: Properties of Material and Constants

Appendix A-1: Drive pipe specification.

Nominal diameter (mm)	Outside diameter (mm)	Internal diameter (mm)
32	31.75	26.95

Appendix A-2: The friction loss factor of valves and different pipe fittings

SN	Valves and fitting components	Equivalent length	Friction loss factor K_L	Condition
1	Gate valve	8	0.15	Fully open
2	Socket	--	0.08	---
3	Elbow	20	0.7	Long radius 90 threaded
4	Swing check valve	100	2	Forward flow
5	Tee	20	0.9	Line flow threaded
6	Entrance loss	--	1	---

Appendix-A: 3 Slam velocity and level of slam [42]

S.N	**Valve type**	**Valve closing velocity (m/s)**	**Level of slam**
1	Silent check valve	0.06	None
2	Resilient hinge check valve with spring	0.09	None
3	Tilted disc check valve	0.09	None
4	Resilient hinge check valve	0.26	Mild
5	Ball check valve	0.61	Sever
6	Swing check valve	0.61	Sever

Appendix-A: 4 Swing check valve specification

Size (in)	Diameter nominal (mm)	A	B	K_v value
½	15	60	42	5.8
3/4	20	70	48	7.1
1	25	80	54	23
1 1/2	40	100	70	82
2	50	110	80	93

Appendix A-5: Optical parameters of ultra-high vacuum (UHV) collector

Collector configuration	η_0	a_1 [w/m^2.K]	a_2 [w/m^2.K^2]
Bare (without mirror)	0.811	0.53	0.0095

Appendix A-6: Properties of liquid, air and vapor

Properties	Water liquid	Air
Density [kg/m^3]	998.2	1.225
C_p [J/kg-K]	4182	1006.43
Thermal conductivity [W/m-K]	0.6	0.0242
Viscosity [kg/m-s]	0.001	1.79e^{-5}

Appendix A-7: Types of Instrumentation used for the experiment

Instrumentation	Number of instruments used
Twidec NPT ¼ inch Type k Thermocouple	2
Twidec NPT ½ inch Type k Thermocouple	1
Bourns 0-500 Psi Pressure Transducer	1
DIGITEN G3/4" Water Flow Hall Sensor	1

Appendix B: Summary of Experimental Test Results

Appendix B-1: Non-Thermal Run Test Card

Date of test	4/22/2020
Name of tester	Dan Inocencio
Test duration	38:24

Supply height (m)	2.18
Delivery height (m)	7.62

Notes	
Time – 36:30	Gate valve opened
Max outlet flow (L/min)	11.72
Max pressure (kpa)	185
Max Temp – chamber (oC)	28.25
*Not able to fully open gate valve	

Initial conditions	
Inlet temp (^oC)	22
Outlet temp (^oC)	22
Pressure chamber (kPa)	5.1
Temperature (internal chamber) (^oC)	26.87

Final conditions	
Inlet temp (^oC)	20.5
Outlet temp (^oC)	22.25
Pressure – chamber (kPa)	70.87
Temperature (internal chamber) (^oC)	26.75

Time (minute)	Temperature – internal chamber (^oC)	Pressure – chamber (kPa)	Inlet temp (^oC)	Outlet temp (^oC)	Inlet flow rate (L/min)	Outlet flow rate (L/min)
1	27	64.81	21.37	21.87	34	0
5	28.25	110.04	20.63	21.87	34	0
10	28.12	135.21	20.37	22.13	34	0
15	27.88	154.86	20.5	22.25	34	0
20	27.6	165.27	20.55	22.35	34	0
25	27.5	172.51	20.36	22.64	34	0
30	27.64	179.75	20.22	22.86	34	0
35	27.5	183.33	20.15	23.50	34	0
36.8	27.12	171.89	20.50	23.50	34	11.72
37.45	26.45	62.54	20.35	22.5	34	0.000473

Appendix B-2: Thermal Run Test Card

Date of test	4/22/2020
Name of tester	Dan Inocencio
Test duration	57:43

Supply height (m)	2.18
Delivery height (m)	7.62

Notes	
Time – 36:30	Gate valve opened
Max outlet flow (L/min)	16.41
Max pressure (kPa)	344.1534
Max Temp – chamber (°C)	106.75
*Not able to fully open gate valve	

Initial conditions	
Inlet temp (°C)	21.63
Outlet temp (°C)	23.87
Pressure chamber (kPa)	12.4
Temperature (internal chamber) (°C)	28

Final conditions	
Inlet temp (°C)	20.5
Outlet temp (°C)	73.75
Pressure – chamber (kPa)	27
Temperature (internal chamber) (°C)	93

Time (minute)	Temperature – internal chamber (°C)	Pressure – chamber (kPa)	Inlet temp (°C)	Outlet temp (°C)	Inlet flow rate (L/min)	Outlet flow rate (L/min)
1	28.51	60.19	21.50	23.76	34	0
5	29.00	121.41	20.25	23.98	34	0
10	29.00	152.44	20.44	24.25	34	0
15	29.12	172.44	20.75	24.38	34	0
20	28.56	178.09	20.10	24.64	34	0
25	42.09	200.98	19.91	24.84	34	0
30	60.00	221.87	20.09	25.09	34	0
35	73.75	242.90	20.25	25.28	34	0
40	83.09	265.31	20.18	25.84	34	0
45	91.00	288.20	20.00	25.25	34	0
50	96.75	310.75	21.25	25.55	34	0
55	103.34	336.81	20.67	26.00	34	0
56.5	106.13	342.32	20.37	26.13	34	0
56.55	106.53	341.22	20.5	25.93	34	0.809
56.63	106.75	243.32	20.25	26.00	34	16.41
57.75	93	27.03	20.50	73.75	34	0

Appendix B-3: Temperature profile of pressure chamber

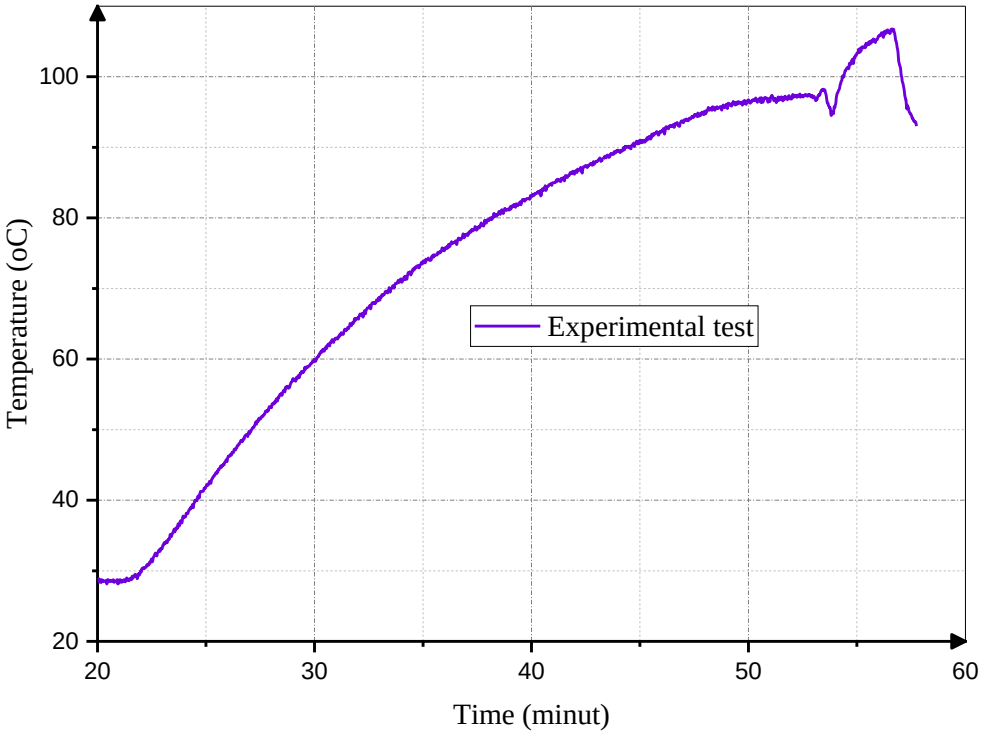

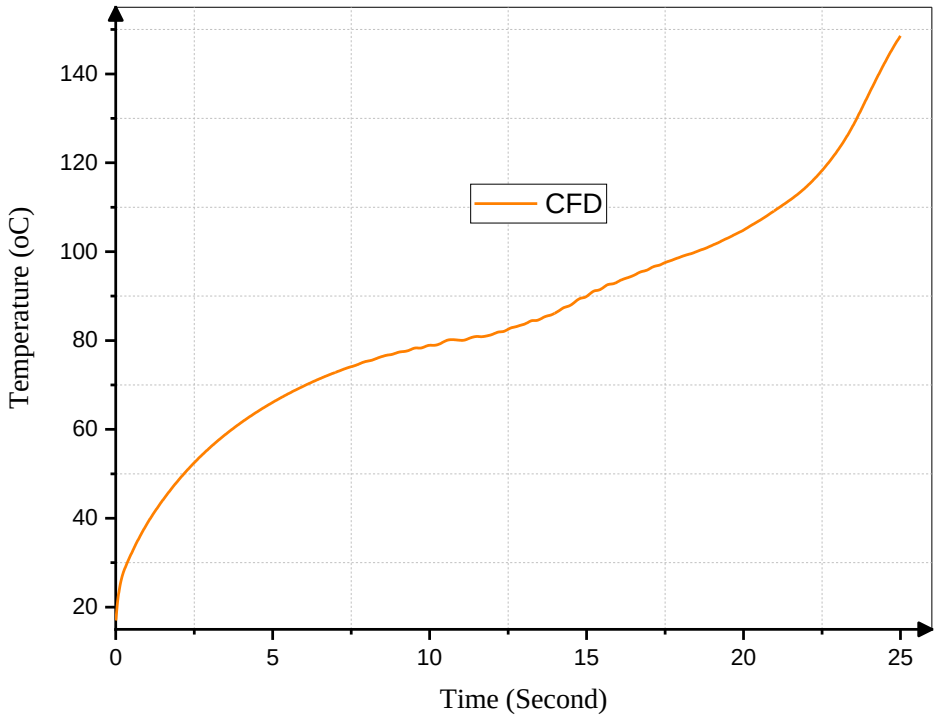

Appendix C: Drawing and Pallets

Appendix C-1: Assembly drawing of ram 25mm nominal diameter ram pump

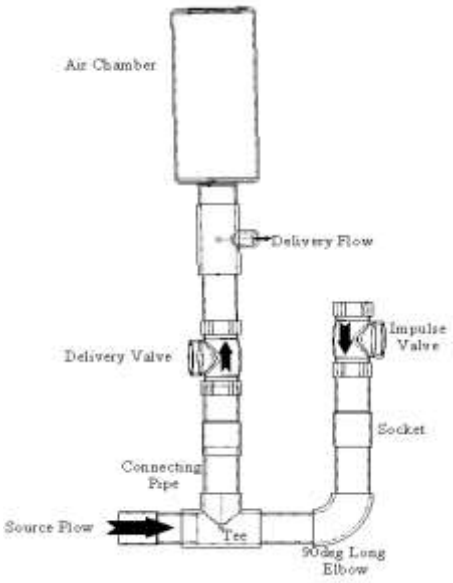

Appendix C-2: Detail real view of the ram pump

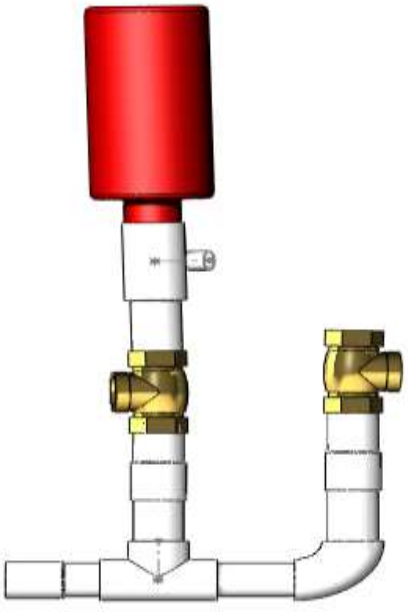

Appendix C-3: Fabrication, assembly and Base plate tub (waste water collecting container)

Appendix C-4: Final feature of the pump and its accessories